

PRELIMINARY DEVELOPMENTAL REPORT
FOR
DEPLOYABLE LARGE AREA
SOLAR ARRAY STRUCTURE

RYAN



AERONAUTICAL COMPANY

REPORT NO. 20869-1

30 JULY 1965

This work was performed for the Jet Propulsion Laboratory, California Institute of Technology, pursuant to a subcontract issued under Prime Contract NAS7-100 between the California Institute of Technology and the United States of America represented by the National Aeronautics and Space Administration.

Prepared for
California Institute of Technology
Jet Propulsion Laboratory
Contract No. 951107

(Subcontract Under NASA Contract No. NAS7 - 100)

183 PAGES

COPY NO. **10**

CONTENTS

SECTION		PAGE
1.0	INTRODUCTION	1
2.0	SUMMARY	3
3.0	DESIGN CONCEPT	5
3.1	Support Beam	7
3.2	Substrate	19
3.3	Roller Drum	21
3.4	Actuation System	22
3.5	Support Structure	24
3.6	Electrical Provisions	25
3.7	Alternate Configurations	28
4.0	DESIGN CRITERIA	57
5.0	THERMODYNAMICS	67
6.0	STRUCTURAL DYNAMICS	77
7.0	STRUCTURAL ANALYSIS	91
8.0	WEIGHT ANALYSIS	137
9.0	MATERIAL AND PROCESS DEVELOPMENT	141
10.0	RELIABILITY	165
11.0	CONCLUSIONS	171
12.0	RECOMMENDATIONS	173

LIST OF ILLUSTRATIONS

FIGURE		PAGE
1	Basic Beam Shapes	9
2	Substrate and Beam Details	11
3	Beam Test Samples	13
4	Substrate Installation	15
5	Deployable Panel Installation	17
6	Solar Array	26
7	Sprocket Drive Mechanism	29
8	Deploying Ribbon Drive Mechanism	31
9	Attachment to Vehicle - Cross and Tubes	33
10	Vehicle Mounts - Rollout Array	35
11	Beam Guide - Rollout Array	37
12	Beam Supports and Guides - Scheme 1	39
13	Beam Supports and Guides - Scheme 2	41
14	Alternate Beam Guide	43
15	Substrate Attachments - Rollout	45
16	Substrate Attachments - Beam	47
17	Panel Attachment to Beams	49
18	Detail of Beam Attachment	51
19	Substrate Samples	53
20	Mockup of Rollout Drum	55
21	Mockup of Rollout Drum	55
22	Periods of Electrical Power	63
23	Solar Irradiance vs Maximum Solar Cell Temperature	63
24	Steady State Temperature	71
25	Solar Cell Surface Temperatures	72
26	Temperature Distribution	73
27	Temperature Distribution - Substrate Attachment	74
28	Modulus of Elasticity vs Buckling Coefficient	98
29	K vs θ -Degrees	104
30	K vs θ -Degrees	105
31	K vs θ -Degrees	106
32	Elevator Temperature Properties	114
33	Solar Array Growth Potential	134
34	Parametric Study	135

LIST OF ILLUSTRATIONS (Continued)

FIGURE		PAGE
35	Weight of Glass Fiber Substrate	140
36	Test Panel for Flexural Strength and Modulus	144
37	Test Sector	151
38	Test Method - Beam Buckling	151
39	Beam Specimens	152
40	Typical Failure Modes	152
41	Contilever Beam Bending Test	157
42	Creep Specimens Before Test	157
43	Creep Specimens During Test	158
44	Creep Specimens After Test	158
45	Substrate After Lamination	164
46	Substrate After Lamination	164

LIST OF TABLES

TABLE		PAGE
1	Thermal Properties	75
2	Summary - Cantilever Beam Tests	101
3	Panel Requirements	145
4	Mechanical Properties of Beam Materials	147
5	Test Sector Requirements	148
6	Wrapping Tests on Beam Sectors	149
7	Bending Moment Tests - Open Beam Sector	150
8	Cantilever Beam Test Results	154
9	Creep at 295° F	160
10	Properties of Silicone Rubber Foam	167

1.0 INTRODUCTION

This report summarizes the results of a Phase I (Preliminary Design Phase) Study conducted by Ryan Aeronautical Company for the Jet Propulsion Laboratory. This study was authorized by JPL Contract No. 951107.

The purpose of the Phase I study was to select and explore a concept for deploying lightweight, large area solar arrays with areas of 150 to 400 square feet, and to develop the design so that an evaluation could be made with respect to the production of manufacturing drawings and fabrication of prototype units.

An area of 200 square feet was selected as representative of near future needs. This area was divided into four units of 50 square feet for mounting within the design envelope supplied by JPL. A roller drum, extendable beam concept was selected because of its inherent adaptability to growth requirements, and the good self-damping qualities of the stowed substrate, which would minimize dynamic deflection problems.

Layout design studies were made in the areas of beams, substrate, support structure, actuation systems and electrical provisions. Analytical support in these areas was provided as required. Sample structural elements were fabricated and tested to provide answers in areas where analytical methods were not applicable, or were too time consuming. Results of this work are contained herein.

2.0 SUMMARY

Preliminary design layout studies, analytical investigations and tests on sample parts and assemblies indicate that the concept presented in the proposal is feasible. Changes have been made in beam shape to optimize the section and torsional characteristics. Design layouts have been made in sufficient detail to indicate that production drawings can be made in the predicted time span. Sample part tests and analyses indicate that the proposed assembly will sustain the design loads and will function reliably.

3.0 DESIGN CONCEPT

Past experience with rigid solar panel substrate structures has illustrated that minimizing panel deflection due to dynamic loads becomes an increasingly difficult design task, as panel size increases. This task could be more easily accomplished if allowable weights could be increased to provide stiffer substrate structures, or adequate damping devices. The demand for advancing the state-of-the-art, however, requires that allowable weights be reduced rather than increased. This fact causes a basic incompatibility in the concept of a large rigid array that is also light in weight.

A concept, such as the roller drum presented herein, reduces the dynamic deflection problems by providing a highly rigid shape due to its large diameter and short length. Using this rigid structure to support and dampen a flexible substrate, maximum advantage of the rigid structure may be realized during the periods of high loads. The design also uses a relatively lightweight substrate and beam assembly to react to the greatly reduced g loads experienced after deployment.

Although the roller drum concept is not new, it has not been utilized to date. Two major reasons for this are: (1) the requirement for large arrays was not critical, (2) a reasonable method of extending the supporting substrate was not available.

The development of a lightweight folding and extending beam compatible with a roller is the major reason for the feasibility of the concept. The first phase effort has developed a beam that fulfills these goals and thus becomes a roller concept that is logical and workable for packaging and extending large area solar arrays. The particular design presented herein fits well within the envelope of a hypothetical spacecraft. Actual space availability and interface structure can be altered to provide even greater capability.

A one-foot-diameter roller was used because of specification requirements, but the beam appears capable of bending to smaller diameters without adverse effects. Another advantageous characteristic for larger envelopes is that the length of the array may be shortened as the roller length increases, thus maintaining the same area. This also decreases the CG moment arm and reduces the required beam section at the root.

The resulting lighter beam requires less torque for retraction. Therefore, a smaller motor will suffice. The ultimate configuration for a particular envelope and area may require additional beams on the array, as area and envelope requirements change. The concept is adaptable to different envelopes and area requirements.

The overall concept is divided into five areas. These are:

- Support beam
- Substrate
- Roller and support structure
- Actuation system
- Electrical provisions

These areas are discussed individually in the following pages. Alternate concepts in each area have been explored, and certain of these are included for comparison.

3.1 SUPPORT BEAM

The preliminary investigation conducted at the time of Ryan's proposal to JPL indicated the feasibility of rolling a structural beam around a one-foot-diameter drum. Subsequent development of this basic idea during Phase I was aimed at optimizing the beam configuration to fulfill design parameters. The essential part of this development was the design of a shape which would be most effective to react the bending loads imposed by the .2 G cruise maneuver. In addition, this shape should be one which would allow flattening of the section with relatively little load and no permanent distortion. Closely coupled to the design of the shape was the selection of a material which would tolerate flattening and wrapping without yielding, and one which would perform under all environmental conditions.

The beam shape presented in the proposal is shown as Design A, Fig. 1. This shape was discarded after further analytical and sample test investigations. The shape selected as the first choice is shown in Design B of Figure 1. Others investigated are shown in Figures 2 and 3.

Reasons for the change to Design B were:

1. The unsupported edges of Design A proved to be critical in buckling when the load direction imposed compression loads on these edges. The side of the beam taking tension loads was required to support approximately 80% of the load. This characteristic caused the beam weight to be high in comparison to the load reacted, because only one-half of the beam assembly was working to react a load normal to the beam.

Conversely, Design B eliminates the unsupported edges by creating a closed section stabilized for buckling by the reversed curvature of the shape. This design utilizes the full height of the beam by working both beam caps at one time, rather than one-half of the beam, to react loads from a particular direction.

2. The open section shown as Design A has very little torsional rigidity. Closing the section, as accomplished in Design B, greatly increases the torsional capability of the beam, thereby increasing the torsional rigidity of the entire panel.

Bending tests were conducted on various materials and section shapes of varying thicknesses. An optimum modulus to weight ratio was selected

which was compatible with such other factors as weight, corrosion, magnetic aspects, creep, etc. This approach also reduced the cap stresses to an allowable value.

The use of a thin material allows the use of smaller radii in the beam cross section, which improves the R/T ratio for cap buckling. The goal was to decrease the radius to a point that the section would still bend to a flat, folded configuration but would exhibit no permanent set. This approach produced the greatest depth beam for a given width. It is possible to produce a beam of a higher-than-required load capability using this philosophy, but the load required to flatten the beam increases also. These two factors must be balanced then to produce a beam with desirable flattening characteristics while maintaining the required beam stiffness and movement capability.

Material investigation was limited to those materials which were non-magnetic. Available materials, glass fiber, aluminum, AM 355 (magnetic), and titanium, were used for the fabrication of test samples to check foldability characteristics. The high modulus required, as explained previously, eliminated aluminum. AM 355 was used to provide initial concept type parts because of its availability in gages required, ignoring its magnetic properties. Fiberglass thicknesses required necessitated excessive flattening loads, which rated this material as second choice. Problems of resin creep at temperature were mainly overcome by the use of proper resins. Titanium exhibited all the desirable qualities needed, and test sample fabrication proved this material capable of fulfilling requirements.

The method of attaching the beam to the drum and substrate is illustrated in Figures 4 and 5. Other methods of beam attachment will be explored on the test drum now being fabricated, and findings will be incorporated into the final design.

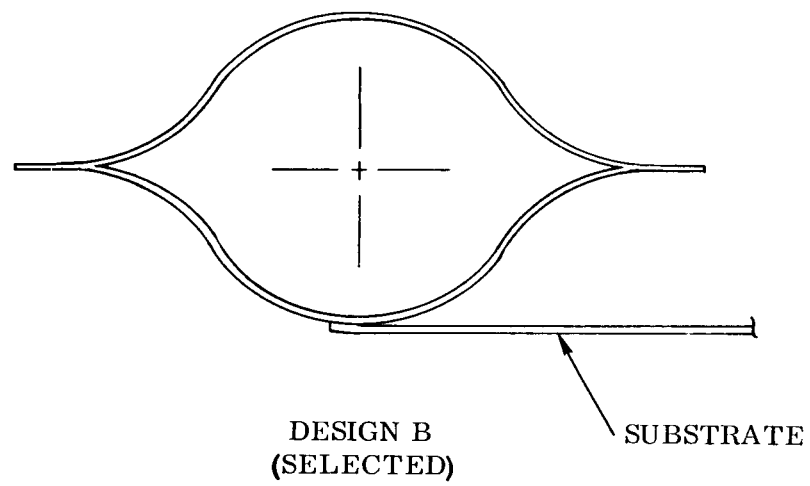
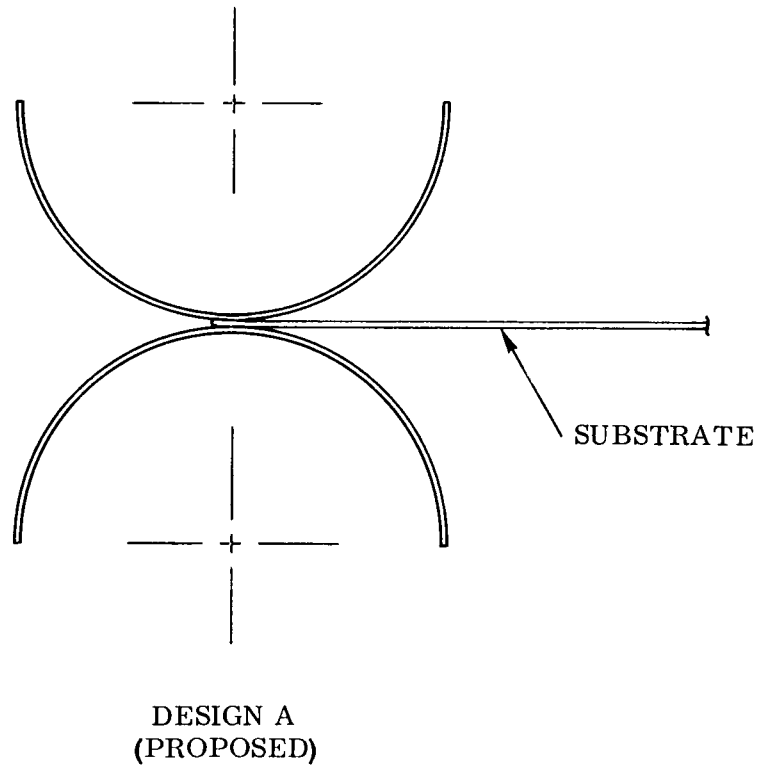
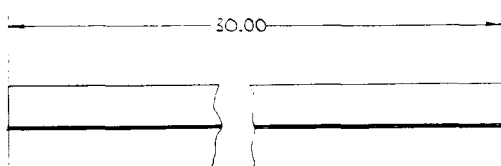
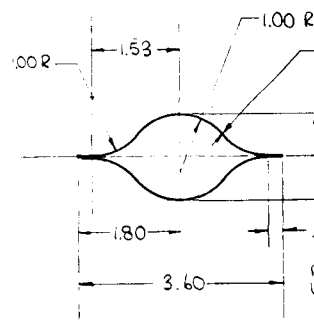


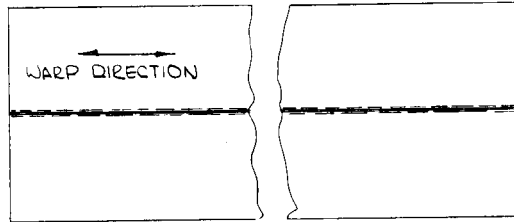
Figure 1 Basic Beam Shapes



MATL: .43 GLASS FIBER WITH EPON 828-2P7A
PER NPD 139

TEST SAMPLE V E

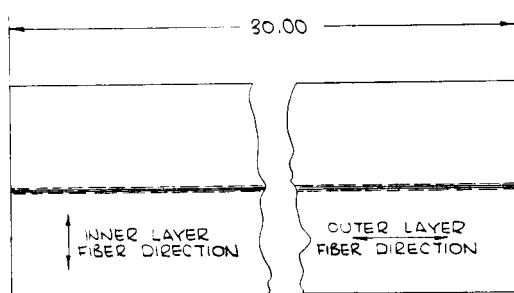
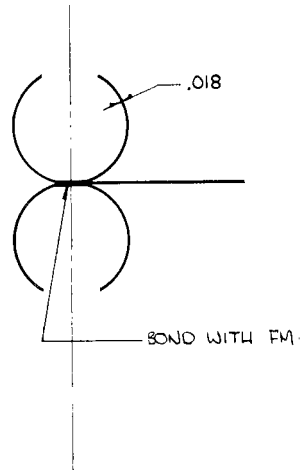




ALL DETAILS SAME AS SAMPLE III D-20
EXCEPT AS SHOWN

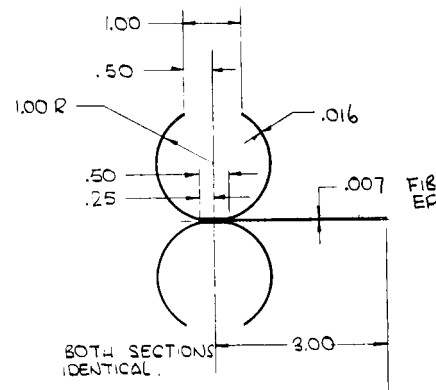
MATERIAL - 143 GLASS CLOTH WITH
EPON 828 AND DION RP-7A PER MPD 139

TEST SAMPLE III E-2



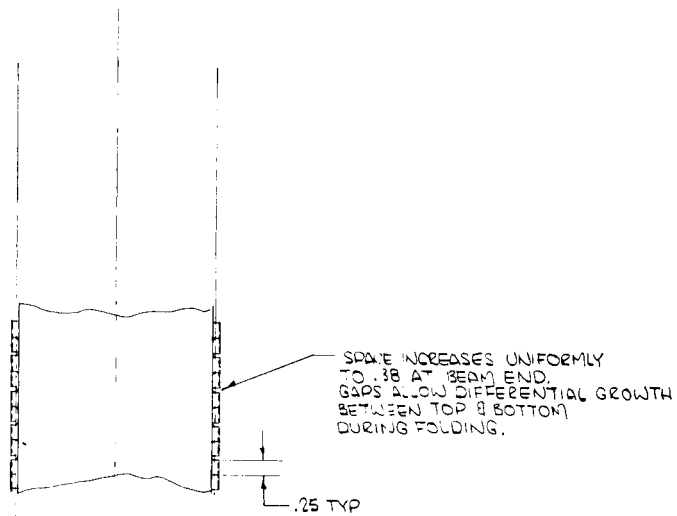
MATERIAL : SCOTCHPLY 1009-26 S
UNIDIRECTIONAL, LOCATE FIBER
DIRECTION AS SHOWN.

TEST SAMPLE III D-20



TEST BEAMS - FIBERGLASS

00



TUBE SECTIONS BRAZED TO CAP TO FORM HINGE SECTIONS, ALLOW BEAM TO FLATTEN.

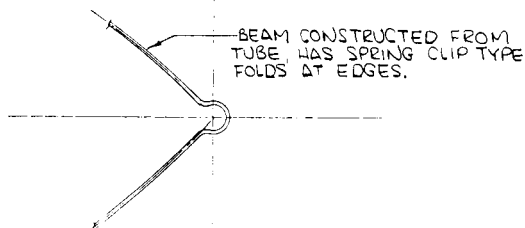
SAMPLE 7

.015 THK —
THICKNESS TAPERS FROM .015 TO .004 OVER THIS LENGTH.

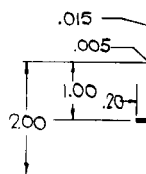
.004 THICKNESS IS .20 CONSTANT OVER THIS WIDTH.

CONTINUOUS SEAM WELD —

1.10 R —
1.25 R —

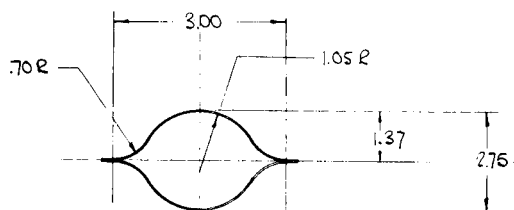


GLASS (128 CLOTH) KY.



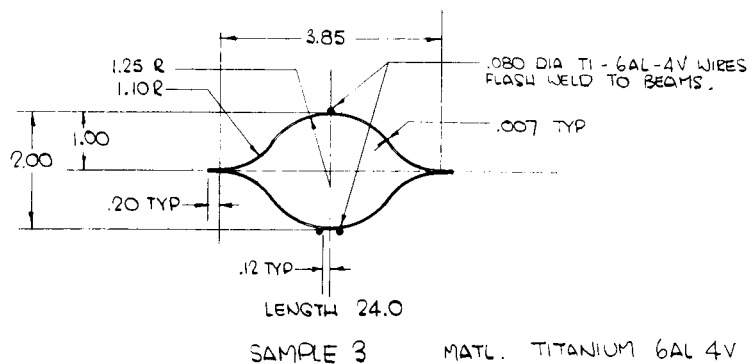
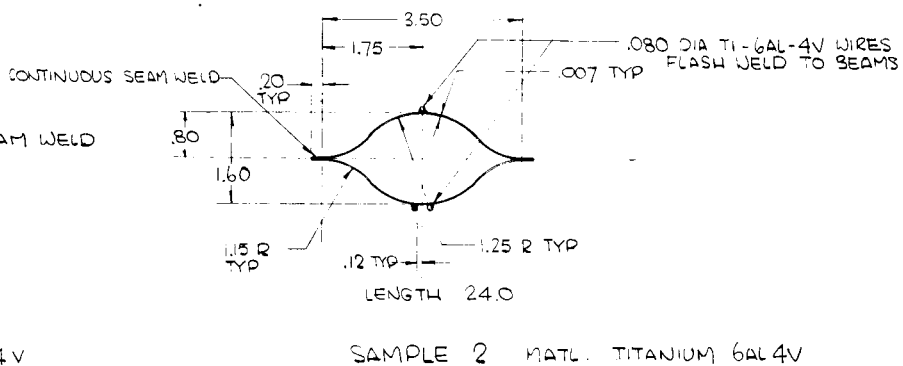
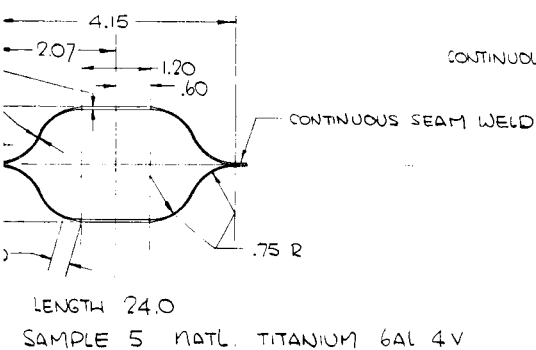
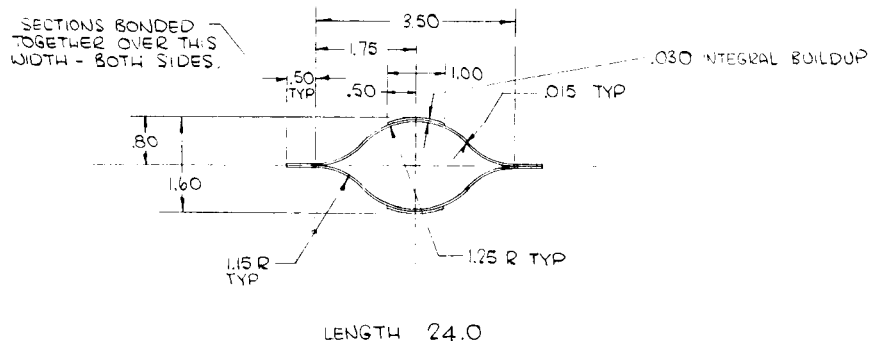
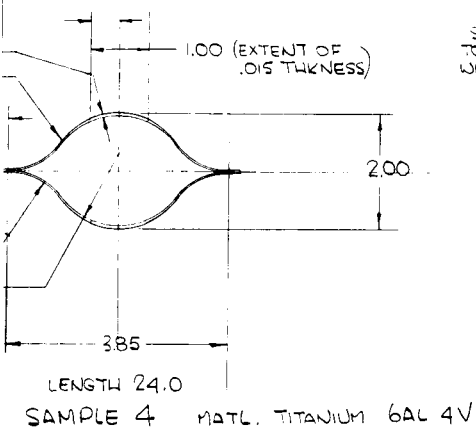
THICKNESS TAPERS OVER THIS LGTH, .3

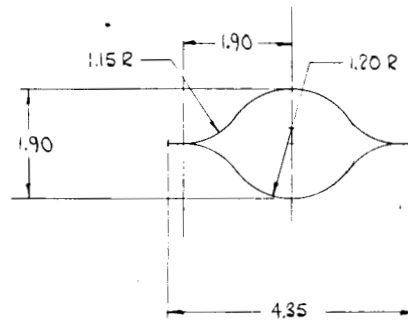
CONTINUOUS FOLDS ALLOW DIFFERENTIAL GROWTH WHEN FOLDED.



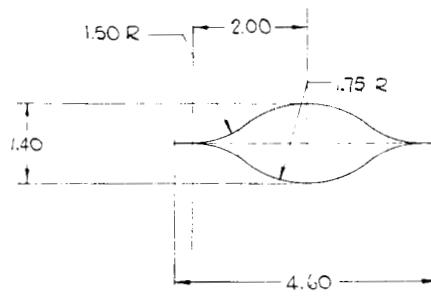
SAMPLE 6

ALTERNATIVE METHODS OF FORMING A HINGE OR FOLDING POINT.

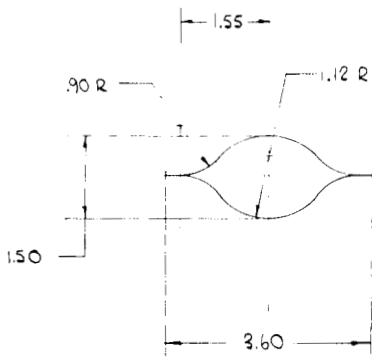




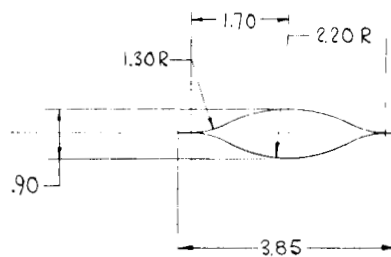
SECTION 3.



SECTION 2



SECTION 4



SECTION 1.

Figure 2 Substrate and Beam Details

5

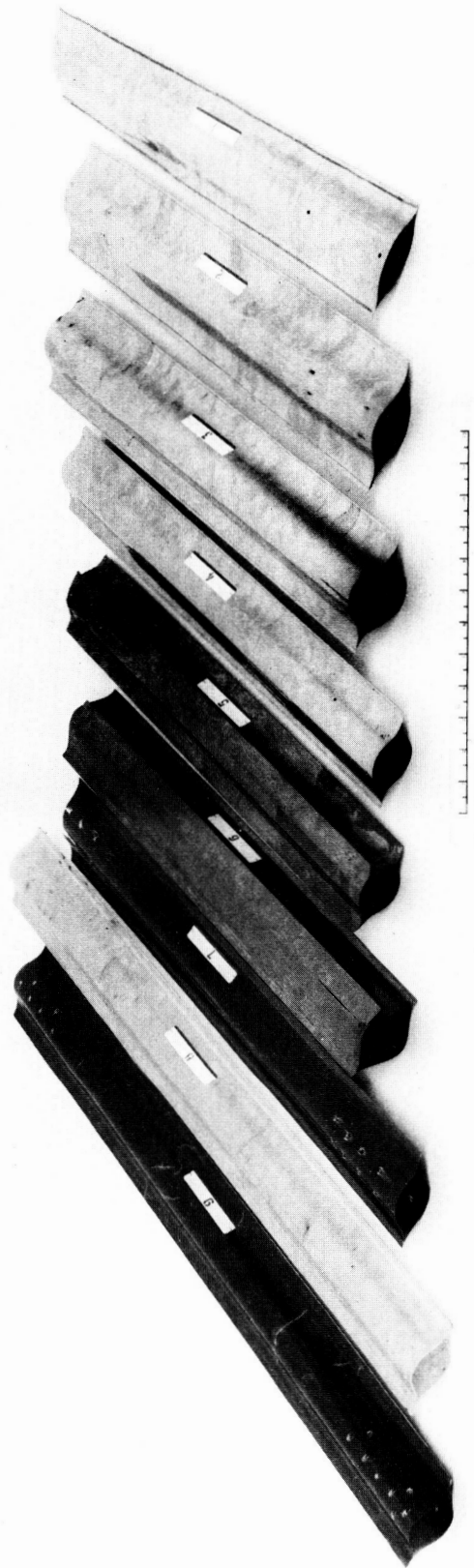
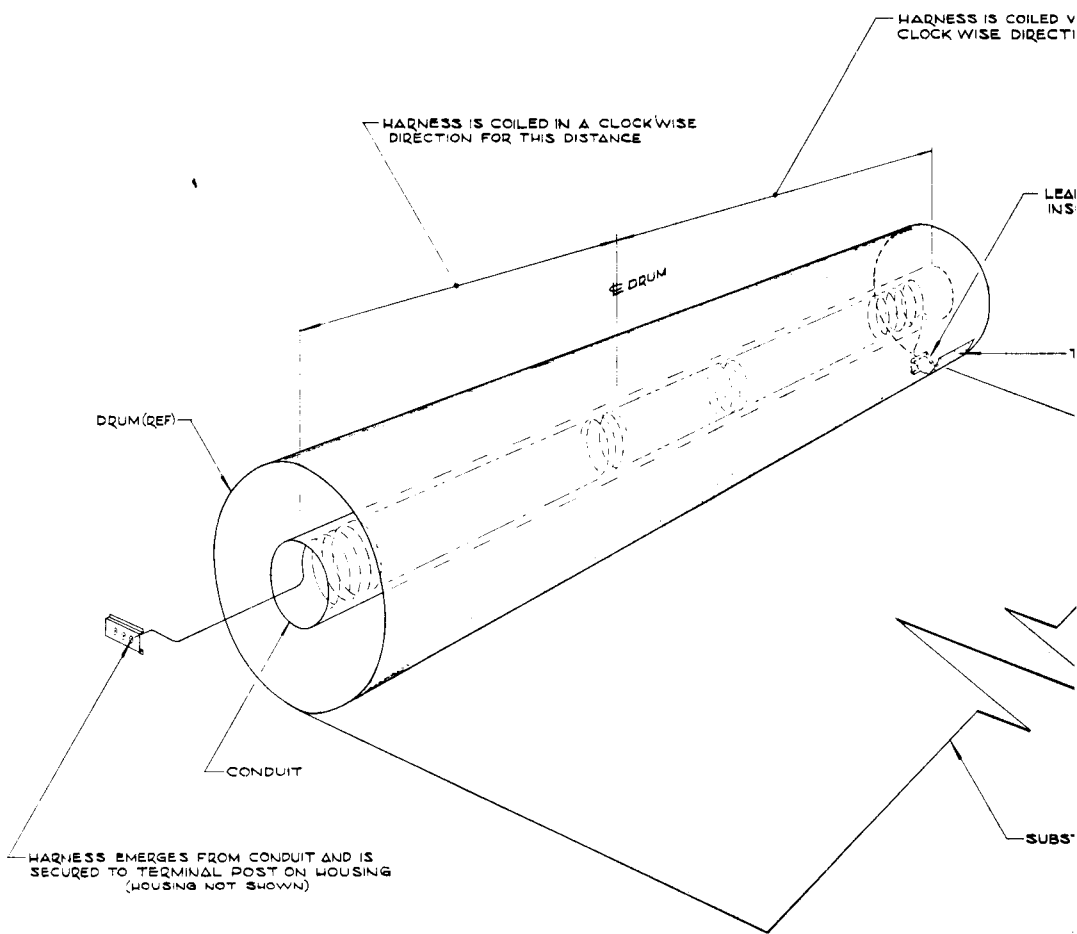


Figure 3 Beam Test Samples



PARTIAL ELECTRICAL SCHEMATIC

THIN CONDUIT IN A COUNTER-
J FOR THIS DISTANCE

ATTACHED TO TERMINAL ON
OF DRUM

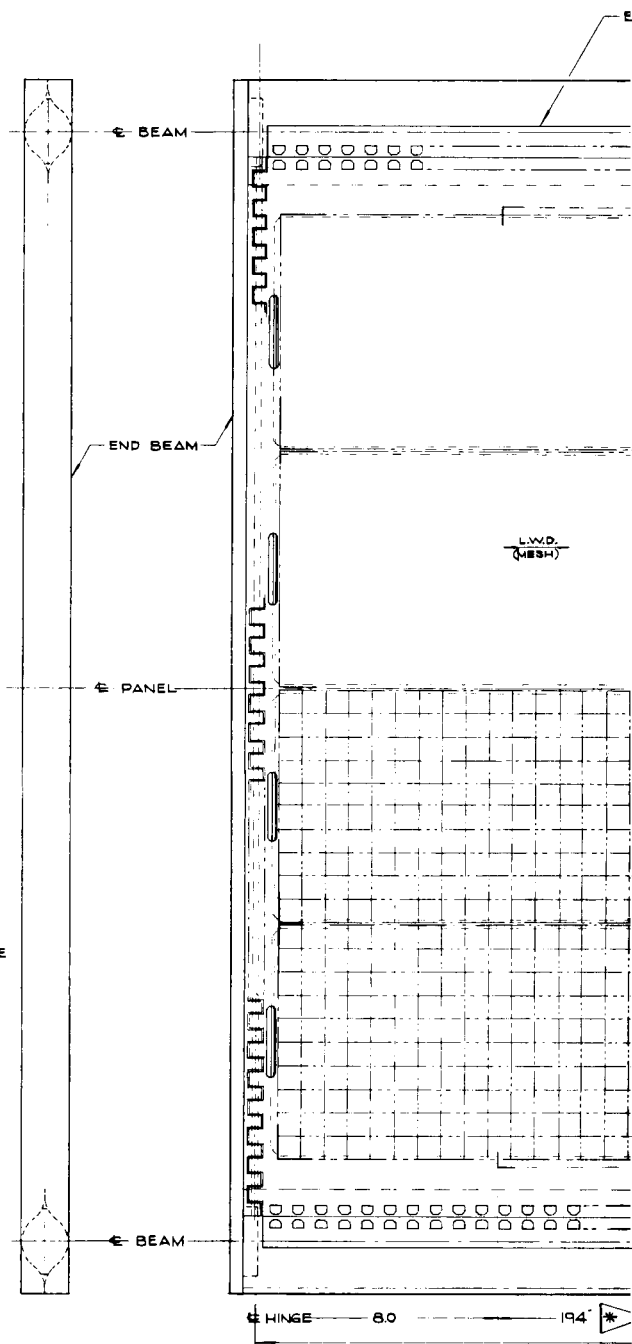
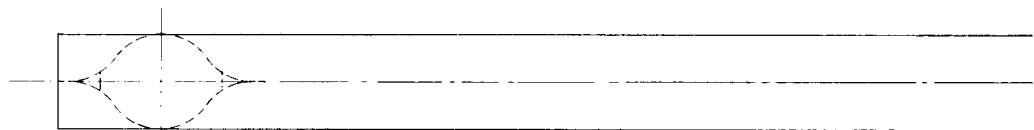
TERMINAL ACCESS DOOR

ELECTRICAL LEADS FROM
CELL MODULES

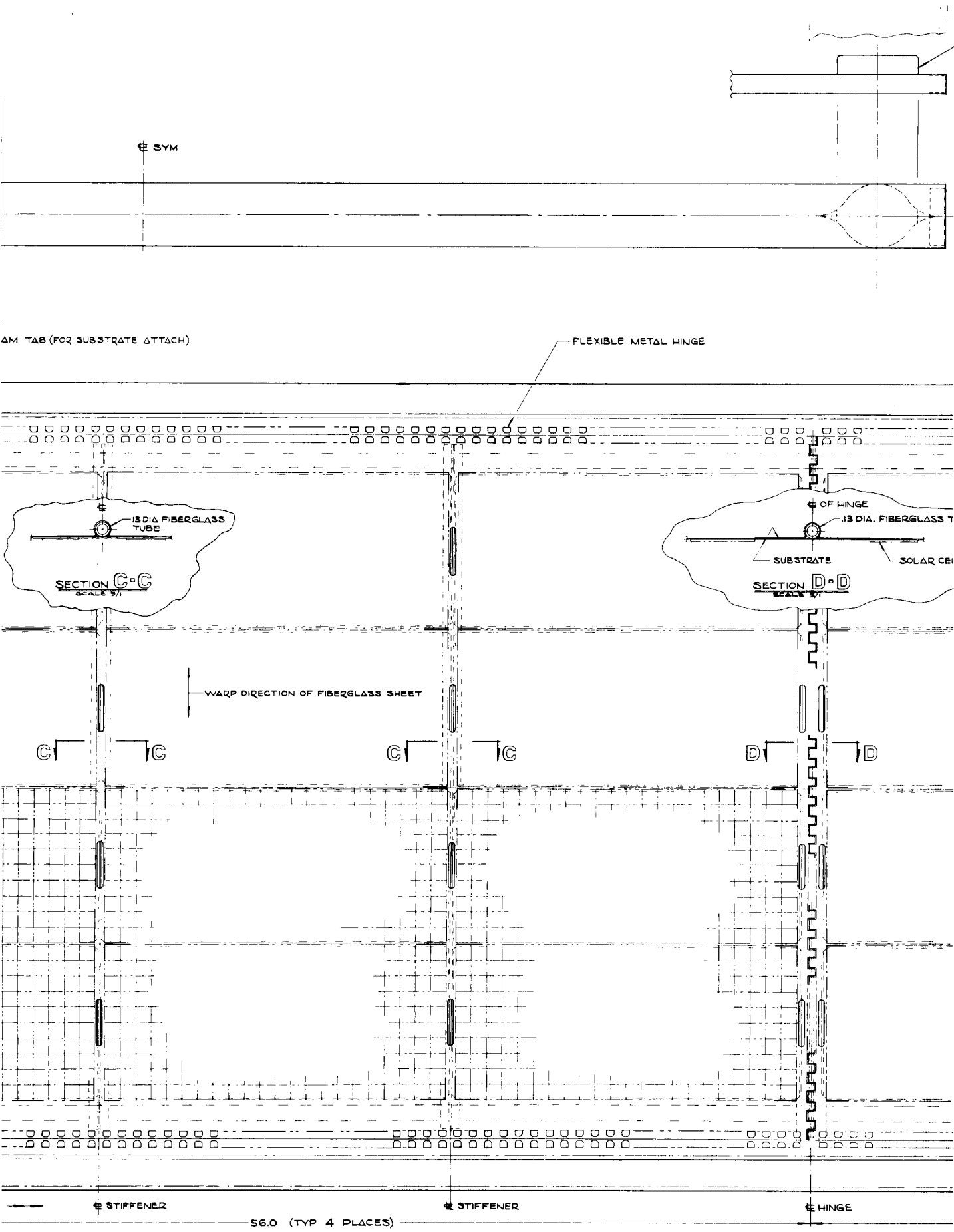
DATE (REF)

SOLAR CELLS (REF)
FIBERGLASS EPOXY SHEET - ONE PLY STYLE 108 (.002)
ADHESIVE - FM-1044 (.001 THICK)
FINE EXPANDED SILVER MESH-FLATTENED / ANNEALED-A₉7-2/0E
FIBERGLASS EPOXY SHEET - STYLE 113 (.003)
RESIN EPON 828 QP7A
SILICON FOAM DAMPING PAD(S) *

AL CROSS SECTION OF SUBSTRATE
NO SCALE



2



A-A VIEW OF FRONT FACE OF PANEL
 SCALE 1/2

3

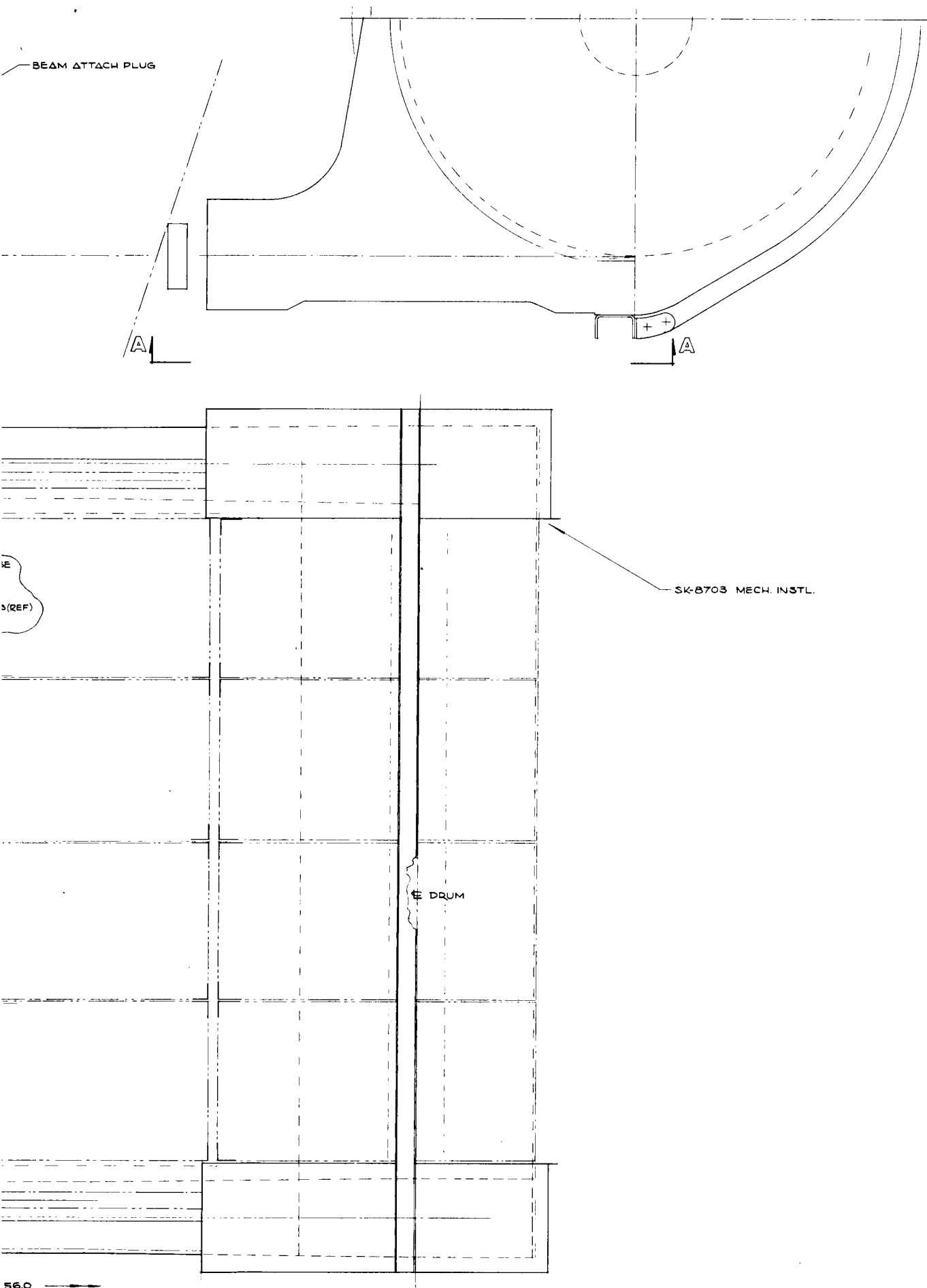


Figure 4 Substrate Installation

4

38.50
BETWEEN CTRS.

BEAM

1.0x1.0 LIPPED ANGLE - 7075-T6 MATL. AL. ALY.
(FULL WIDTH)

INNER WEB
.040-7075-T6 MATL. AL. ALY.

SECTION A-A

SHEAR WEB
032 7075-T6
AL. ALY.

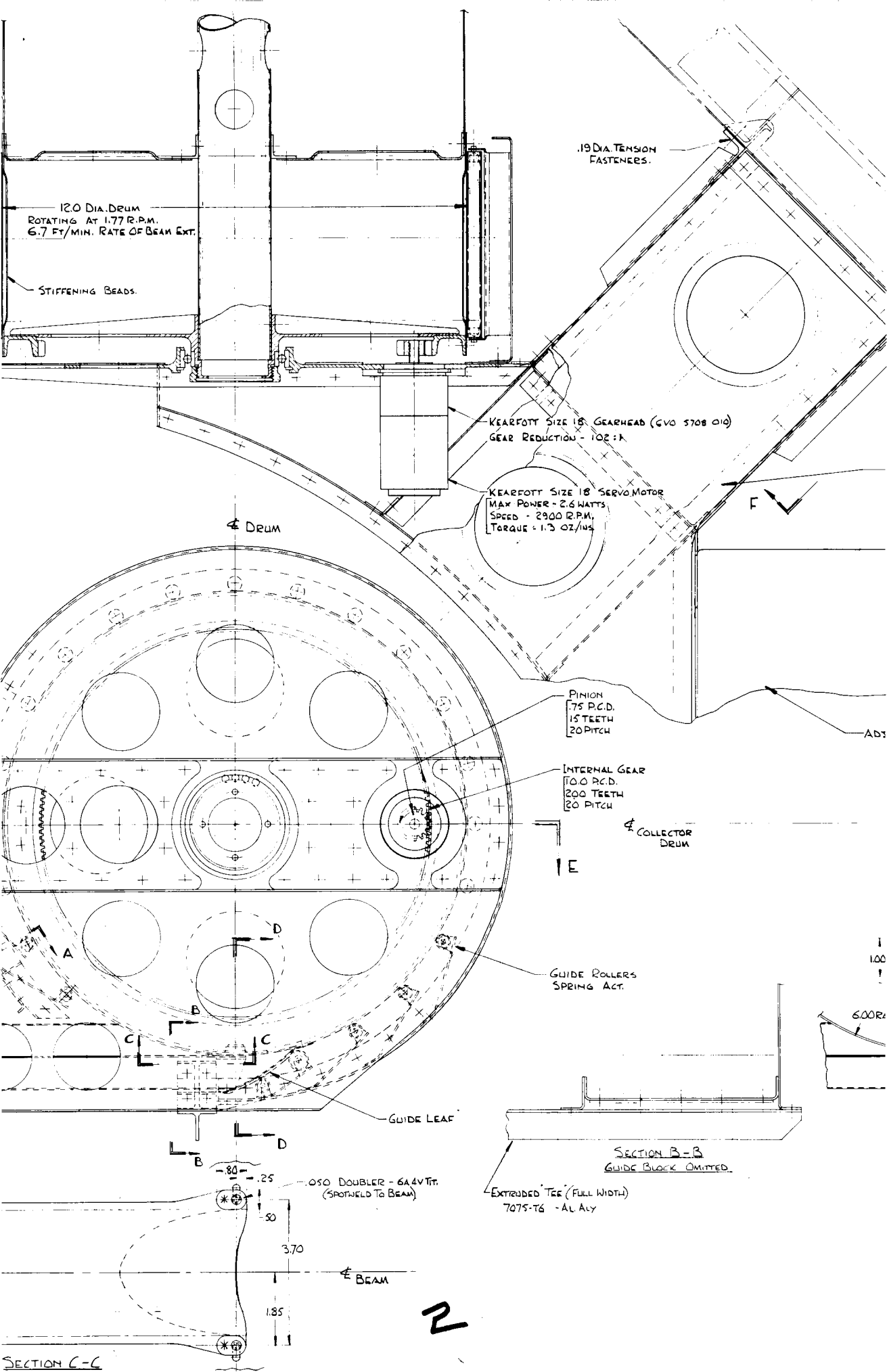
SPACECRAFT ENVELOPE

E

BEAM

END COVER
.040-7075-T6 MATL. AL. ALY.

1



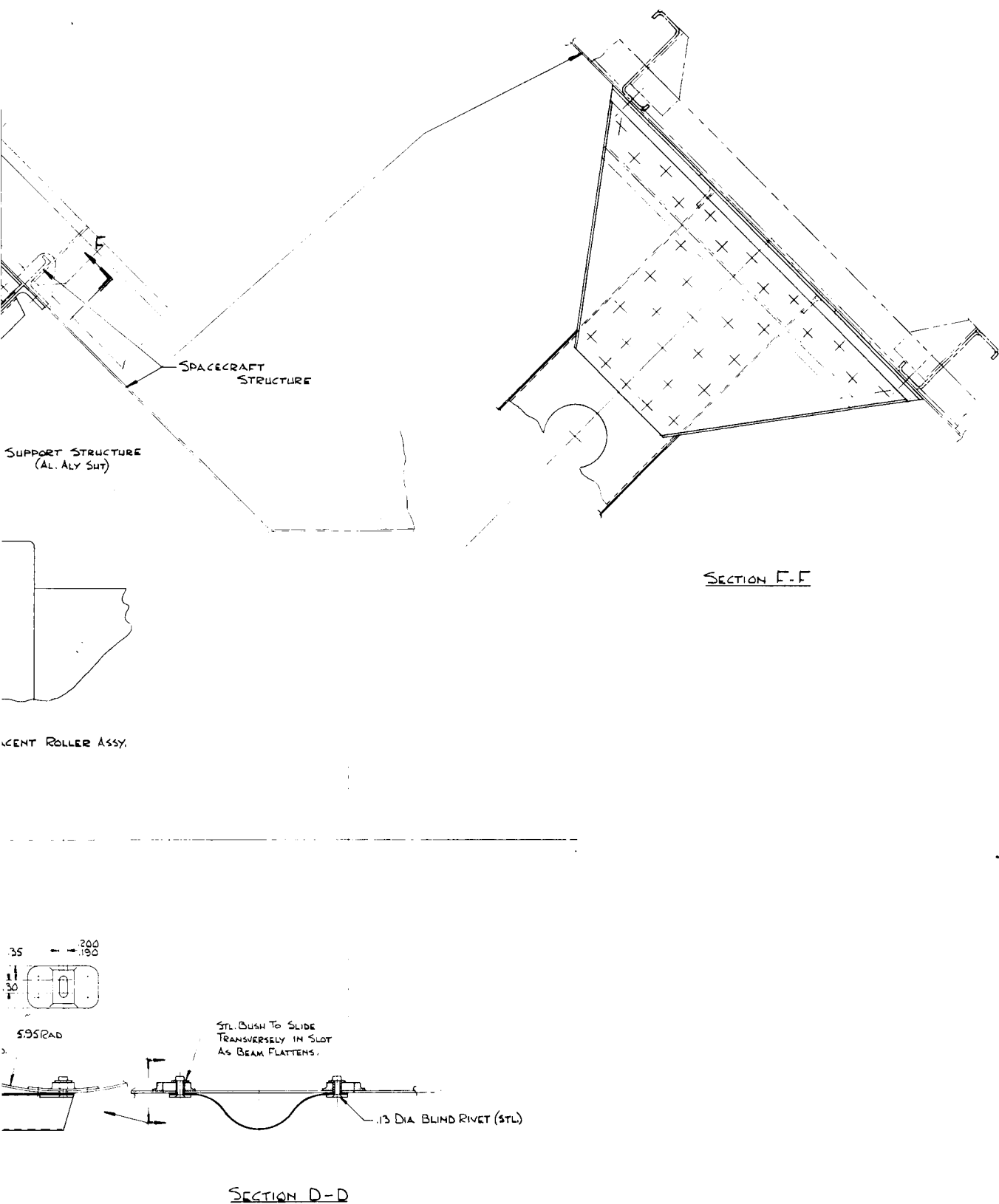


Figure 5 Deployable Panel Installation

3

3.2 SUBSTRATE

The substrate in its most simple form can consist of a semi-rigid sheet of material mounted directly to the beams and roller and bonded permanently in place. The weight and stress analysis for the system was conducted for this condition and then recalculated. Figure 4 illustrates this approach, which offers sufficient advantages to justify a slight weight increase.

The basic substrate consists of a .003-inch-thick, resin-impregnated fiberglass cloth. Ribbons of fine, expanded silver mesh are placed in a pattern corresponding to the solar cell submodules for purposes of cancellation of magnetic effects of current flow. This mesh becomes the center layer of the total substrate when a .002-inch thickness of resin-impregnated fiberglass cloth is added as a dielectric layer. Cutouts in this dielectric layer provide for electrical connection from the cells and terminal strips to the mesh.

Joints are provided to facilitate installation and removal of the substrate from the beams and drum and to allow the 18-foot length to be fabricated in more easily handled units. This also provides for more practical sizes for the layup and checkout of solar cells. These joints are of two types, depending on their direction. The transverse joints, which experience little bending, simulate piano-type hinges. The hinge pin may be removed to separate the joint. This joint also provides some transverse stiffness. Stiffeners of approximately the same size are provided about every 18 inches. Thus, a removable section would be approximately 54" long x 36" wide. The longitudinal attachment of substrate to spar must bend over the one-foot-diameter drum and must therefore be relatively flexible. This is accomplished by the use of sections of tab connectors, which are inserted through slots in the beam tie flange and substrate and are then bent over to form a secure attachment. These also permit removal of the panel by removing the clip sections. The substrate will be increased in thickness at these attach points to reduce local bearing stresses.

Damper strips are mounted to the back of the substrate to protect the solar cells when the panel is packaged. These silicone foam strips will be bonded approximately every four inches and extend longitudinally in the areas where this contact is required.

No cover or protection is planned for the exposed solar cells on the outside of the package since this would add extra weight. Furthermore,

there is little need for such protection, as demonstrated by the unprotected cell surfaces of the fixed panels used for Ranger and Mariner spacecraft.

3.3 ROLLER DRUM

The primary purpose of the roller drum is to provide a rigid backup structure for storing the substrate and beams during periods when the array is not functioning. The critical time of support is obviously during boost phase, when the high G loads caused by acceleration and vibration are present. The drum must also react torsional loads due to the drive input, which is introduced at one side of the drum only and must be transferred to both beams to provide the force for extension and retraction. Any torsional deflection in the drum would cause relative lateral movement of the beams and introduce shear into the substrate.

The drum is constructed of a rolled, one-foot-diameter aluminum cylinder, with end plates machined to accommodate a bearing and drive gear. There are lightening holes in the drum to decrease weight, and bulkheads are installed at four points to provide additional support for leaf-spring and substrate loads. A short section of fiberglass sheet is secured permanently to the drum and extends outward to the center of the previously described disconnect joint at the inboard end of the substrate. A glass fiber tube extends through the center of the drum to provide a support conduit for a coiled electrical lead. Provisions for an access door and an electrical terminal board are also incorporated in the drum.

3.4 ACTUATION SYSTEM

Three major methods of deployment are studied in this phase. Briefly these are as follows:

- a. Central drum drive
- b. Sprocket drive
- c. Strap drive

The central drum drive (Figure 5) was selected for use on the array. Alternate methods are shown as Figures 7 and 8.

The principal reason for the selection of this concept was the relative simplicity, which is directly coupled with system reliability and weight. The basic differences between the systems are as follows:

- a. The drum drive uses only one motor to extend and retract the substrate and is controlled by electrical switching, with no clutching or mechanical drive disconnects. Pressure contact rollers are required to prevent the folded beam from buckling from the compression load induced by the drum during the deployment cycle. This method requires no alterations or sprocket holes in the beam.
- b. The sprocket drive system may employ one or two motors. The layout presented in Figure 7 uses only one motor. The drum is disconnected by an overrunning clutch, for the deployment phase, as the toothed sprockets pull the beams from the roll. The toothed sprockets are disconnected by reversal of motor direction, which reverses the direction of load and moves an idler gear out of mesh. The motor then drives the drum directly thru the overrunning clutch.
- c. The strap drive clutching and disconnect system is similar to the sprocket drive. In this system, however, the shaft, instead of driving a sprocket, drives a spool containing deployment ribbon. When this spool is engaged by the idler gear, the ribbon rotates the drum and provides support for the folded beam to allow it to deploy without buckling away from the drum. To retract the substrate, motor direction is reversed. The drum is then driven through the overrunning

clutch, which pulls and wraps the beams around the drum. At this time, the idler gear disengages the ribbon spool and the ribbon is wrapped back onto the drum as the retraction cycle continues.

Preliminary tests have been conducted to examine the characteristics of the beam as the section makes a transition from flat to full section, along with tests in the area of the flat wrapped section. Two major factors which influence the compression load in these sections are the support guide friction and the spring roller friction. The magnitude of these values cannot be determined until completion of a full-scale test module, which is being fabricated to simulate the selected concept. Favorable results will justify the design as presented. Unfavorable results will require modification to increase the buckling strength of the beam. Roller spacing and pressure will be varied to achieve optimum results with minimum friction.

In the absence of test results, expected frictional forces were estimated to allow the selection of a motor and reduction gear box. It was estimated that a torque of five foot-pounds would be required to overcome this frictional force. A motor and gear reduction unit was selected to operate the system with this torsional force and a rate of six feet a minute (total time, three minutes) was set as reasonable for deployment and retraction time. Minor changes in interchangeable gear heads may be required to accommodate loads if values fall far outside those estimated. The present power requirement for the motor is approximately 2.6 watts.

3.5 SUPPORT STRUCTURE

The portion of the hardware considered as support structure falls into two divisions:

- a. The end caps, which support the drum, spring rollers, beam guides and drive motor.
- b. The adaptor support structure, which supports the entire roller and substrate assembly from the spacecraft interface.

These are illustrated in Figure 5. Alternate methods of support are shown in Figures 9, 10, and 11.

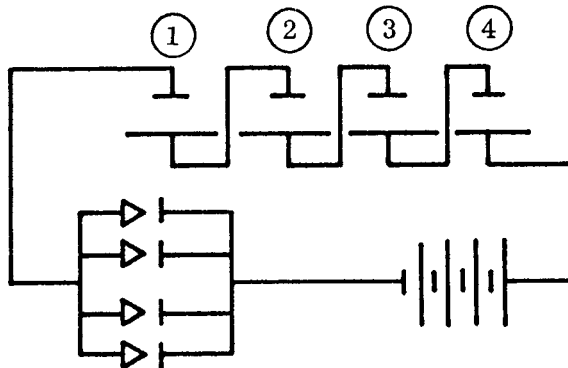
The end caps are designed to form a rigid mounting surface to support the loads induced by the roller springs. The end panel provides the base of this structure. A partial cap, which encompasses all but 45° of the drum, provides the mounting surface for the leaf springs which hold the rollers. This cap is prevented from deforming by means of a cutout panel at the inboard side of the end-cap assembly which completes the load path. The beam-support guides tie directly to these two end panels, which form good load reacting pads for the beam in extended condition. The combined drum, substrate, drive, and end cap weight, as magnified by boost and dynamic load conditions, is supported by a Y-shaped torque box constructed from aluminum sheet. See Figure 5. The Y support attaches to the adjacent ends of two assemblies and transmits the load directly to the spacecraft structure. This support must react the 12-G boost load coupled with the dynamic load of the deployable roller and substrate assembly. A ± 12 -G dynamic load is superimposed on the 12-G boost load in the longitudinal direction, which produces a 24-G load down and a zero-G load up. The possibility that the adjacent ends of the adjoining roller drums will be out of phase requires that the structure have sufficient torsional strength to react these loads. Simultaneously with these loadings, a 6-G lateral load occurs, and this must also be reacted by the support structure.

The support is designed to provide a good load path for the above conditions and to spread these loads out evenly to the spacecraft structure. It is assumed that alterations in either bus structure or roller support structure may be made to accommodate interface design.

3.6 ELECTRICAL PROVISIONS

An electrical layout was made using the available area and geometry of the structure shown in Figure 6. A general description of the buildup is as follows:

1. The solar array consists of 4 blades
2. Each blade consists of four 54" x 34" panels (total dimensions, 217" x 34")
3. Each panel consists of three electrical strings (cell groups)
4. Each string (cell group) consists of four electrical modules
5. Each electrical module consists of 22 submodules
6. Each submodule consists of 10 - 2cm x 2cm cells
7. The electrical connections are ten cells in parallel and 88 cells in series for each string
8. Each string is terminated with 4 blocking diodes, as shown below:



With the cells connected as described above, electrical characteristics of each cell group are as follows, for the conditions noted:

1. At 28° C and rated power output of 140 mw/cm² with a 10% efficient cell - 40.48 VDC @ 1.156 A = 46.8 watts
2. At 59° C and rated power output of 140 mw/cm² with a 10% efficient cell - 37.31 VDC @ 1.156 A = 43.12 watts

The quantities of cells required for the previously described electrical units are as follows:

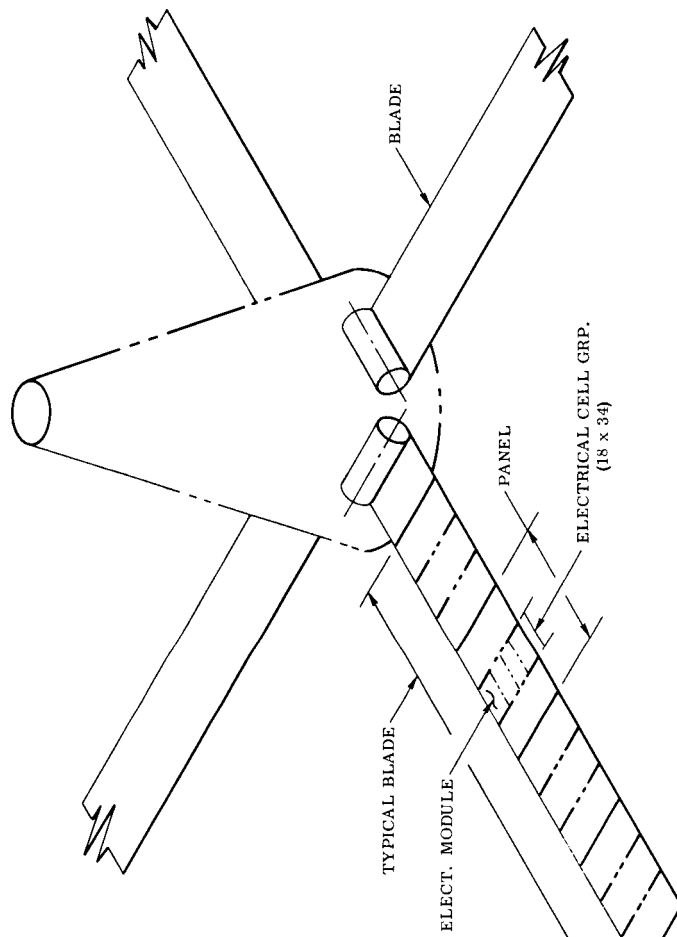
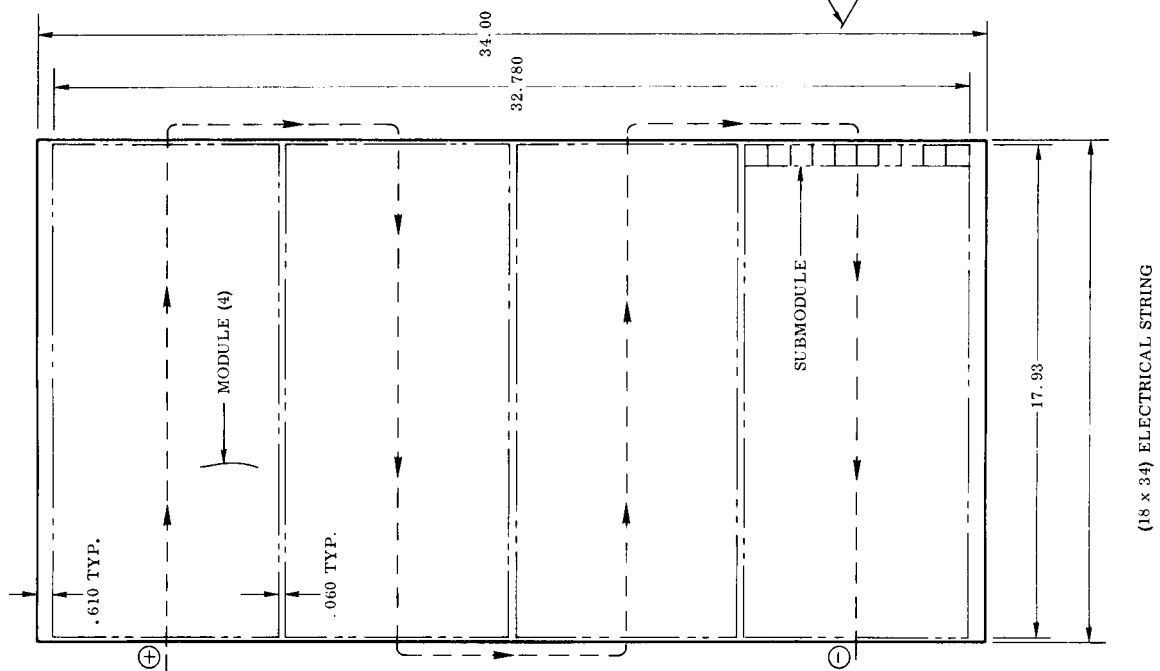


Figure 6 Solar Array

1.	Submodules	10 cells (all parallel)
2.	Module	220 cells (22 in series)
3.	Cell group (string)	880 cells (88 in series)
4.	Panel	2,640 cells (3 strings in parallel)
5.	Blade	10,560 cells (4 panels in parallel)
6.	Solar array	42,240 cells

The power outputs for these units are:

1.	Cell group	43.125 watts
2.	Panel	129.375 watts
3.	Blade	517.5 watts
4.	Solar Array	2,070 watts

NOTES:

The substrate area required is 205.4 ft. ²

The cell area required is 188.9 ft. ²

Packing factor = 91.9%

The number of cells per sq. ft. = 206

Individual cell area including spacing = .664 in. ²

The foregoing layout was investigated to check the feasibility of the geometry to produce 2,000 watts. The 2,070-watt output of this layout proves its feasibility. This electrical design is submitted as one which is compatible with the selected mechanical design and spacecraft electrical requirements.

3.7 ALTERNATE CONFIGURATIONS

The following figures are presented as supporting data and represent alternate configurations and layout investigations.

SILICON FACED ROLLERS
DRIVE OUT BEAMS.

BACK-UP ROLLERS APPLY
PRESSURE TO BEAM
FLANGES

ALTERNATIVE DRIVE METHOD
UTILISING FRICTION ROLLERS.

TORQUE SHAFT SUPPLIES POWER
TO OPPOSITE SIDE DRIVE
MECHANISM.

IDLER SWINGING ARMS.

SIZE 18 GEARHEAD
300:1 REDUCTION

BU ORD SIZE 18
REVERSING SERVO-
MOTOR

DRIVE SPROCKETS
2.867 PCD
9.00 CIRCUM
24 REVOLUTIONS
SERVO MOTOR S
WORKING SPE
TORQUE AT U
SIZE 18 GEARHEAD
RATIO 300:1
TIME TO EXTEND

IDLER GEAR ON SWING
ENGAGES BEAM DRIVE
DEPLOYING BEAM -
WHEN WINDING IN.

BEAM DRIVE SPROCKETS SLIDE
LATERALLY TO ALLOW FOR
LATERAL GROWTH OF BEAM
WHEN BEAM IS FLATTENED.

BEAM DRIVE SPROCKET M
WITH SPROCKET HOLES IN
FLANGES.

BACK-UP PLATE KEEPS BE
FLANGES IN MESH WITH
SPROCKETS

SECTION A-A.

1

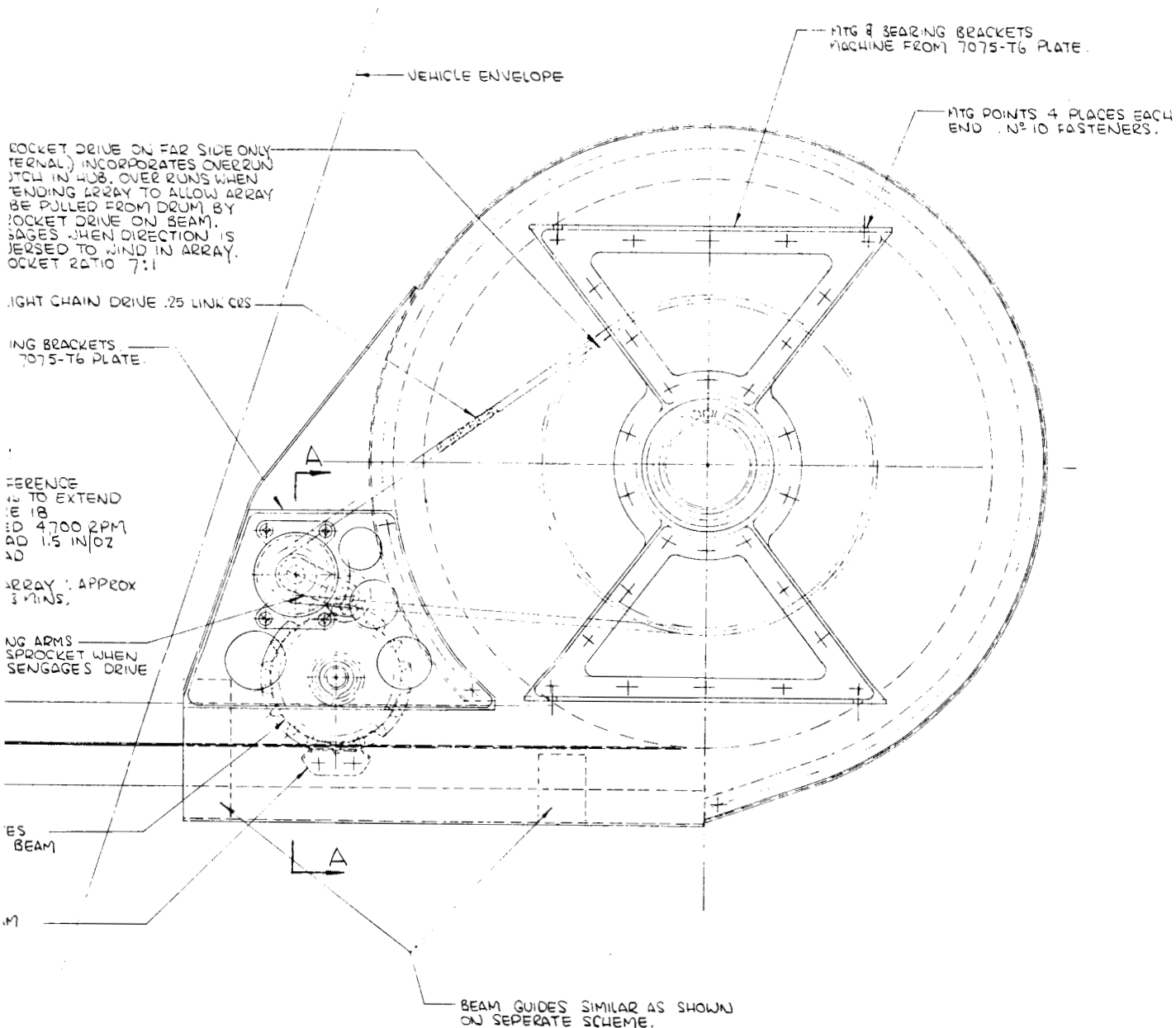


Figure 7 Sprocket Drive Mechanism

2

SPROCKET
(EXTERNAL
CLUTCH IN
EXTENDING
TO BE PULLED
DEPLOYING
ENGAGES
REVERSED
SPROCKET

LIGHT CH

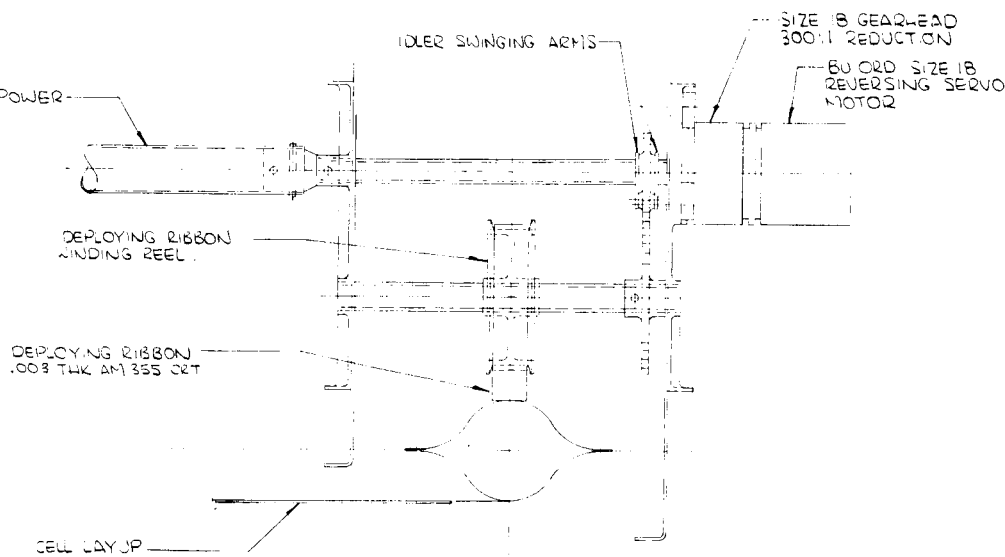
BEARING/MOUNTING BR
MACHINE FROM 7075-

IDLER GEAR ON SWINGING
ENGAGES DEPLOYING REEL
REEL WHEN DEPLOYING A
DISENGAGES REEL WHEN V
ARRAY.

DEPLOYING RIBBON WINDING
REEL

DEPLOYING RIBBON
INTER-WRAPPED WITH BEAM
PULLS OUT BEAM WHEN PULLED
FROM DRUM.

TOQUE SHAFT SUPPLIES POWER
TO OPPOSITE SIDE DRIVE
MECHANISM.



SECTION A-A.

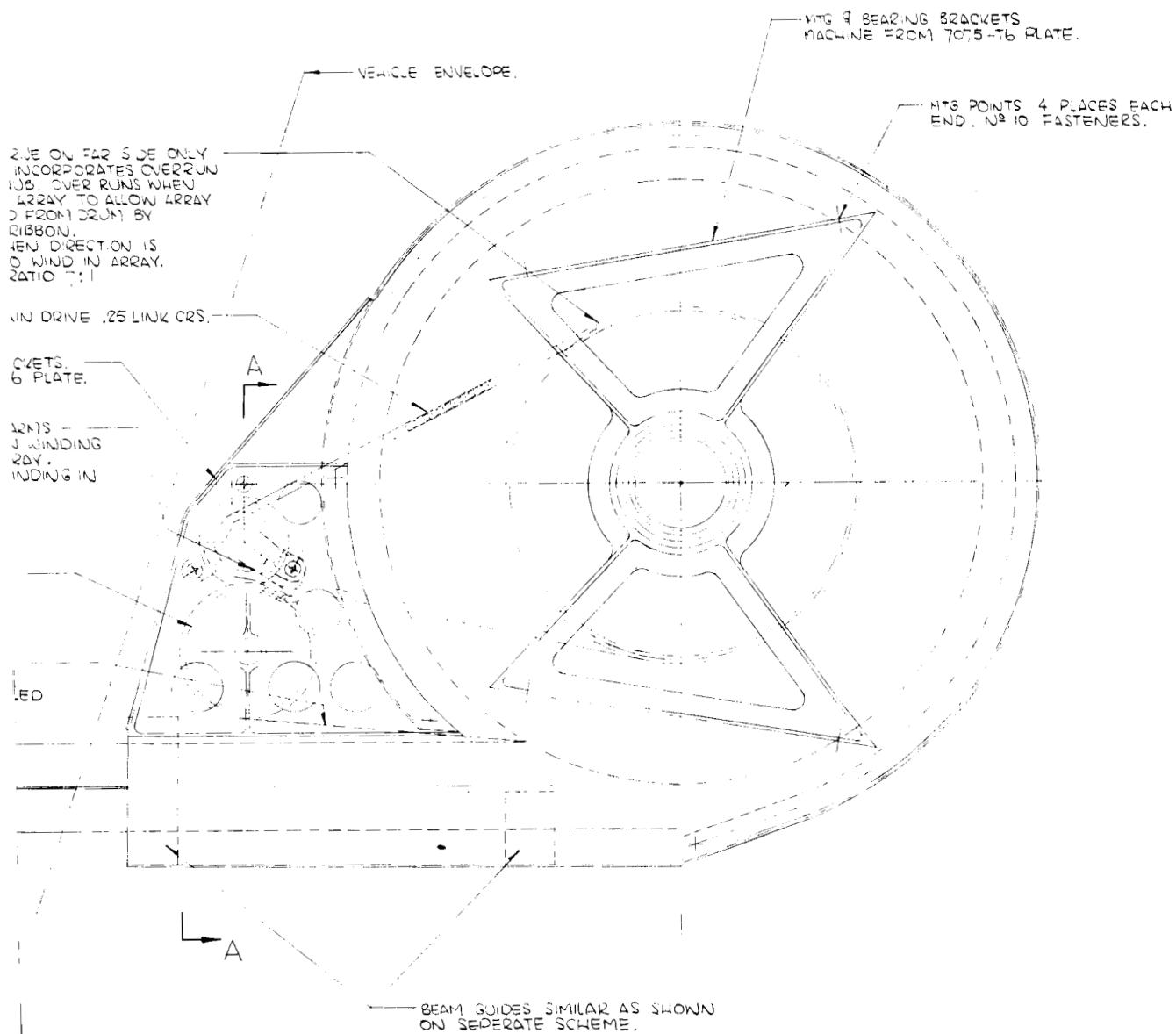
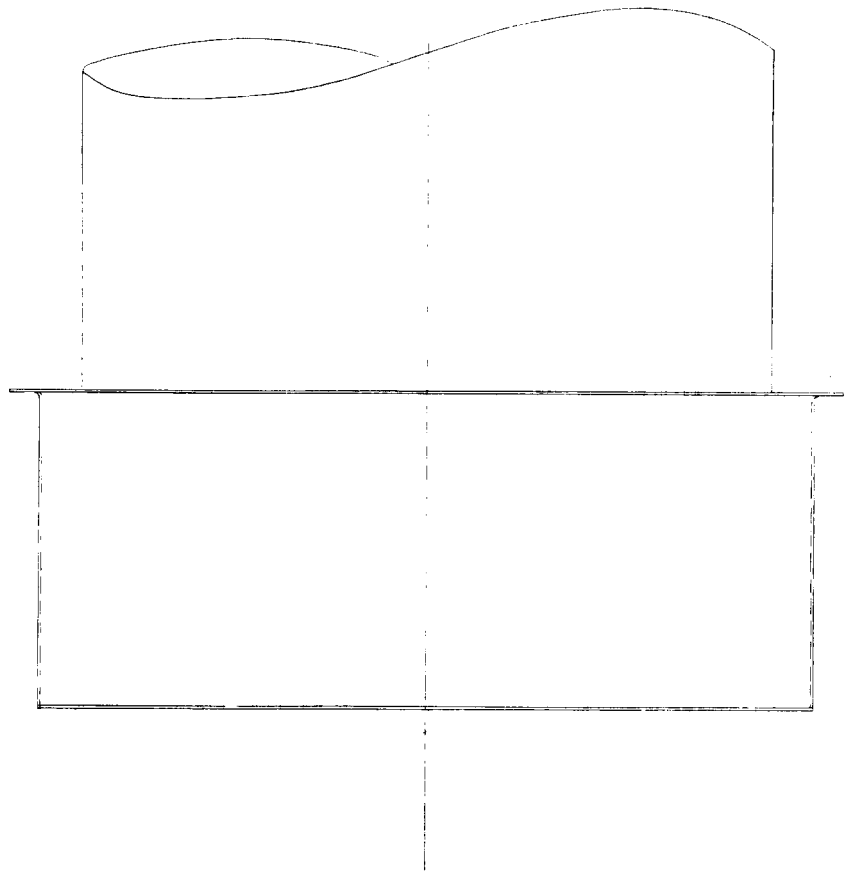
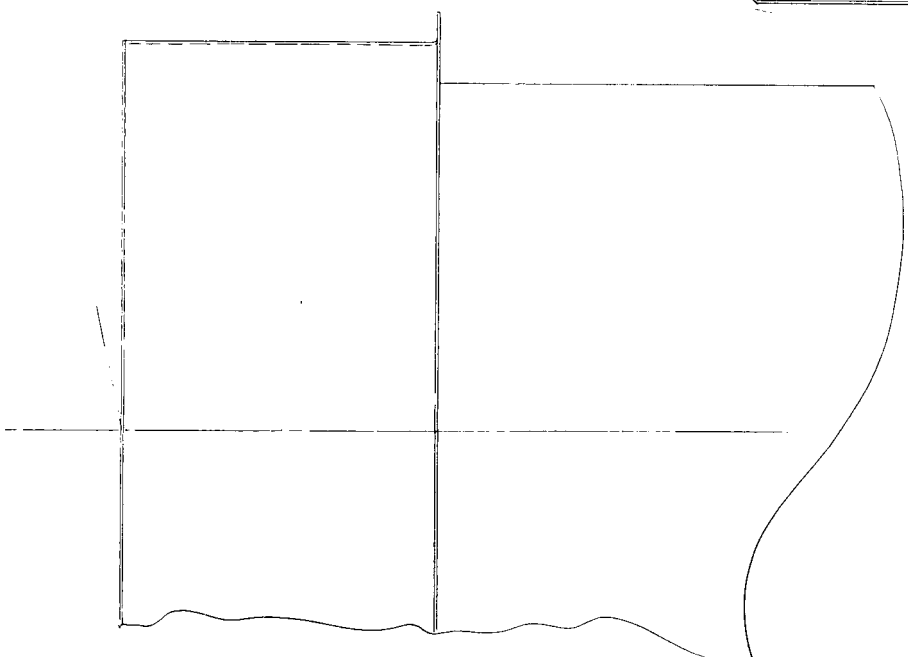
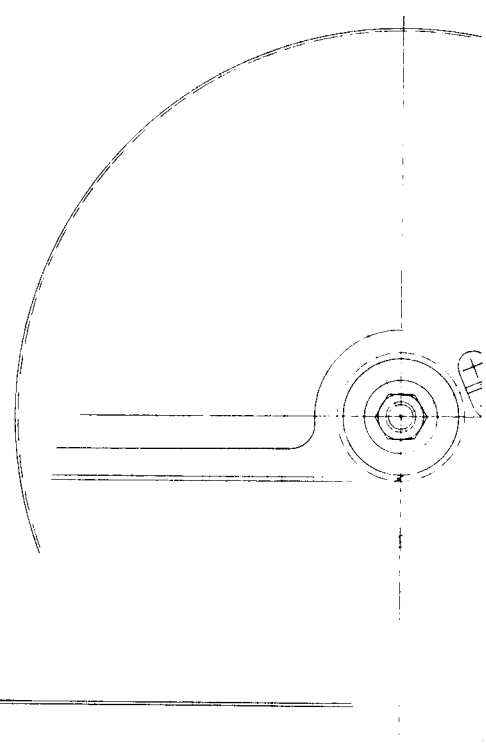
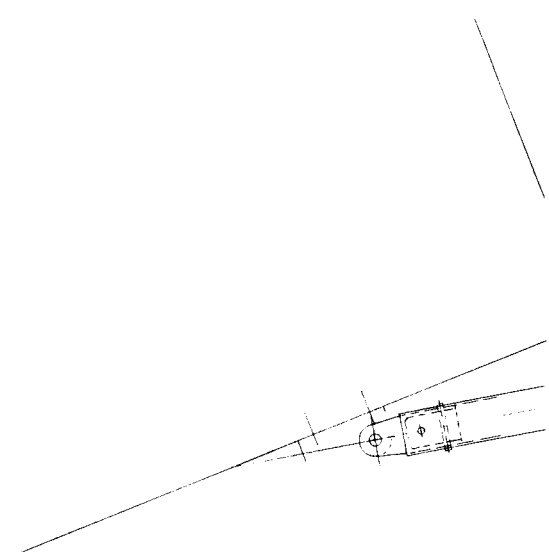
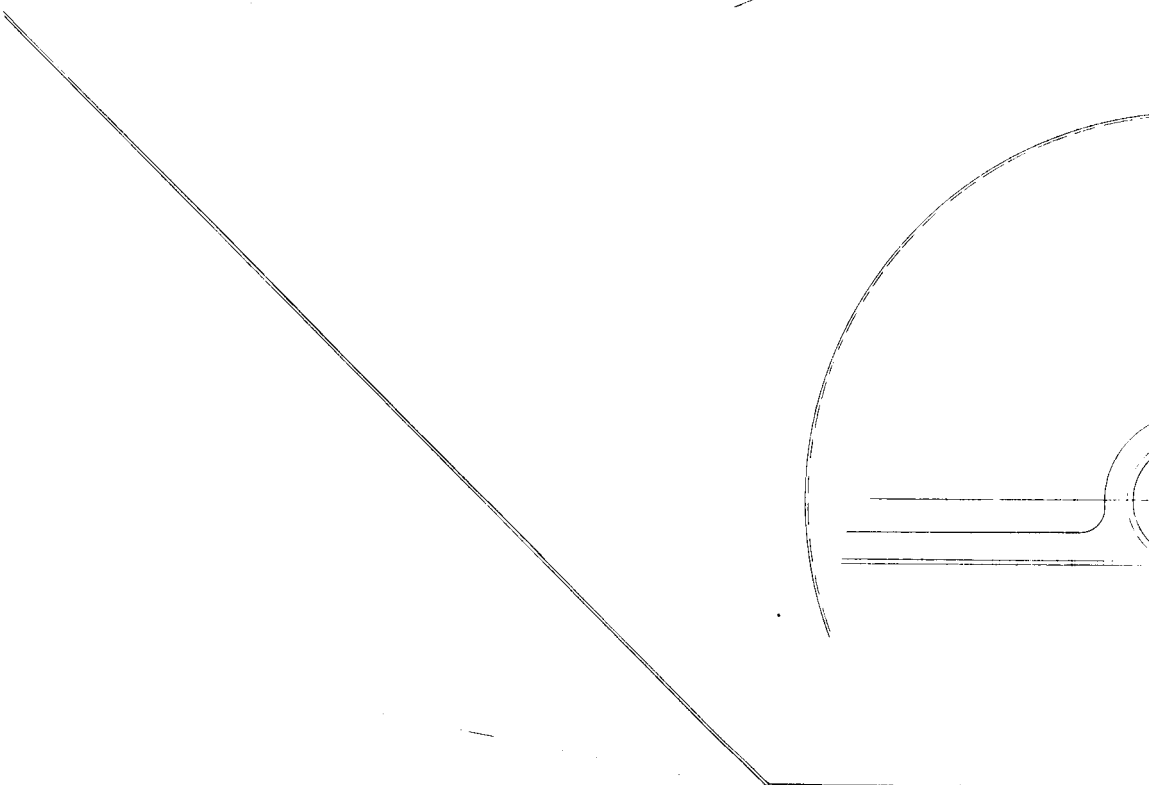


Figure 8 Deploying Ribbon Drive

2





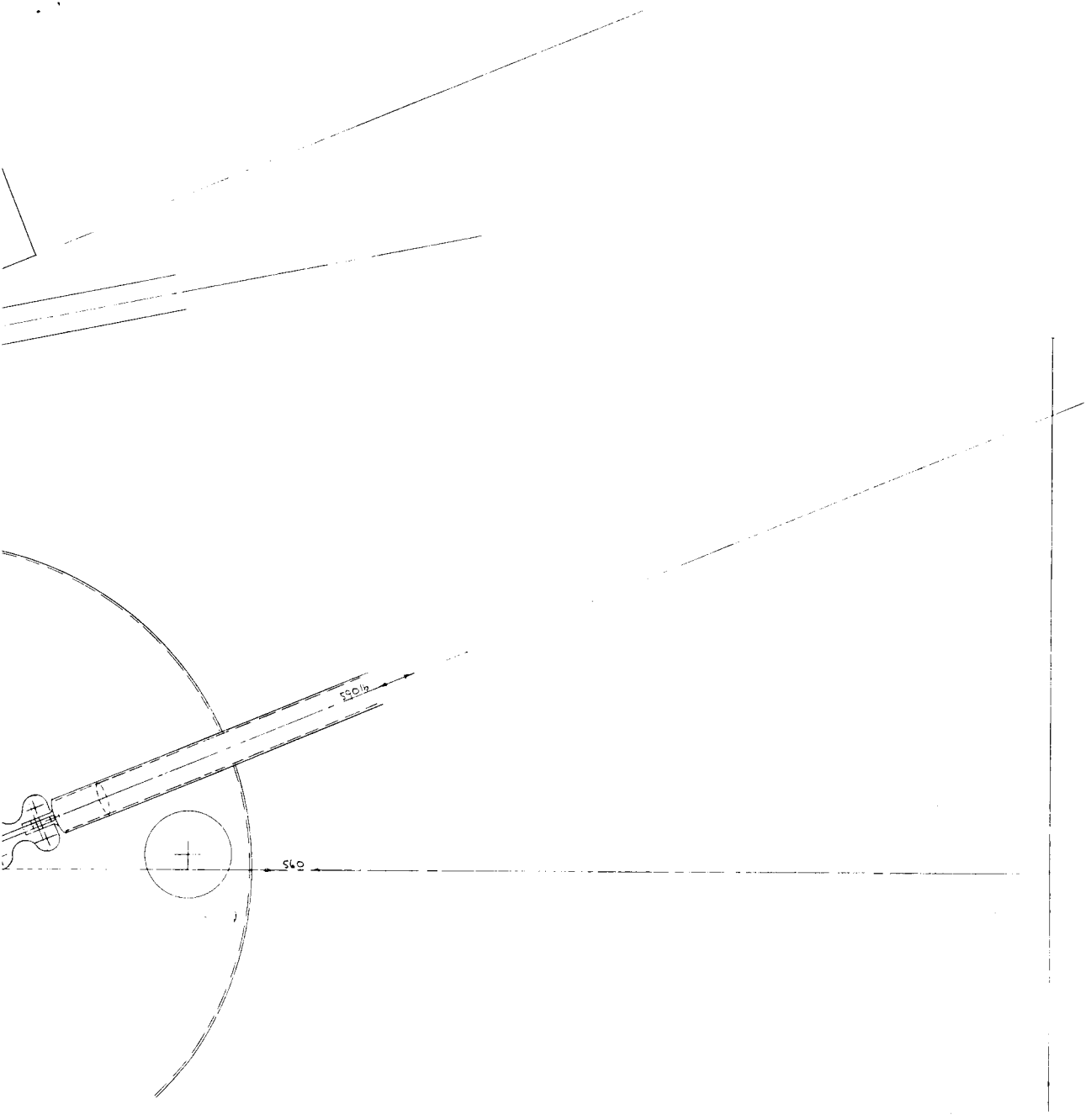
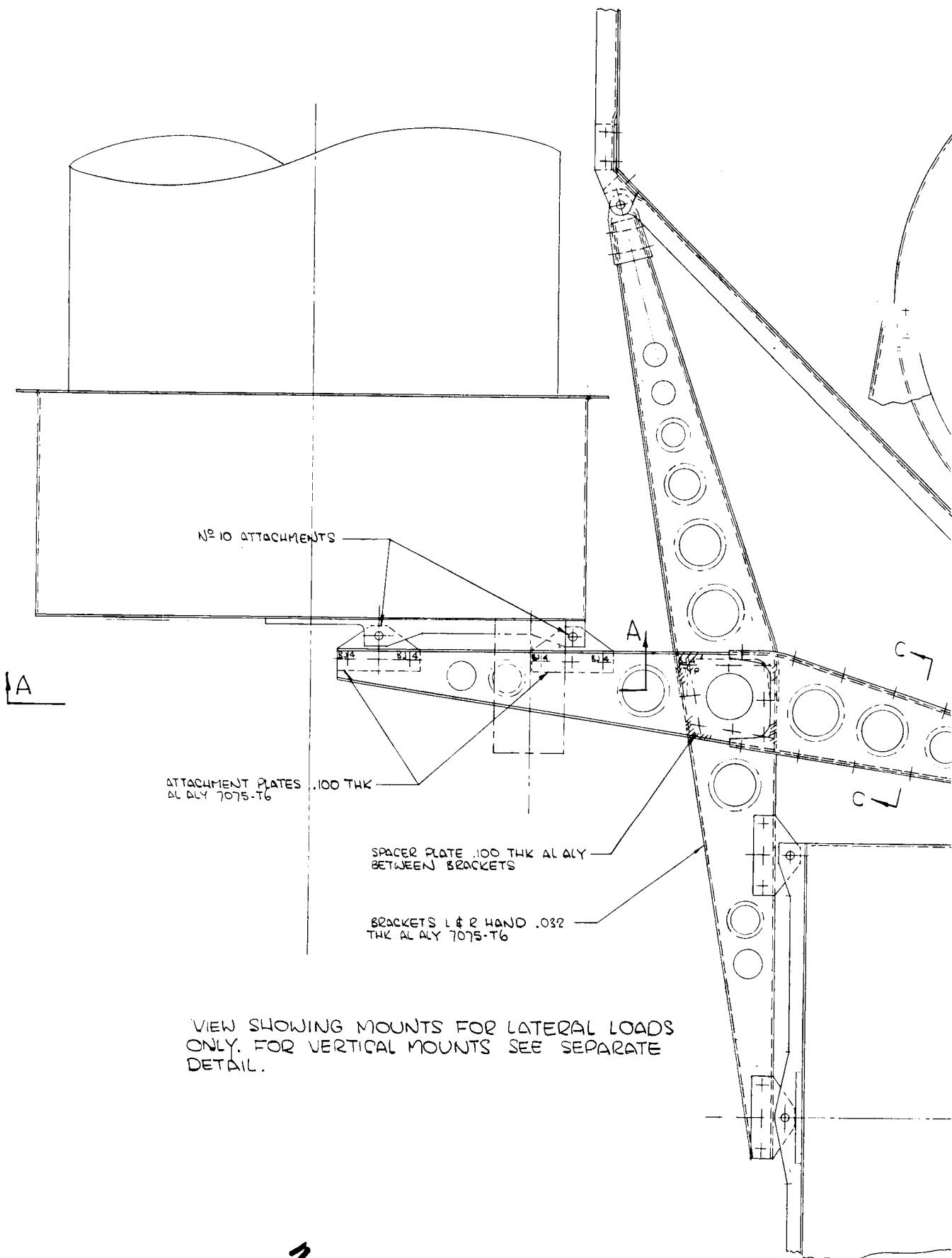
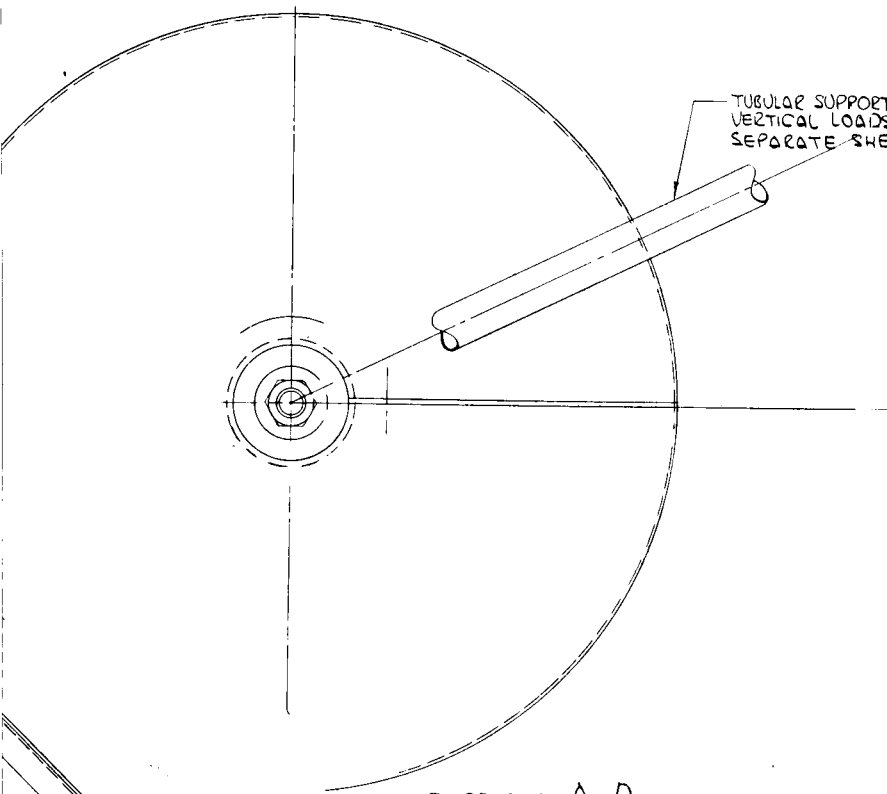
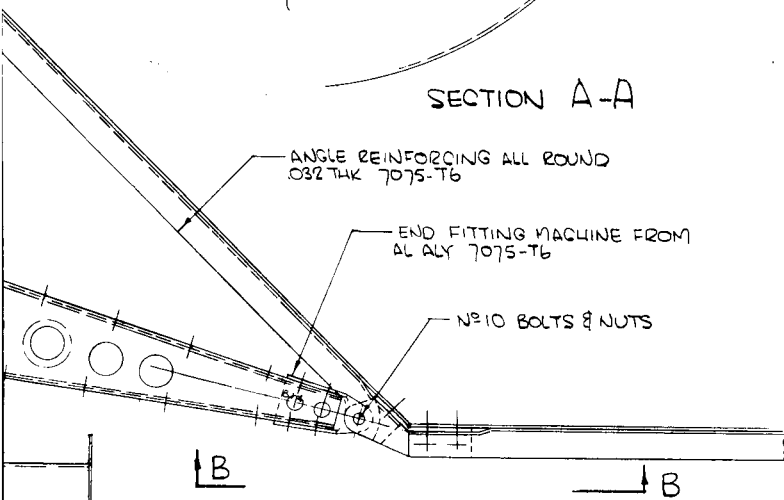


Figure 9 Attachment to Vehicle - Cross and Tubes

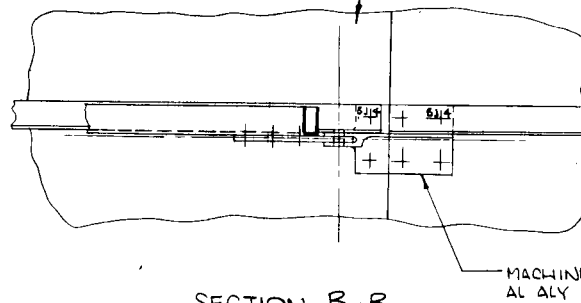




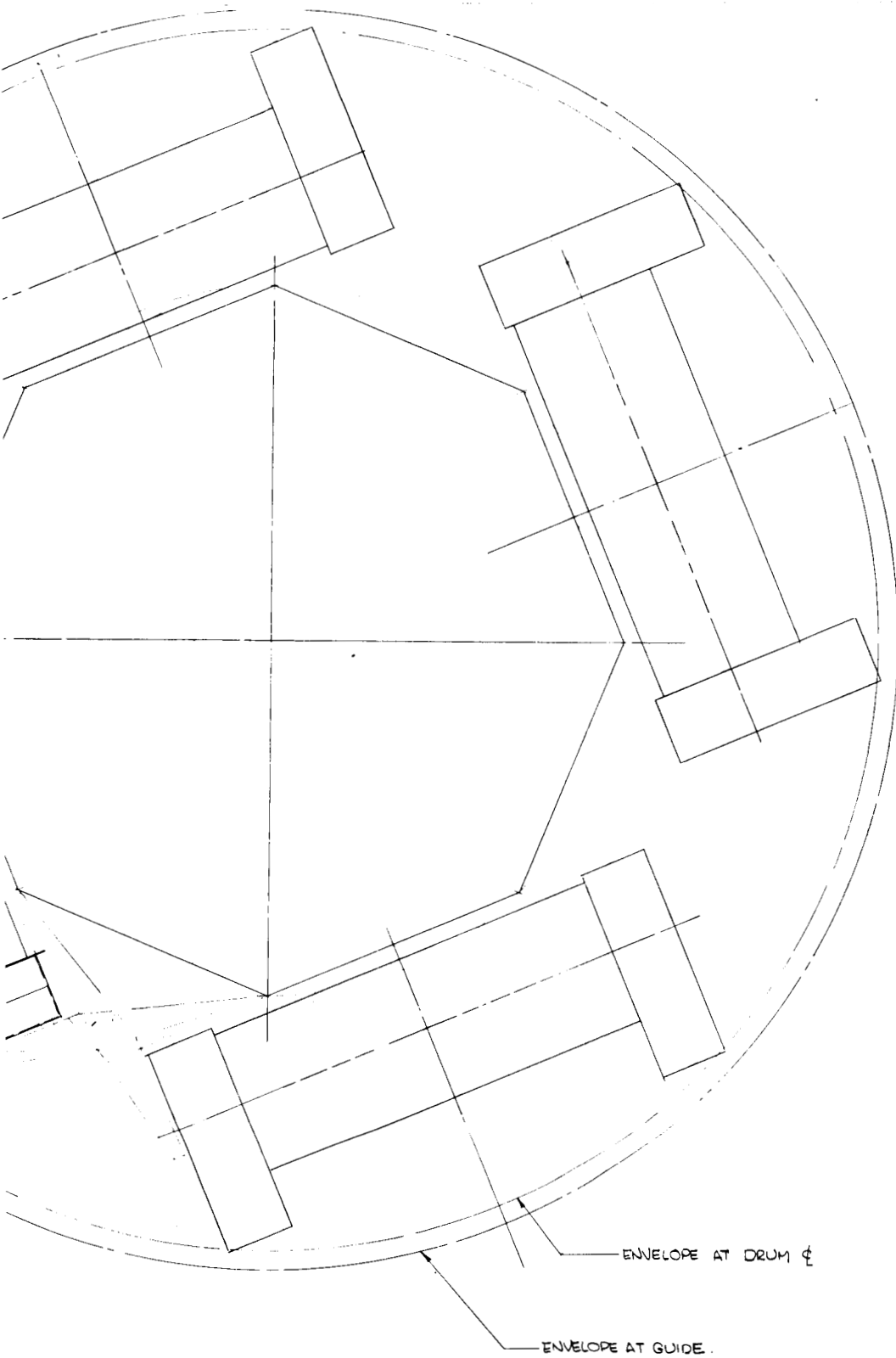
SECTION A-A



VEHICLE OCTAGONAL BODY

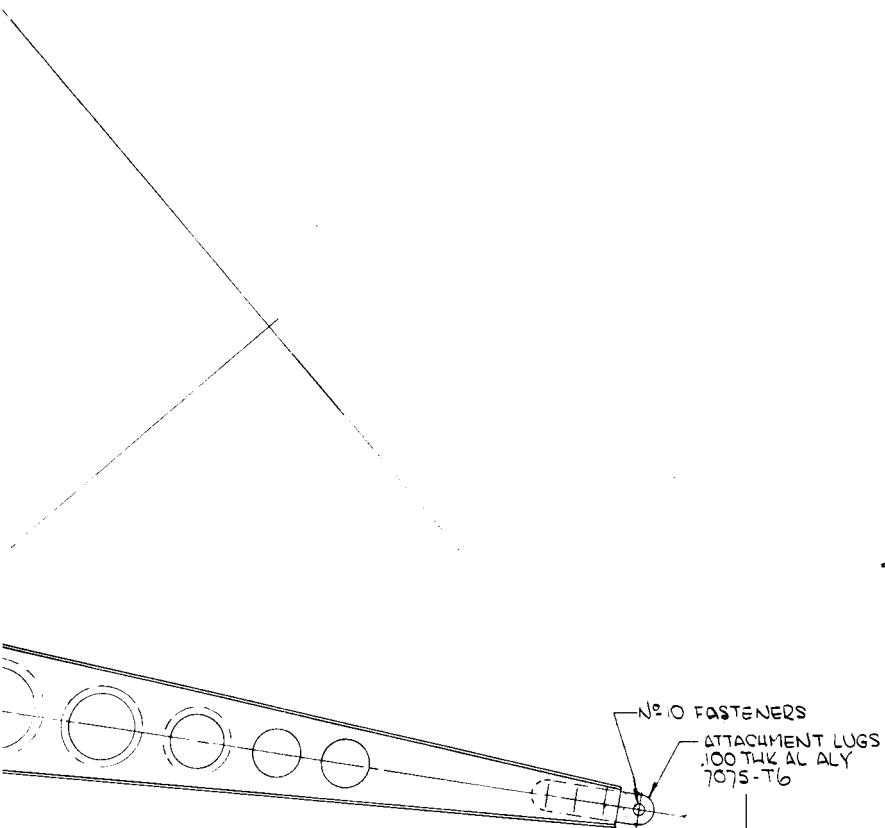


SECTION B-B



FITTING
15-T651

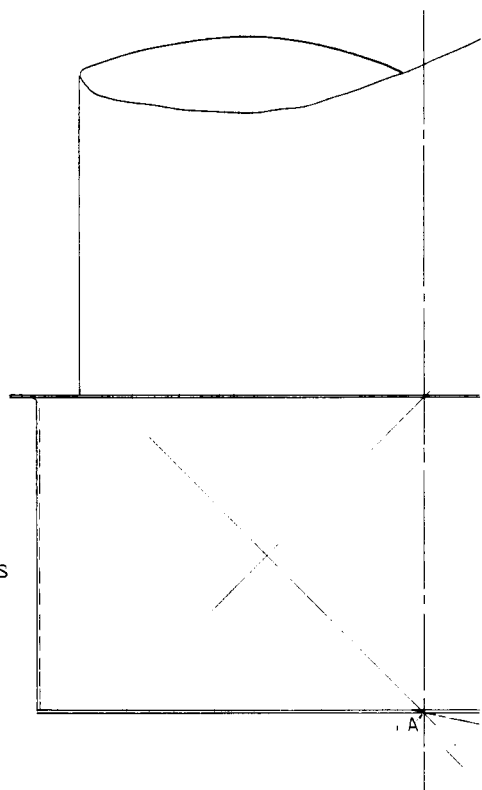
Figure 10 Vehicle Mounts - Rollout Array



SPACER (SHADED) .100 THK
AL ALY 7075-T6

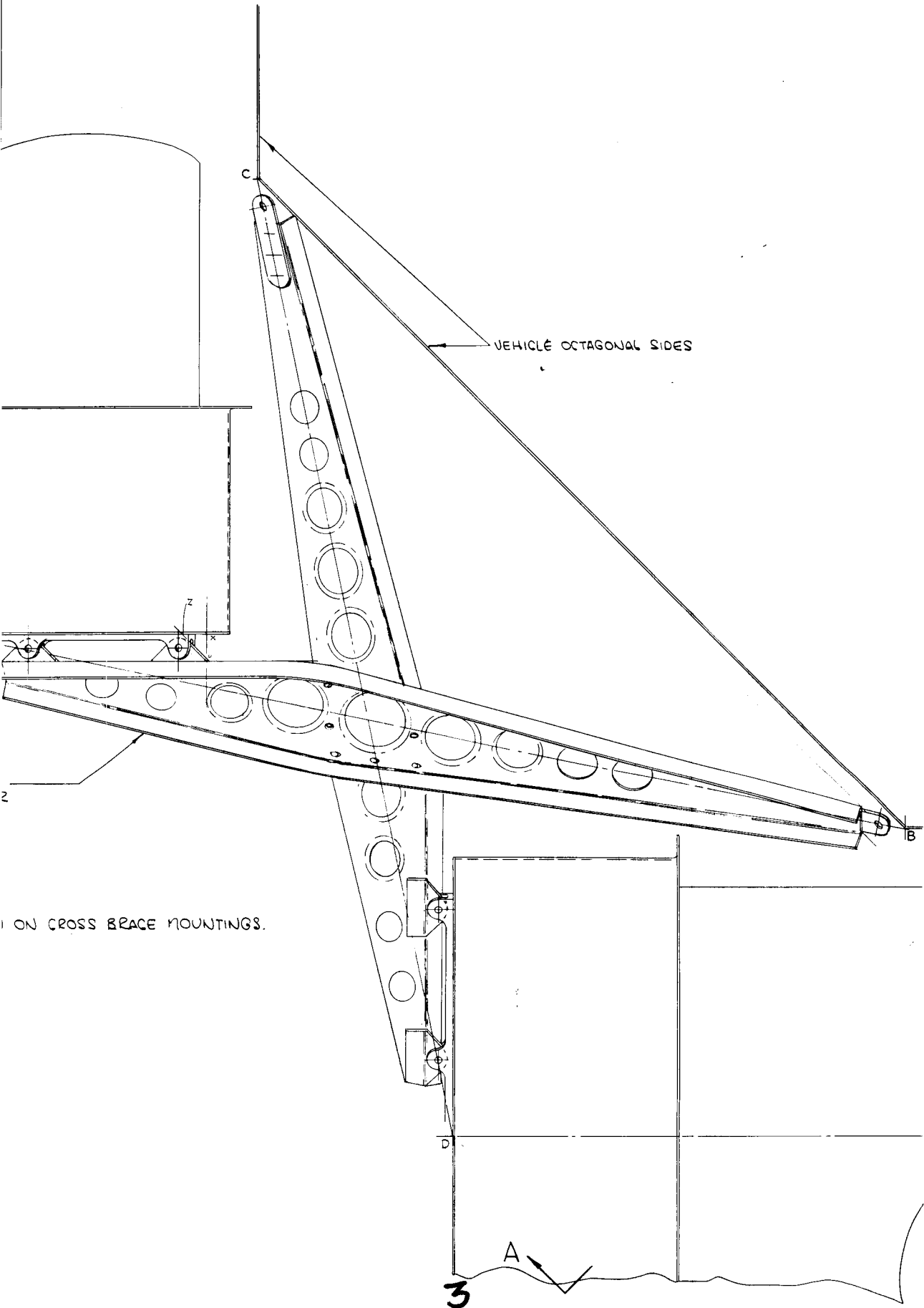
.50 FLANGE
TYP

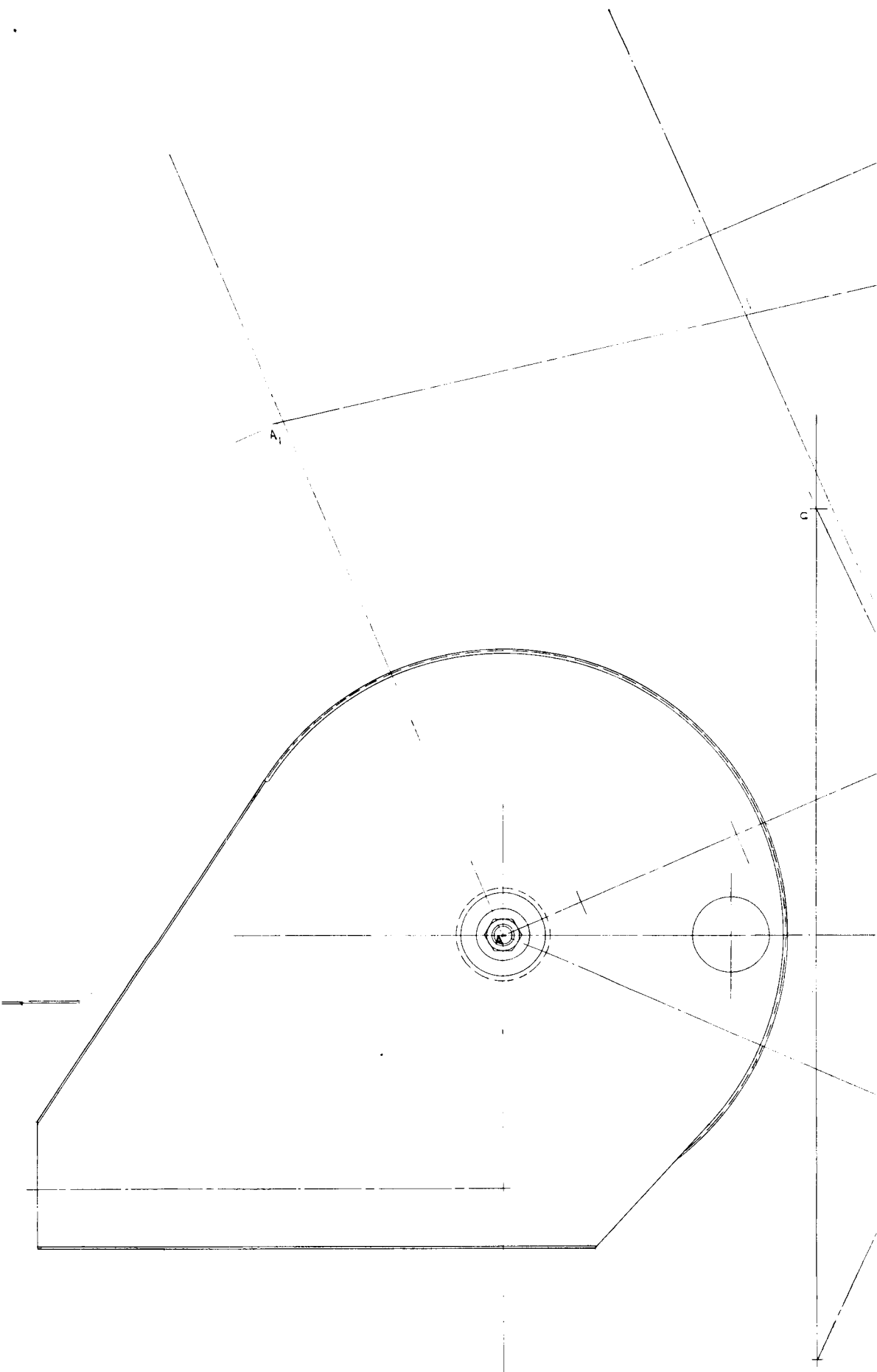
SECTION A-A



UPPER CROSS BRACE SHOWN
LOWER CROSS BRACE SIMILAR
BUT OPPOSITE HAND.

PLAN VIEW





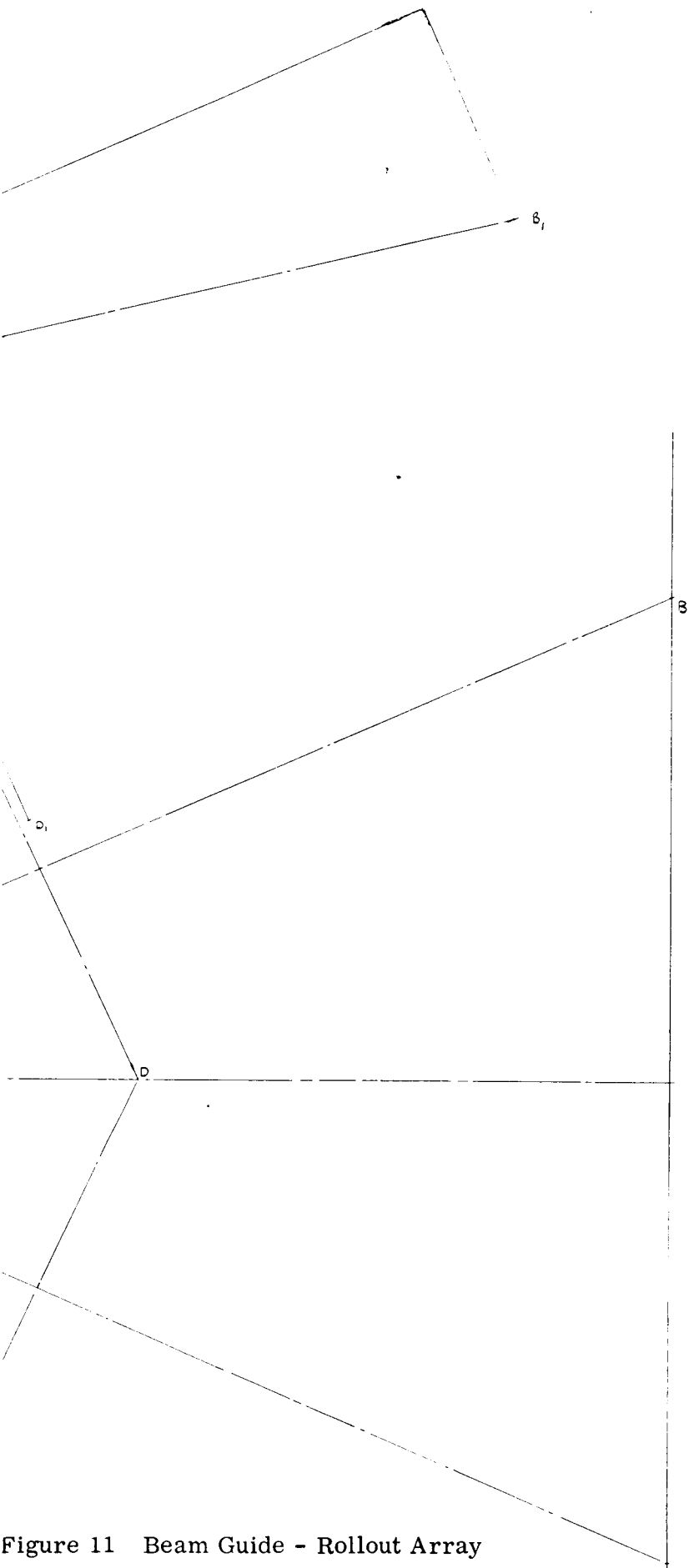
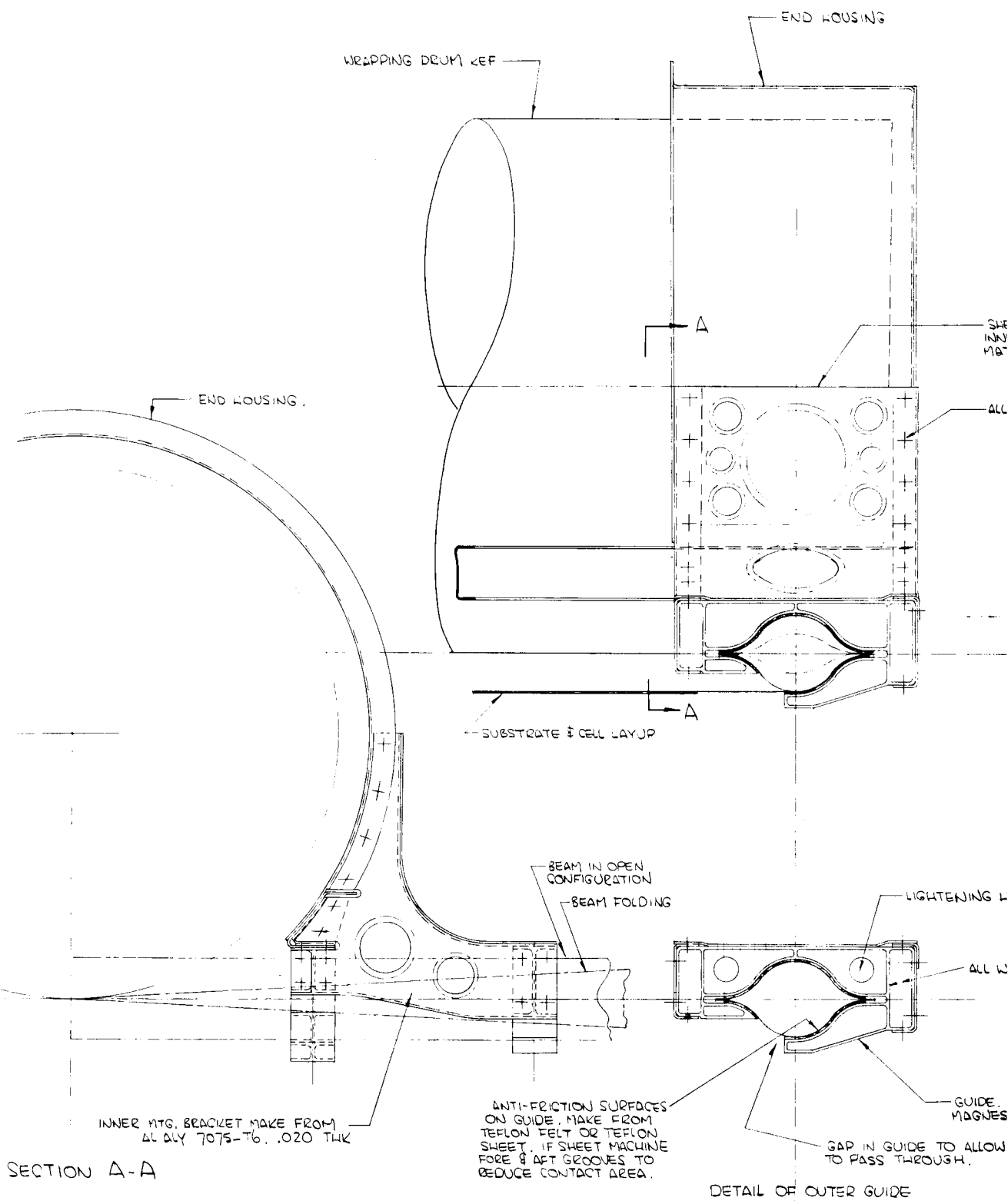
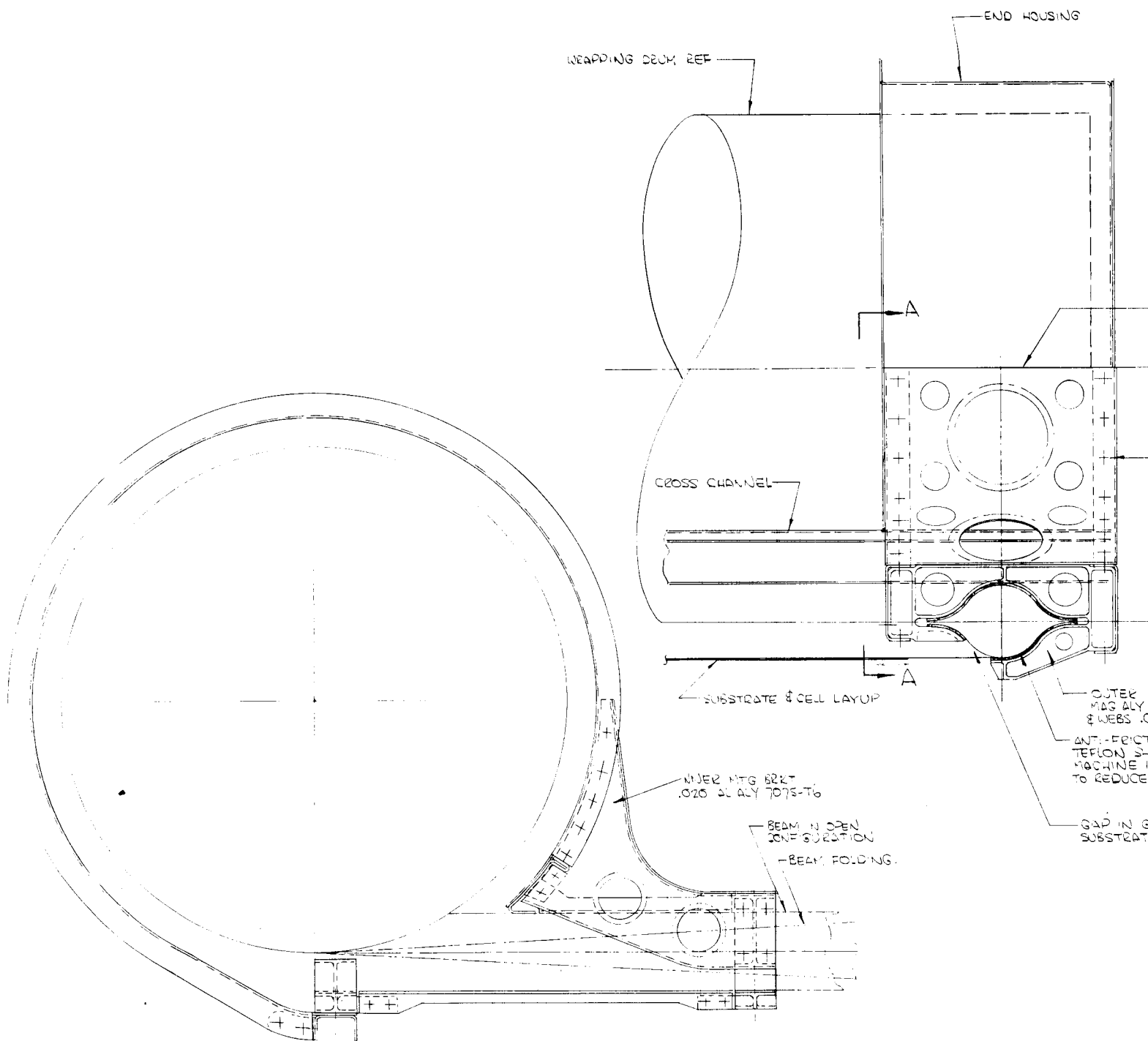


Figure 11 Beam Guide - Rollout Array





SECTION A-A

7

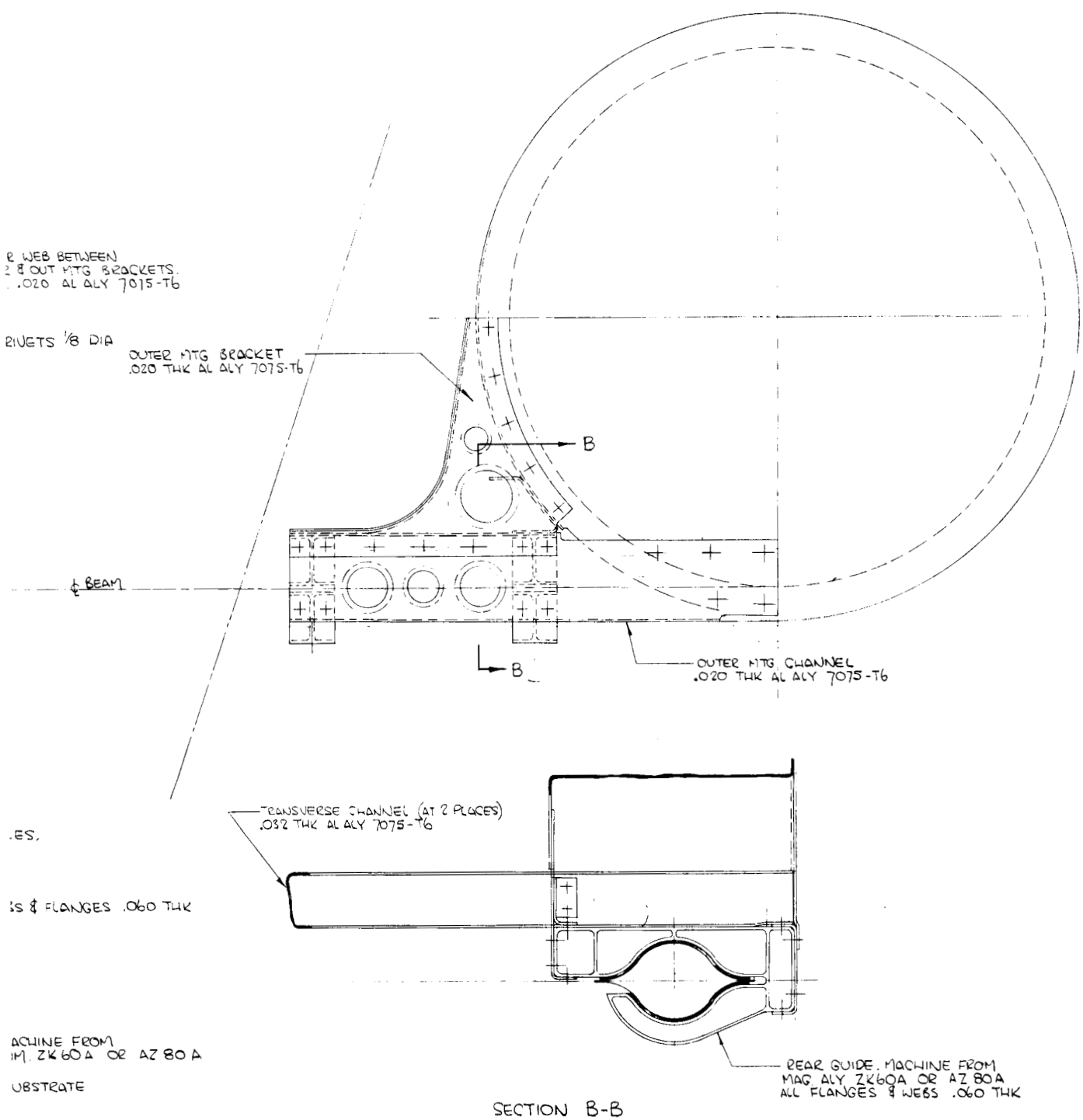


Figure 12 Beam Supports and Guides - Scheme 1

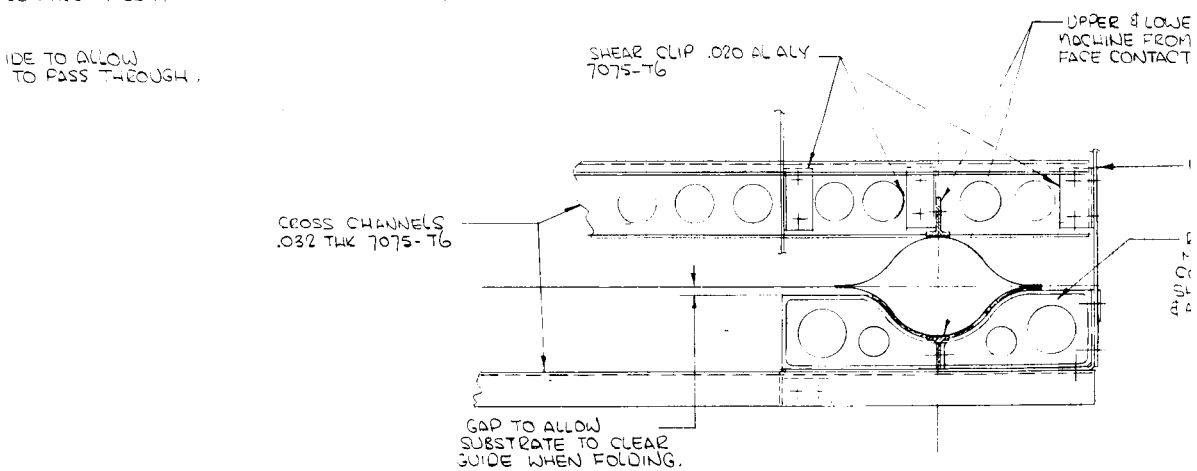
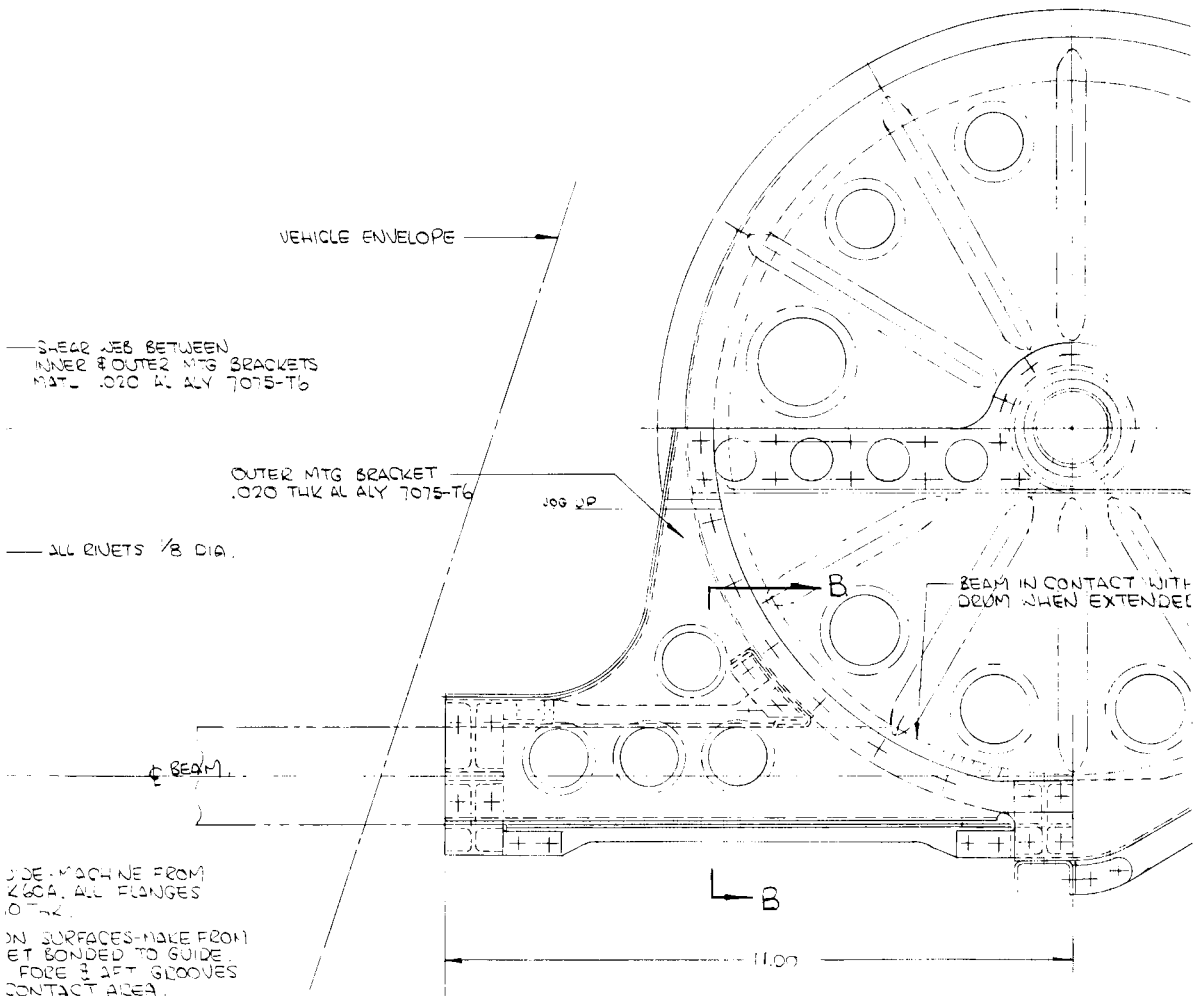
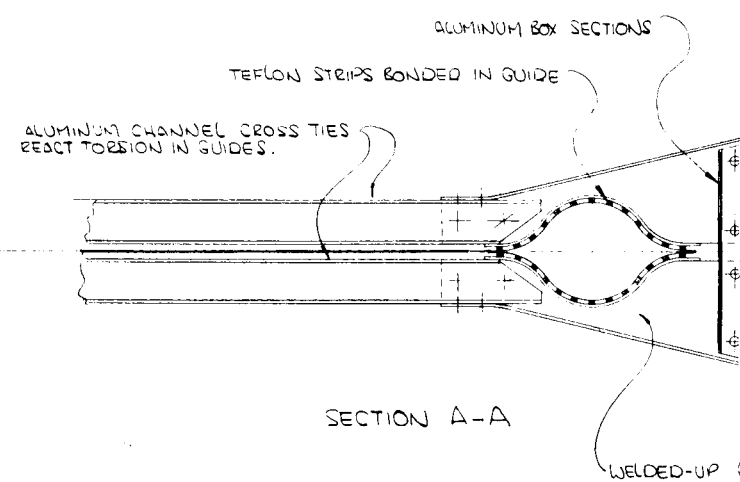
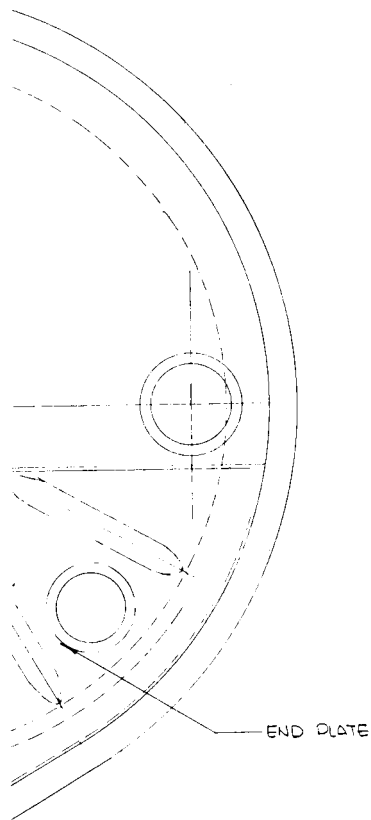


Figure 13 Beam Supports





2 GUIDES
MAG ALLOY ZK60A
AREA WITH TEFLON.

END PLATE

REAR GUIDE MACHINE FROM
MAG ALLOY ZK 60A. FACE
CONTACT AREA WITH TEFLON
REAR. MACHINE GROOVES FOR
FIT TO REDUCE FRICTION AREA.

and Guides - Scheme 2

3

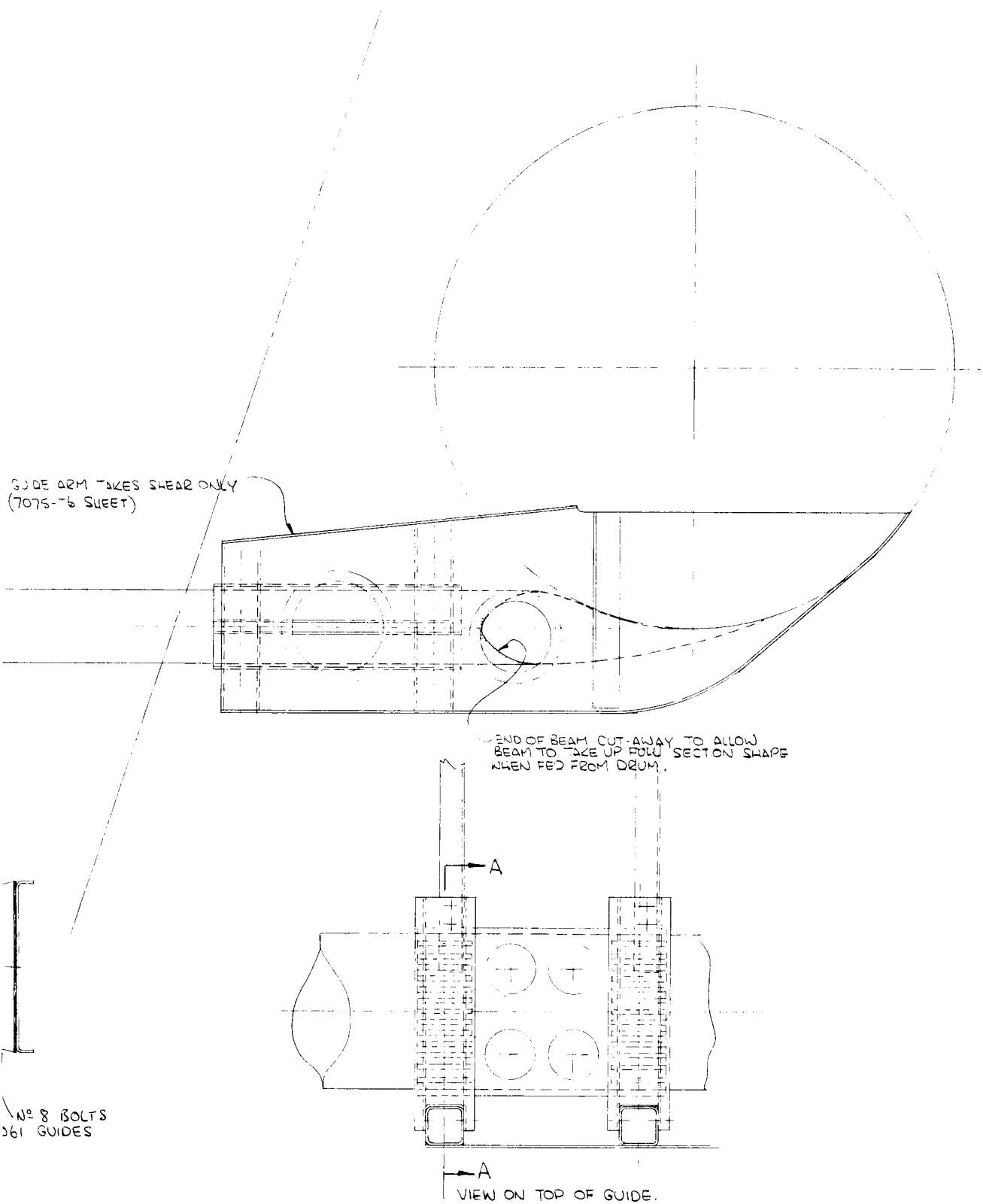
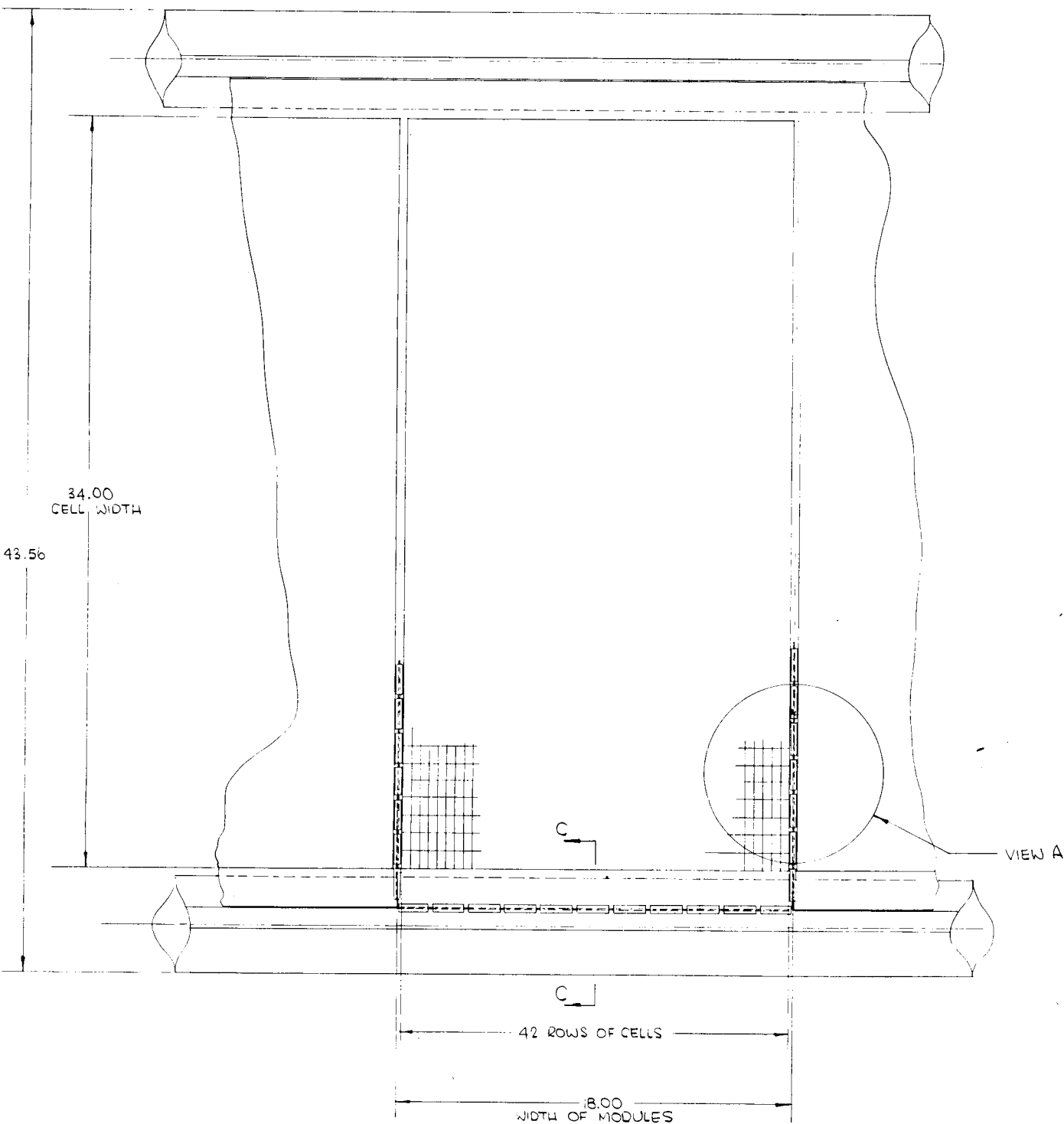


Figure 14 Alternate Beam Guide

2



PARTIAL VIEW ON EXTENDED PANEL ,
SCALE $\frac{1}{2}$

1

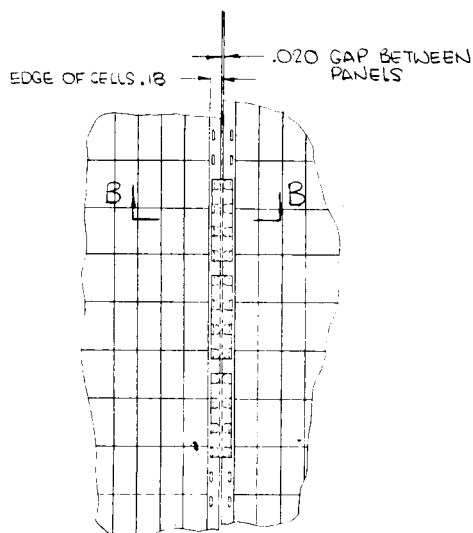
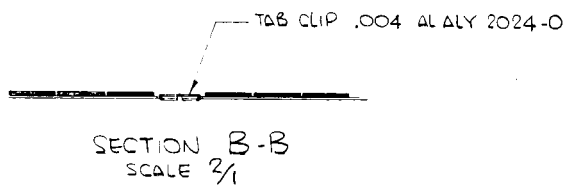
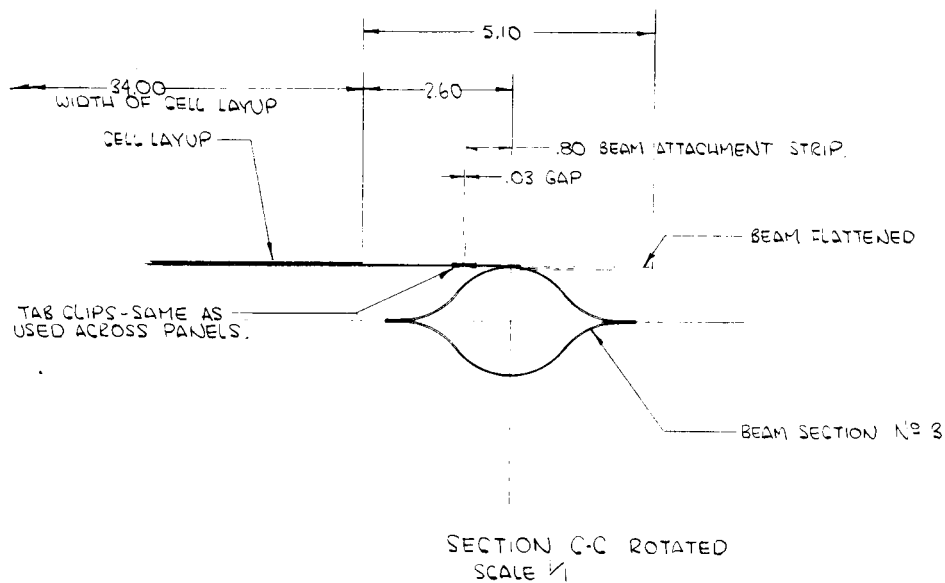
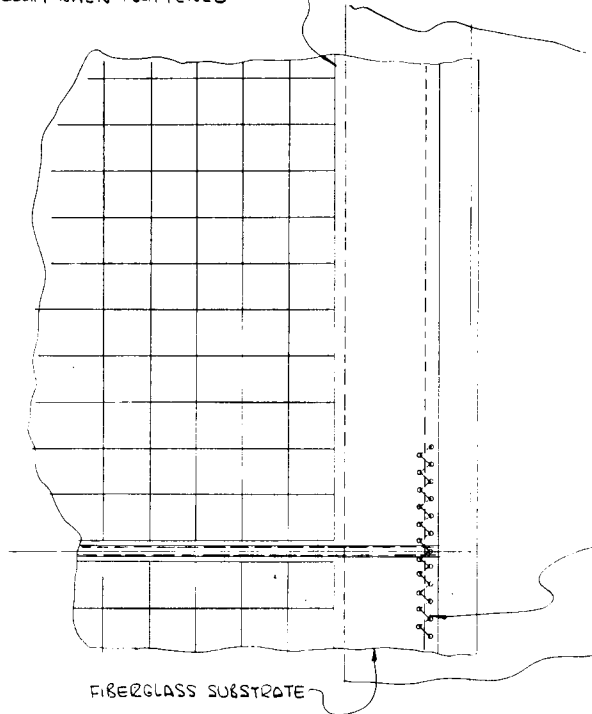


Figure 15 Substrate Attachments - Rollout

CELLS SET BACK TO CLEAR
BEAM WHEN FLATTENED



FIBERGLASS SUBSTRATE

SUBSTRATE LACED TO ATTACHMENT
STRIP WITH NYLON MONOFILAMENT.

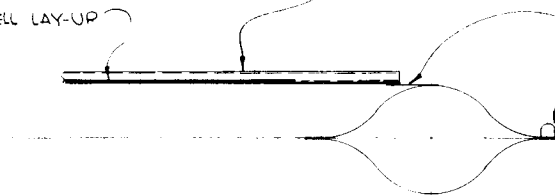
CELL LAYUP

SECTION

BE
FL

ALUMINUM TUBE STIFFENERS
MOLDED INTO SUBSTRATE

CELL LAY-UP



.005 THK TITANIUM 6AL4VA
ATTACHMENT STRIP SEAM
WELDED TO BEAM.

SPACERS TO COMPENSATE
FOR SUBSTRATE & BEAMS.

7

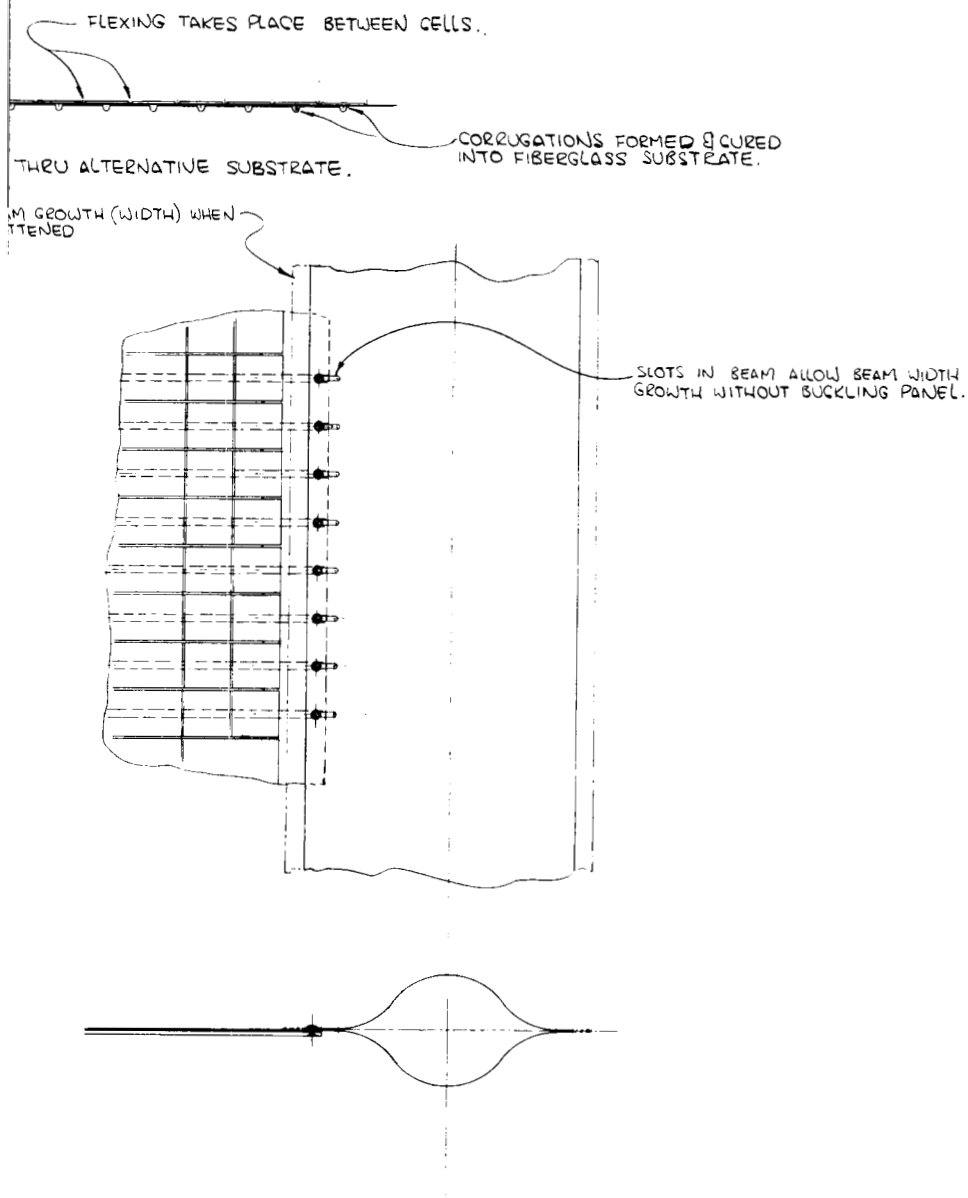
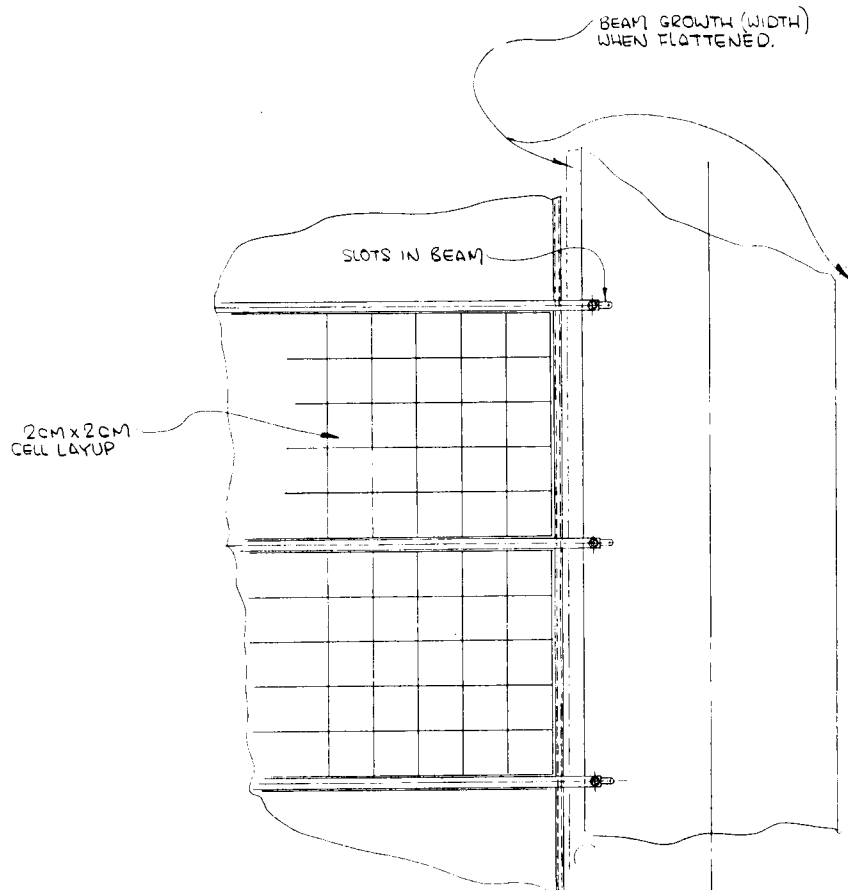


Figure 16 Substrate Attachments - Beam

2



2cm:
LAYU

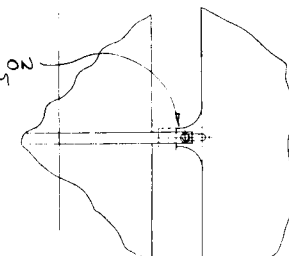
FIBERGLASS MOULDED PANEL WITH INTEGRAL MOULDED-IN CROSS STIFFENERS & EDGE BEADING.

SPACERS COMPENSATE FOR THICKNESS OF PANEL.

SLOT IN STIFFENER ALLOWS BEAM TO GROW WHEN FLATTENED.

TAB ON BEAM

METHOD 1.



ALTERNATIVE METHOD OF SLOTTING. (THIS INCREASES OVERALL WIDTH OF OF PANEL BY .90)

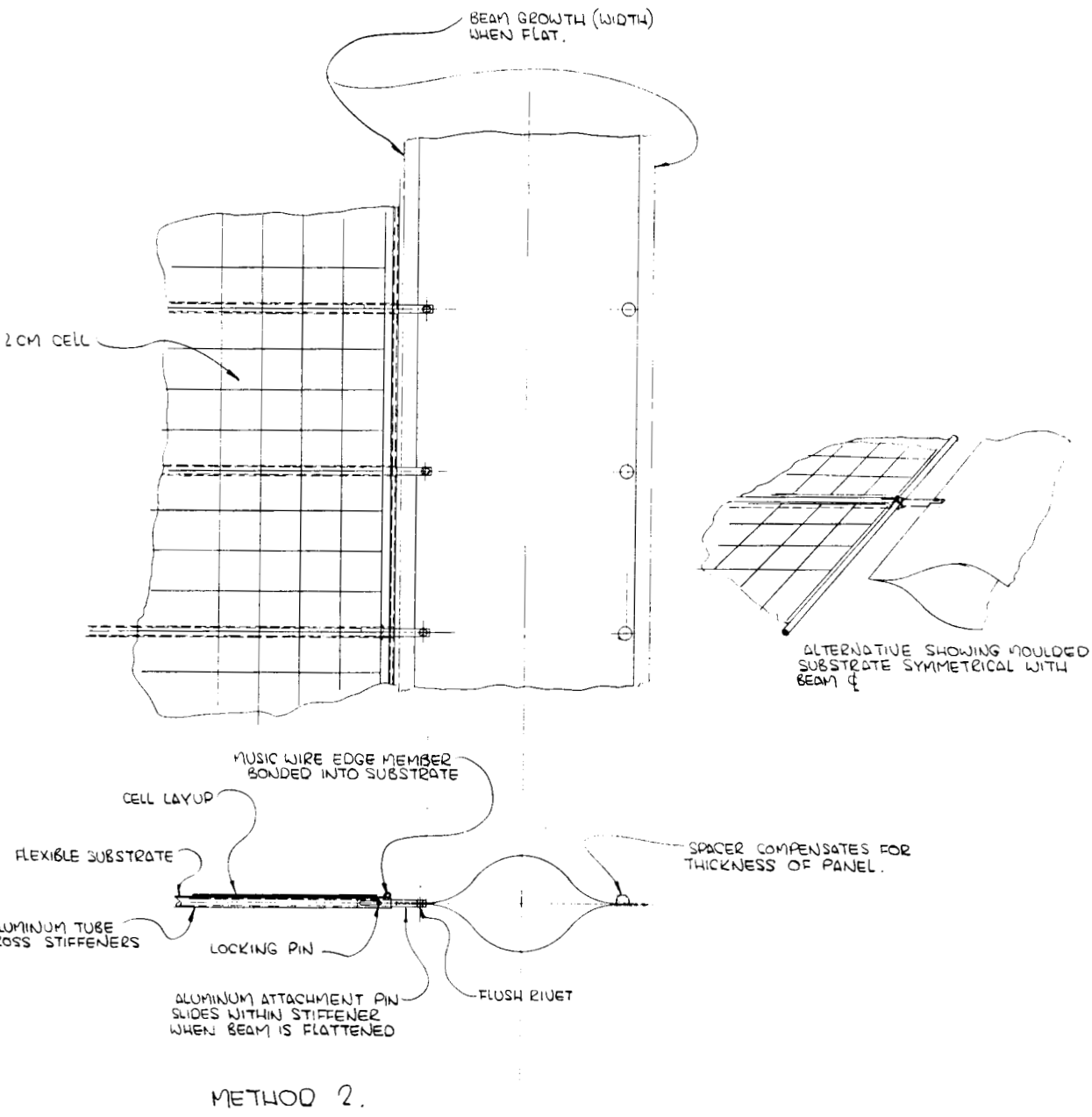
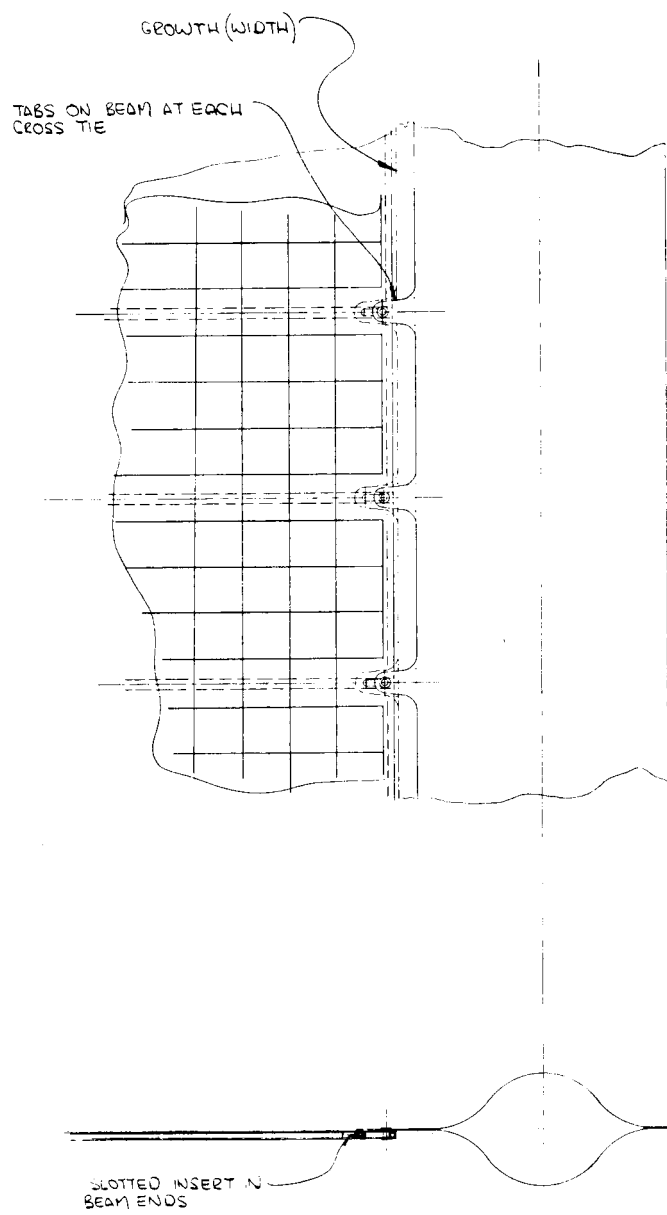


Figure 17 Panel Attachment to Beams

2



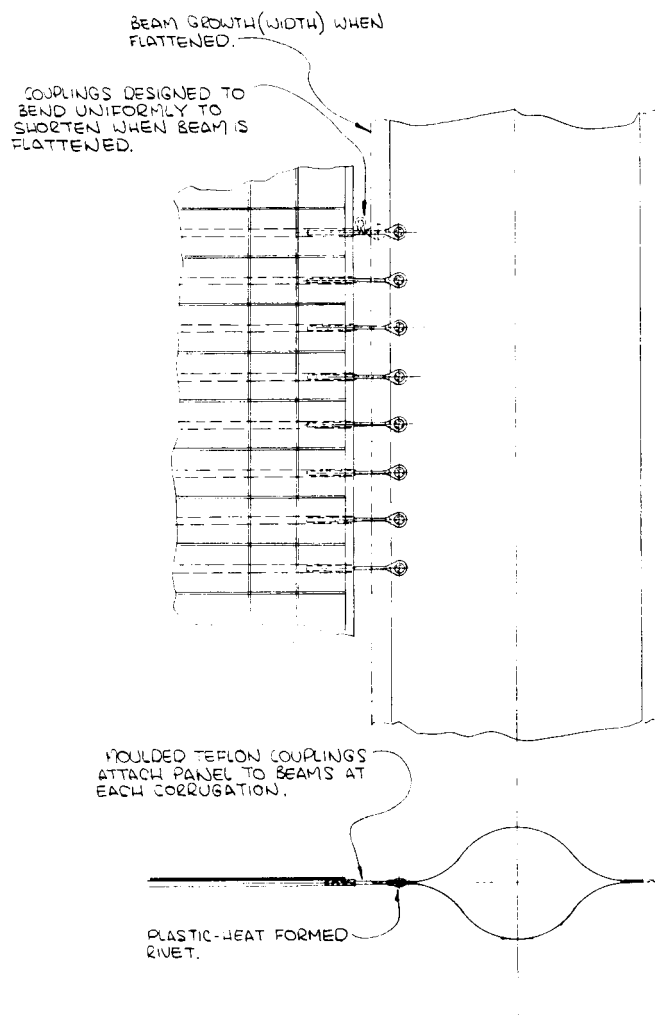
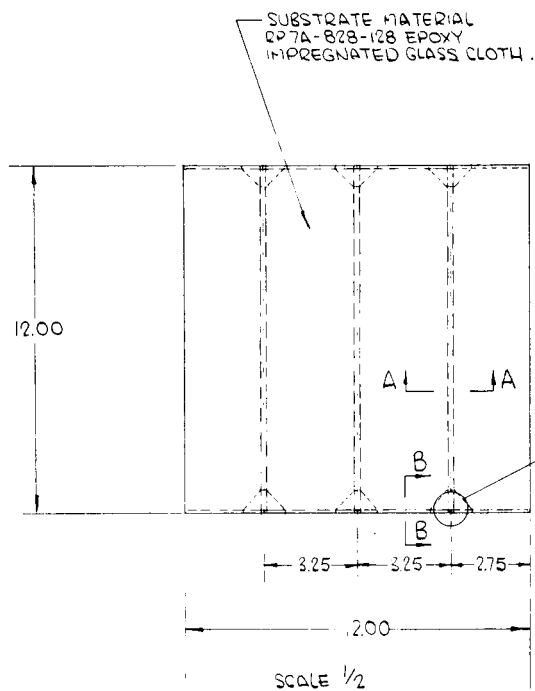
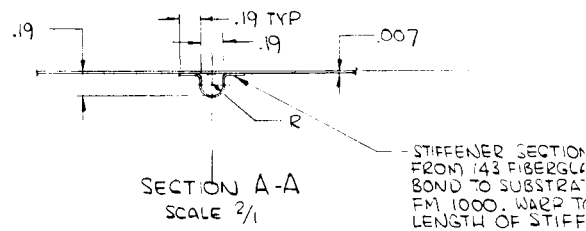


Figure 18 Detail of Beam Attachment



SAMPLE N^o 1.



.10 DIA SOLID FIBERGLASS
ROD BONDED TO
SUBSTRATE.

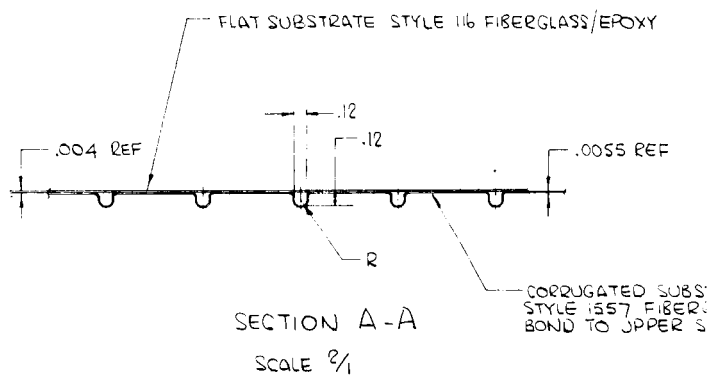
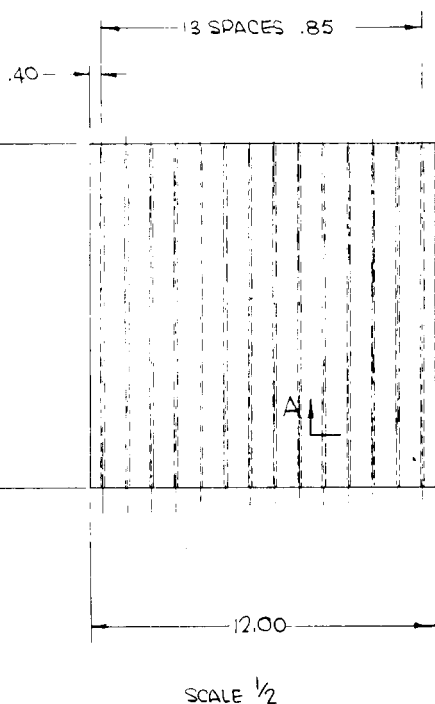
DETAIL 'C'

SECTION B-B
SCALE $\frac{2}{1}$

FIBERGLASS GUSSET-SAME
MATERIAL AS SUBSTRATE. BOND
TO PANEL

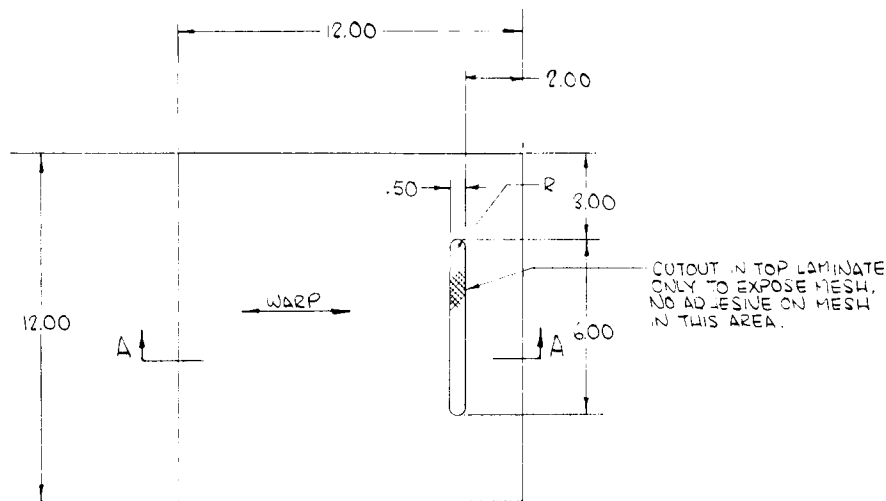
EDGE MEMBER IS
CONTINUOUS

DETAIL 'C' REVERSED
SCALE $\frac{2}{1}$

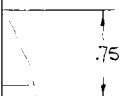


SAMPLE N^o 2

FORMED
SS/IEPOXY
E WITH
RUN
NER.



SCALE 1/2



TYP 6 PLCS

EXPANDED SILVER MESH
2 AG 7-2/0E FLATTENED
& ANNEALED.
BOND MESH TO OUTER SHEETS
USING FM 1000 .002 THK
BOND AT 50 PSI MIN.

2 LAYERS TYPE 108 GLASS CLOTH
EPOXY SHEET BOND WITH EPON
828-DION RP7A



SECTION A-A (NO SCALE)

- 1 AS SHOWN
- 3 SAME AS -1 EXCEPT USE 116 GLASS CLOTH

SAMPLE 3.

RATE
GLASS/EPOXY
SHEET AFTER

Figure 19 Substrate Samples

2

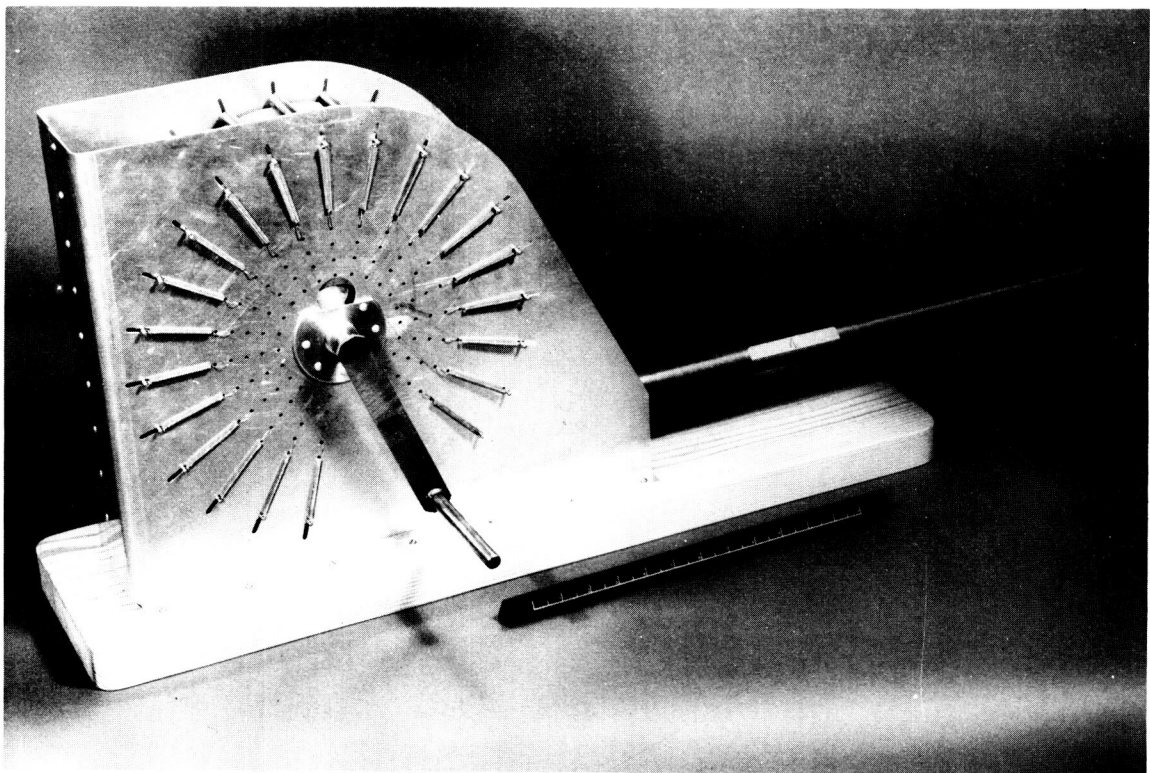


Figure 20 Mockup of Rollout Drum

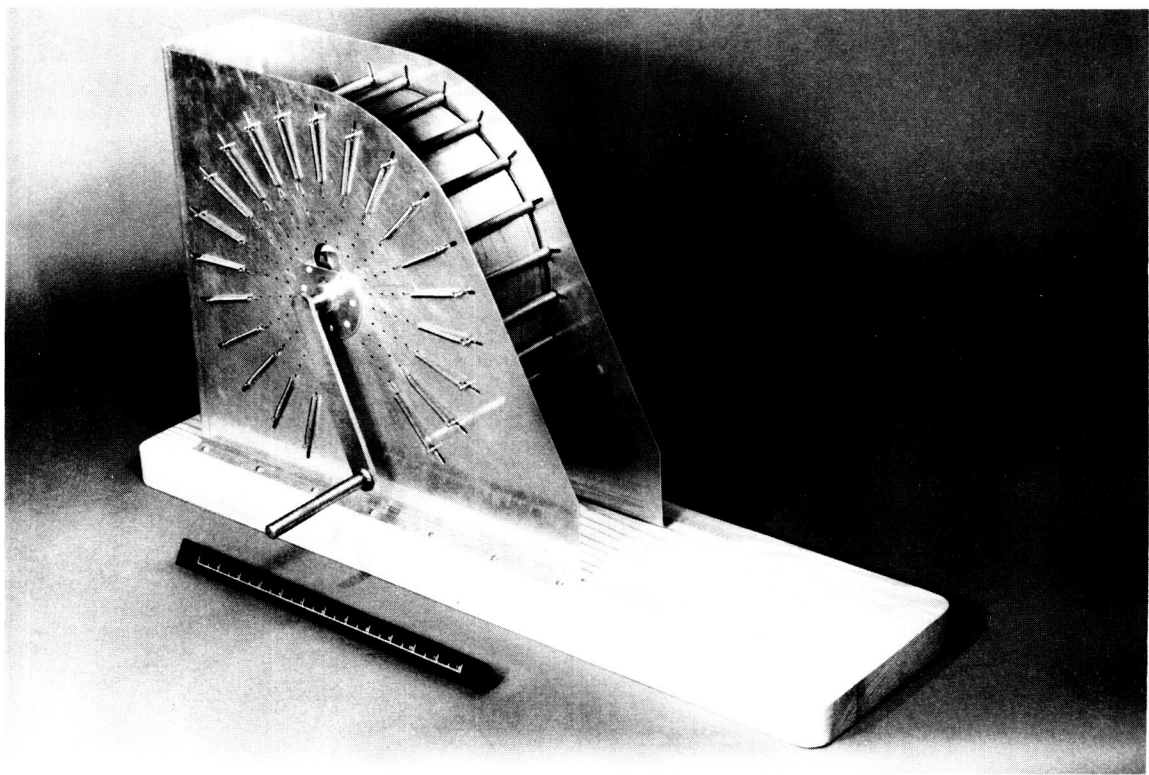


Figure 21 Mockup Rollout Drum

4.0 DESIGN CRITERIA

The design criteria utilized in the preliminary design and analysis of the Deployable Large Area Solar Array Structure are taken in whole from the data and information presented in the Statement of Work of the pertinent contract.

4.1 CONFIGURATION DESIGN CRITERIA

1. No provisions shall be required on the array structure to support unrelated spacecraft components such as power regulating zener diodes, cold gas attitude control systems, and/or vernier solar pressure vanes.
2. During the launch phase, the array structure shall remain within the envelope shown on JPL Drawing No. J-4190680 (Sheet 1). This drawing reflects the available packaging regions for a broad range of typical Mariner spacecraft systems under study for use in the 1969-197X era. The drawing depicts a standard Surveyor class shroud on an Atlas-Centaur vehicle. The spacecraft is arbitrarily defined to be an octagonal frame, fifty-eight inches across on the major diagonal. Primary array structure attachment to the spacecraft may be accomplished along any of the corners or vertical edges of the hypothetical spacecraft frame.
3. The basic array structure shall be designed to have a minimum number of different components. This requires that the total array structure be composed of not more than four sub-elements or panels.
4. Total available surface for solar cell mounting shall be between one hundred fifty and four hundred square feet. For initial planning and conceptual study purposes, a target area of two hundred square feet shall be assumed. The geometry of the array structure shall be based upon a rectangular modular solar cell array of 18 inches x 34 inches, having a weight of 0.30 pound per square foot. This weight shall include cells, filters, modular wiring, and secondary cabling.

5. Any mechanical latch points or devices located on the cell surface shall not shade the solar cell surface when the array structure is oriented $\pm 5^\circ$ from the normal incidence angle of illumination.

4.2 STRUCTURAL DESIGN CRITERIA

Under the hypothetical environmental conditions set forth in the Environmental Criteria for a useful life of eighteen months:

1. The array structure shall have the capability of surviving normal ground handling during fabrication, assembly, qualification testing and storage. The array structure shall also have the capability of being repaired when subject to minor damage.
2. The array structure shall have the capability of surviving all dynamic loads, including transportation, cruise course correction, and retromaneuver at planetary encounter. It is implicitly assumed that the array structure will be in the undeployed configuration during launch, and in the deployed configuration during course correction motions. Depending upon the nature of the array structure, either deployed or undeployed, either configuration may or may not be used during the retro-maneuver. The retro-maneuver thrust shall not be used to initiate or power the retraction, if required, of the array structure. Upon the completion of the retro-maneuver, the array structure shall be in the deployed configuration suitable for power production.
3. The rear surface of the array structure shall be designed to minimize heat radiation traps in order to minimize local front surface hot spots.
4. All array structure components shall have provisions for pressure equalization between internal elements and the external flight environment.
5. To preclude real or potential degradation of the solar cells mounted upon the array structure, the curvatures induced in the cells shall be limited as follows:
 - (a) The radius of curvature of the undeployed, or stowed, array structure shall at no time be less than six inches.
 - (b) Under dynamic conditions, the angular change of the cell substrate per unit length shall be less than 1.0 degree/inch.

6. To avoid servoelastic coupling of the array structure and hypothetical spacecraft control system, the inertial and response characteristics for the array structure shall be as follows:
- (a) During powered flight (boost, retro), due to allowable tolerance variations in the fabrication process, the first mass moment of the array structure (undeployed or deployed) shall vary less than 5% as measured about the spacecraft centerline (boost axis).
 - (b) If deployed, the array structure shall further have the following characteristics:
 - (1) The undamped first cantilever natural frequency of the array structure shall be between 0.5 and 5.0 cps.
 - (2) The ratio of damping to critical damping in the first cantilever mode shall be in the range .15 to 0.7.
 - (3) In the first cantilever mode of the array structure the ratio of generalized stiffness to generalized mass (k/m) shall vary less than 10% due to all allowable tolerance variations in the fabrication processes.
 - (c) During cruise phase (including course correction maneuver), the requirements shall be as defined in Paragraphs 6 (b)(1) and 6 (b)(3).
7. Structural criteria given below are stated in terms of limit loads (yield design loads). Induced stress levels shall be computed for all loading conditions stated in Paragraphs (7(a) and 7(b). Critical conditions shall be clearly identified and carefully evaluated. Margins of safety on stresses induced by these limit design loads are as follows:

$$M.S. = \frac{Y.S.}{L.S.} - 1 \geq 0$$

$$M.S. = \frac{U.S.}{1.25 (L.S.)} - 1 \leq 0$$

where M.S. = Margin of Safety

L.S. = Stresses resulting from Limit Loads

Y.S. = Yield Stress

U.S. = Ultimate Stress

The yield and ultimate stress values shall be those for the appropriate material as given in the latest editions of MIL-HDBK-5 and MIL-HDBK-17.

- (a) Thermal Cycling: this cycling represents the effects of spacecraft orbit about a planet as well as spacecraft attitude reorientations associated with cruise course corrections. The design limit thermal loads for this array structure are equivalent to the levels experienced during the following test environment:
- (1) Pressure - The maximum pressure shall be 10^{-4} mm Hg.
 - (2) Free space background - The free space background or heat sink shall be simulated by a blackened wall having a total absorptivity of greater than 0.80 at liquid nitrogen temperatures, as viewed from the array structure surface.
 - (3) Heat Cycling - A heat input to the array structure surface of 80 watts per square foot shall be held until temperatures stabilize. The electrical power source shall then be turned off for a 1-1/2-hour period. The subsequent step changes in electrical power input from 0 to 80 watts per square foot define the start of a cycle. Periods of applied electrical power shall be for a 1-1/2-hour duration. Periods of non-applied electrical power shall be for a 1-1/2-hour duration (see Figure 22). The array structure shall be subjected to 10 periods of applied heater power for a total test time of approximately 40 hours.
- (b) Limit Structural Design Loads: the following table contains the applicable limit accelerations for use in the determination of the appropriate limit loads. These accelerations

define the environment at the array structure-spacecraft interface. The array structure shall be checked for structural adequacy under both static and vibratory criteria. Static and vibratory loads are not to be superimposed for design purposes.

CONDITION	STATIC	
	<u>Long.</u>	<u>Lat.</u>
a. Max. q & Mach. 1	4g	3g
b. Booster Burnout	12g	2g
c. Booster Tailoff	2g	0
d. Cruise Maneuver	0.2g	.05g
e. Retro Burner	6g	1g

CONDITION	VIBRATORY		
	<u>Level</u>	<u>Range (cps)</u>	<u>Rate Minute/Octave</u>
a. Max. q & Mach 1	-	-	-
b. Booster Burnout	1.6g rms	2-20	1 min/oct
	4.0g rms	20-200	1 min/oct
	Noise 0.2g ² /cps	200-2000	180 seconds
c. Booster Tailoff	-	-	-
d. Cruise Maneuver	0	-	-
e. Retro Burner	0.8g rms	2-20	0.5 min/oct
	2.0g rms	20-200	0.5 min/oct
	Noise 0.2g ² /cps	200-2000	180 seconds

4.3 THERMAL DESIGN CRITERIA

1. All components shall meet the following sterilization requirements:

- (a) Withstand exposure to 3 thirty-six hour periods of heat at 145° C (295°F) in dry nitrogen (a total of one hundred eight (108) hours)
 - (b) Withstand exposure to a gas mixture of 12% ethylene oxide, 88% freon gas for ten hours at a relative humidity between 30% and 50%
- 2. The temperature at any point on the solar cell surface, as a function of solar irradiance, shall be less than the values defined in Figure 23. This is a maximum temperature for any position on the front surface of the array structure. These temperatures may be achieved by requiring that exposed surfaces on the rear and edges of the array structure have a total hemispherical emissivity of greater than 0.80 in the temperature range of -30° C to 80° C.
- 3. The rear surface of the array structure shall be designed to minimize heat radiation traps in order to minimize local front surface "hot spots".
- 4. Thermal cycling represents the effect of spacecraft orbit about a planet as well as spacecraft attitude reorientations associated with cruise course corrections. The design limit thermal loads for this array structure are equivalent to the levels experienced during the following test environment:
 - (a) Pressure - The maximum pressure shall be 10^{-4} mm Hg.
 - (b) Free Space Background - The free space background or heat sink shall be simulated by a blackened wall having a total absorptivity of greater than 0.80 at liquid nitrogen temperatures as viewed from the array structure surface.
 - (c) Heat Cycling - A heat input to the array structure surface of 80 watts per square foot shall be held until temperatures stabilize. The electrical power source shall then be turned off for a 1-1/2-hour period. The subsequent step changes in electrical square foot define the start of a cycle. Periods of applied electrical power shall be for a 1-1/2-hour duration, periods of non-applied electrical power shall be for a 1-1/2-hour duration. (See Figure 22) The array structure shall be subjected to ten periods of applied heater power for a total test time of approximately forty hours.

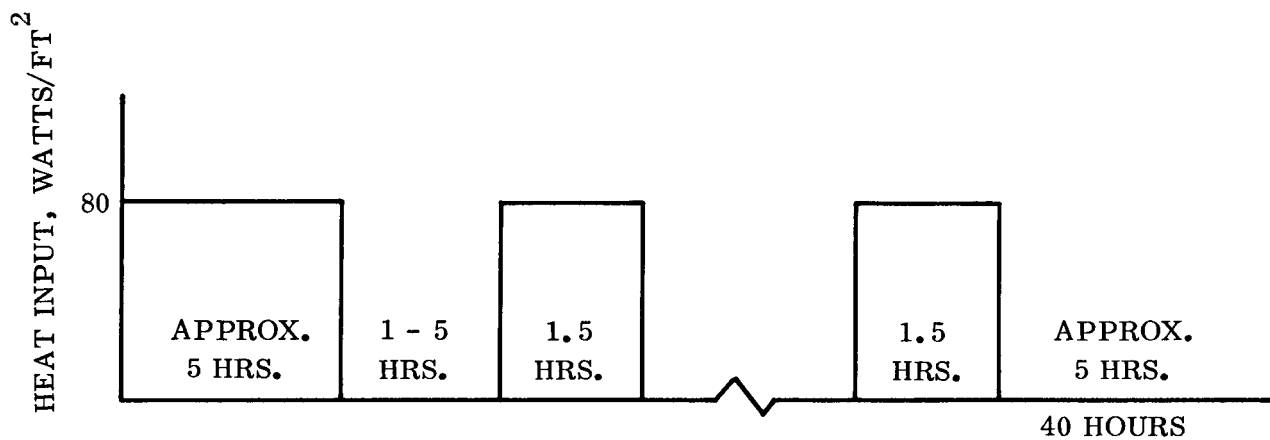


Figure 22 Periods of Electrical Power

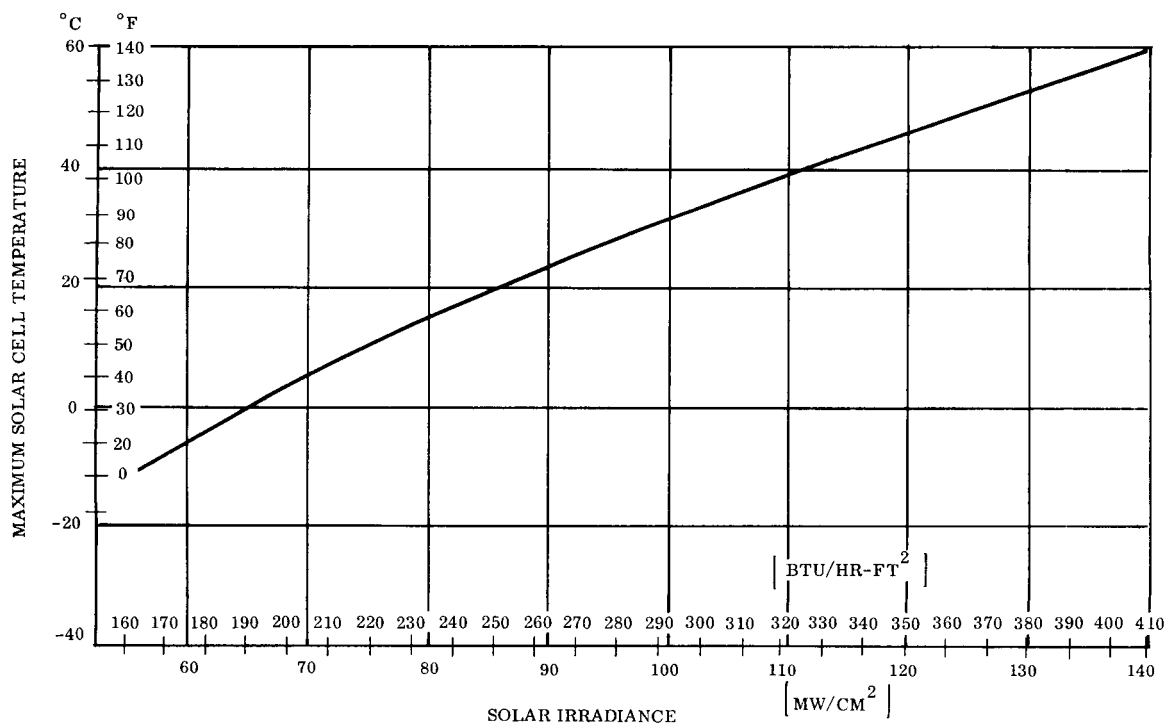


Figure 23 Solar Irradiance vs Maximum Solar Cell Temperature

4.4 MATERIAL DESIGN CRITERIA

1. The cell mounting surface shall be capable of being cleaned with solvents, or mild acid etching techniques prior to cell mounting.
2. The cell mounting surface shall be fabricated of, or coated with, a material that is an electrical insulator. This material shall be capable of withstanding the rigors of cell-mounting techniques. This material shall survive and be capable of repair, in the event that a damaged or defective cell must be removed. The insulation resistance shall be greater than 100 megohms, measured at a test potential of 200 VDC volts between the cell mounting surface and any metallic portion of the substrate.
3. The use of any material shall be predicated upon the proven ability of the material to withstand the deep space environment for a time in excess of eighteen months.
4. All components shall meet the following sterilization requirements:
 - a. Withstand exposure to three thirty-six hour periods of heat at 145° C (295° F) in dry nitrogen a total of one hundred eight hours.
 - b. Withstand exposure to a gas mixture of 12% ethylene oxide, 88% freon gas for ten hours at a relative humidity between 30% and 50%.
5. The exposed surfaces on the rear and edges of the array structure shall have a total hemispherical emissivity of greater than 0.80 in the temperature range of -30° C to 80° C.
6. Magnetic materials shall not be used in any of the array structure components, except when array structure reliability is affected by use of such materials.

4.5 WEIGHT DESIGN CRITERIA

1. A design objective shall be to keep the weight of the array structure and deployment mechanisms below 0.6 pound per square foot, including solar cells, cabling and wiring.

2. The solar cell array shall have a weight of 0.30 pound per square foot. This weight shall include cells, filters, modular wiring and secondary cabling.

5.0 THERMODYNAMICS

The thermodynamics effort for the development phase of the program is presented in this section. The analysis which has been conducted is parametric in nature rather than specific, in that much of the design criteria are very general. A Mars mission has been arbitrarily selected for the analysis. The conditions which might exist during this mission have been used where a specific mission condition is required in the analysis. The data and methods of analysis are presented in a form compatible and applicable to many design concepts.

5.1 SOLAR CELL STEADY STATE TEMPERATURES

Figure 24 is the result of the solution of a steady state equation which equates the solar flux absorbed to the thermal flux emitted by both the solar cell and the back of the substrate or painted surface. Properties of the back of the substrate have been varied to illustrate the influence on temperature of view factor to space and choice of paint or coating (infrared emissivity of surface).

$$\alpha_{sc} S = \delta (\epsilon_c F_c + \epsilon_s F_s) T^4 \quad (1)$$

where

$\alpha_{sc} S$ = heat absorbed by cell

α_{sc} = solar absorptivity = 0.84

S = solar flux

δ = Stefan-Boltzman constant

$\delta = 0.173 \times 10^{-8} \text{ BTU/hr-ft}^2 - ^\circ\text{R}^4$

ϵ_c = infrared emissivity of cell = 0.81

F_c = view factor of cell to space $\cong 1$. (no obstructions of view to space, i.e., no radiation traps)

T = temperature (it is assumed gradients through material are small, $T_{\text{cell}} \cong T_{\text{substrate}}$)

$\epsilon_s F_s$ = emissivity-view factor product of back of substrate

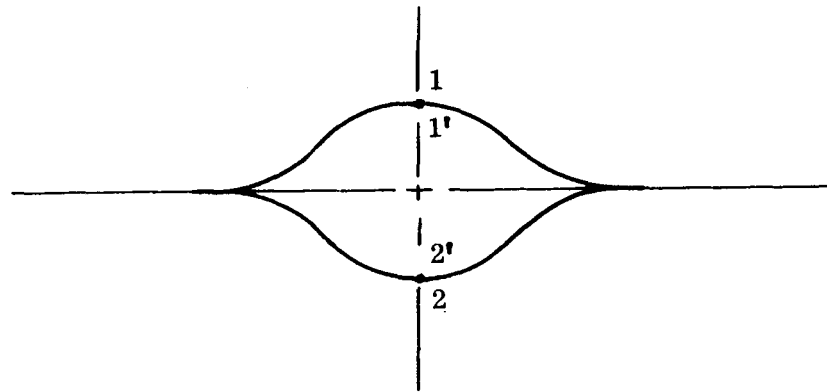
5.2 SOLAR ARRAY TEMPERATURE DISTRIBUTION

Figure 25 is a steady state temperature distribution based on Equation 1. View factors are based on an approximation of geometry illustrated on the figure and the equations and tables of Reference 1. An emissivity of the basic substrate of 0.8 was used (References 2 and 3) and emissivities of the order of 0.9 are obtainable from a selected group of paints (Reference 4). It appears, on the basis of this figure, that neither temperature level nor temperature distribution will present a great problem for the substrate-solar cell assembly in an earth-Mars mission.

5.3 DEPLOYABLE BEAM TEMPERATURE

Equation 2 and Table 1 are presented in a thermal study of the solar array-supporting cantilever beam. For bare titanium surfaces subjected to a solar flux of 440 BTU/hr-ft² (earth vicinity) the anticipated temperature levels are of the order of from 540° to 850° R, and the temperature difference of sunlight side to shaded side ranges from 120° R to 190° R, depending upon the degree of oxidation of the titanium surfaces.

To reduce the temperature difference (to minimize beam curvature effects caused by unequal thermal expansion) the inner surfaces of the beam can be given a coat of highly emissive paint. This has the effect of cutting the temperature difference approximately in half for the partially oxidized titanium beam. An even more effective method of reducing this temperature difference is by decreasing the emissivity of the outer surface of the shaded side of the beam, such as by using vapor deposited aluminum or an adhesive foil. This could cut the temperature difference to approximately one-sixth of the original value. If both of the above methods are used on the partly oxidized titanium beam, a low temperature difference of one-twelfth of the original can be achieved.



$$\alpha_{s1} S - \sigma \epsilon_1 T_1^4 = \frac{\sigma}{1/\epsilon_{1'} + 1/\epsilon_{2'}} \left[T_1^4 - T_2^4 \right] + \frac{2K \frac{A_x}{A_R} (T_1 - T_2)}{L_{1-2}} \quad (2)$$

$$= \sigma \epsilon_2 T_2^4 \quad (2)$$

where

S = solar flux (earth vicinity, 440 BTU/hr-ft²)

σ = Stefan-Boltzman constant, .173 x 10⁻⁸ BTU/hr-ft² °R⁴

α_s = Solar absorbtivity

ϵ = Infrared emissivity

k = thermal conductivity

A_x = cross-sectional area of conduction

A_R = radiating area

L = distance of conduction heat transfer path

T = Temperature subscripts 1 and 2 refer to outside surfaces of points and 1' and 2' refer to inside surfaces of points

Figure 26 is a result of solution of an electrical analogy with junctions indicated (numbered 1 through 8). The circuitry of the analogy includes:

- (1) Solar flux input (current in) to junctions 1, 2, 3, 7 and 8
- (2) Thermal flux emission (current out) to space from all junctions
- (3) Internal radiation (current) between junctions 1-5, 2-4 and 8-6
- (4) Flux (current) transfer through conduction from junctions 1 to 5 via routes 1-2-3-4-5 and 1-8-7-6-5

Thermal property values used in calculation of electrical components in the above analogy can be found in Table 1 under the description, "Bare, partly oxidized titanium surfaces".

Figure 27 amends Figure 26 to include the effect of the substrate's shading half the cantilever beam. Note that the sunlit portion of the beam has been considered painted with an appropriate paint (such as a suitably stable black with solar absorptivity and infrared emissivity of 0.85). This has been done to decrease the temperature gradient over the titanium surface (from point 3 to point 7) as well as to lower the higher temperatures of the beam.

References

- (1) F. Kreith, "Radiation Heat Transfer", International Textbook Co., Scranton, Pa. 1962, Appendix V.
- (2) S. S. Oleesky and J.G. Mohr, "Handbook of Reinforced Plastics", Reinhold Publishing Co., New York, P. 459.
- (3) A. Goldsmith, et al, "Thermophysical Properties of Solid Materials", WADC-TR-58-476, v. 4, November 1960, Pages 785-788.
- (4) "Space Materials Handbook", ML-TDR-64-40, January 1965, Pages 155, 605-606.

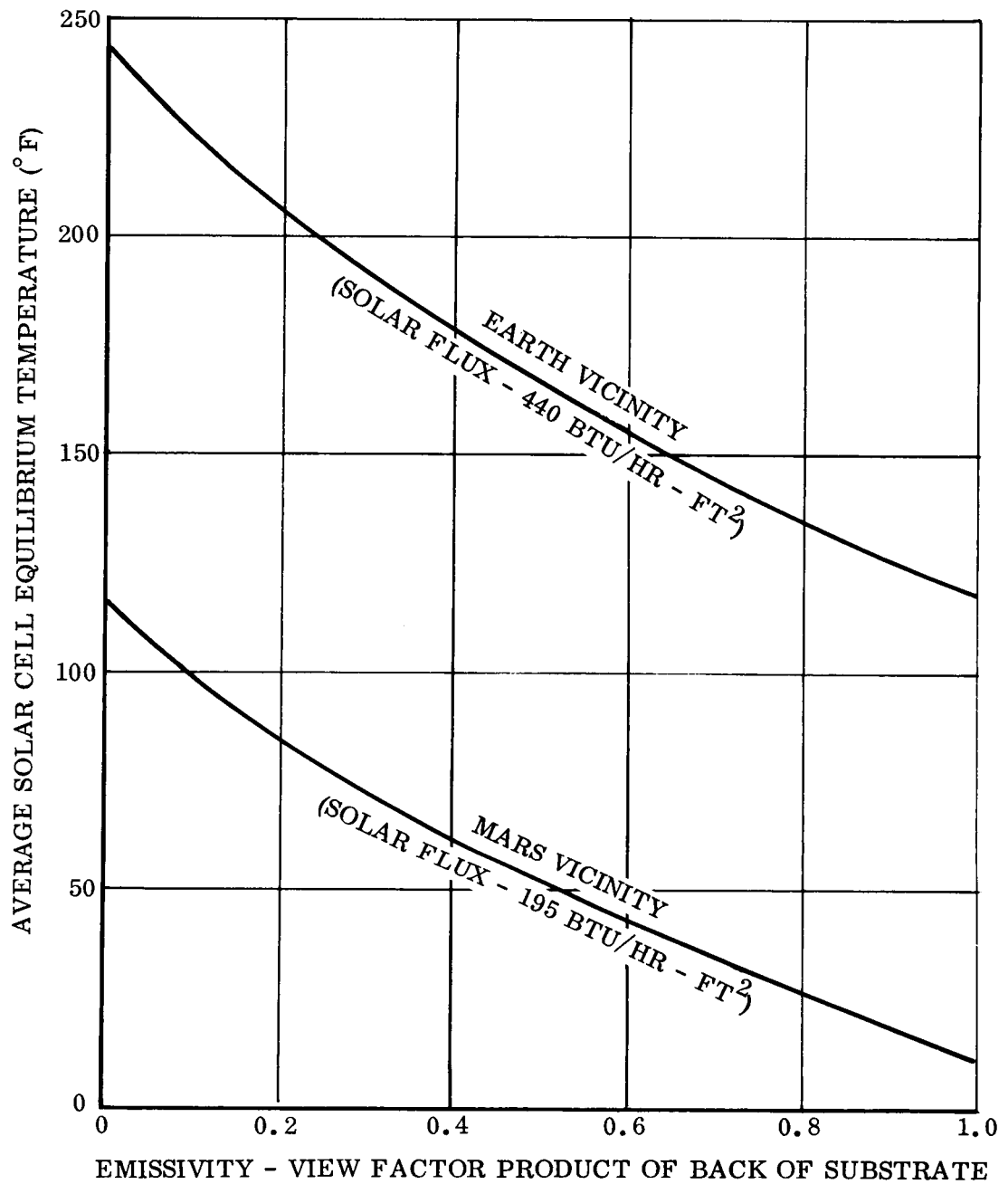


Figure 24 Steady State Temperatures

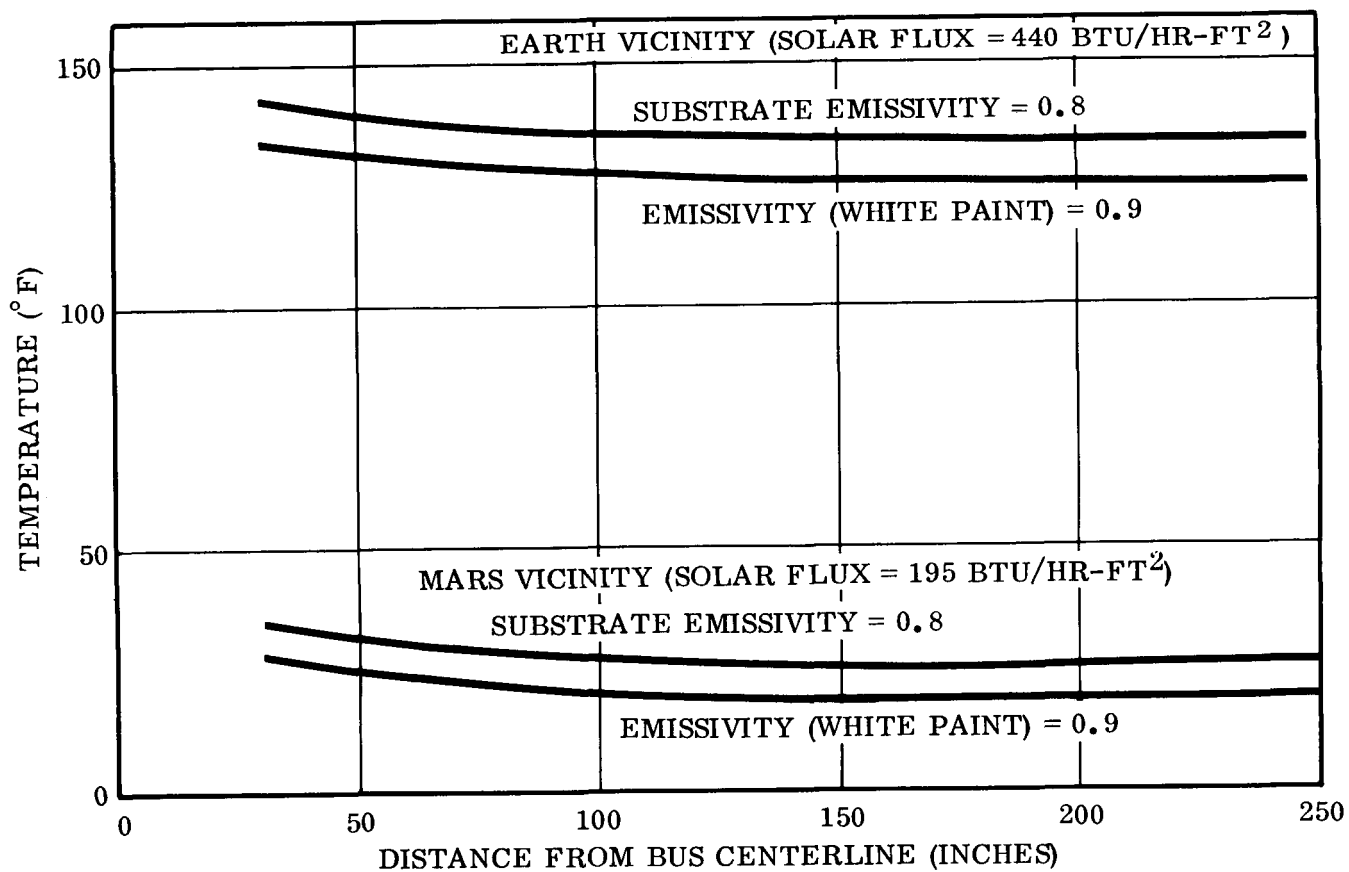
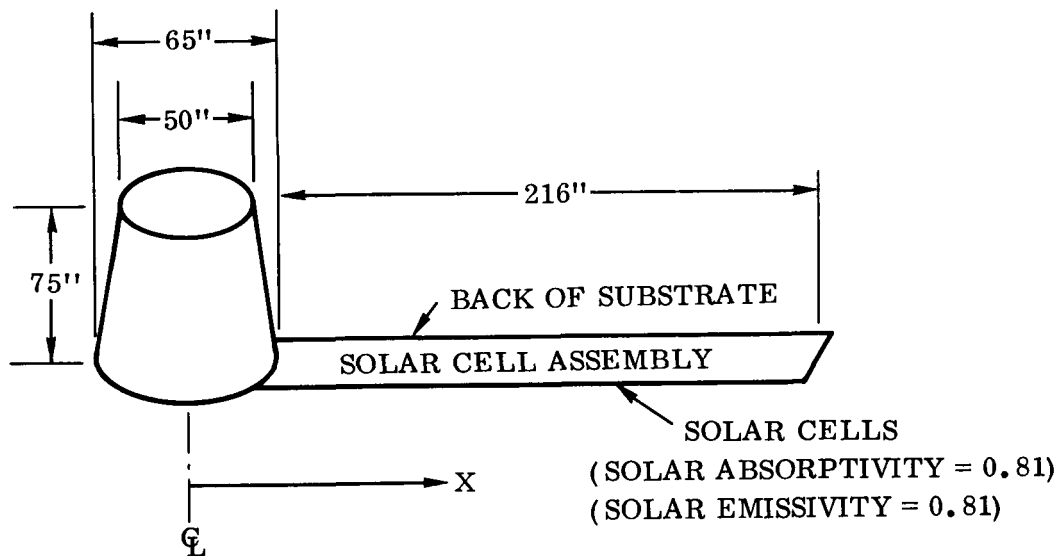


Figure 25 Solar Cell Surface Temperatures

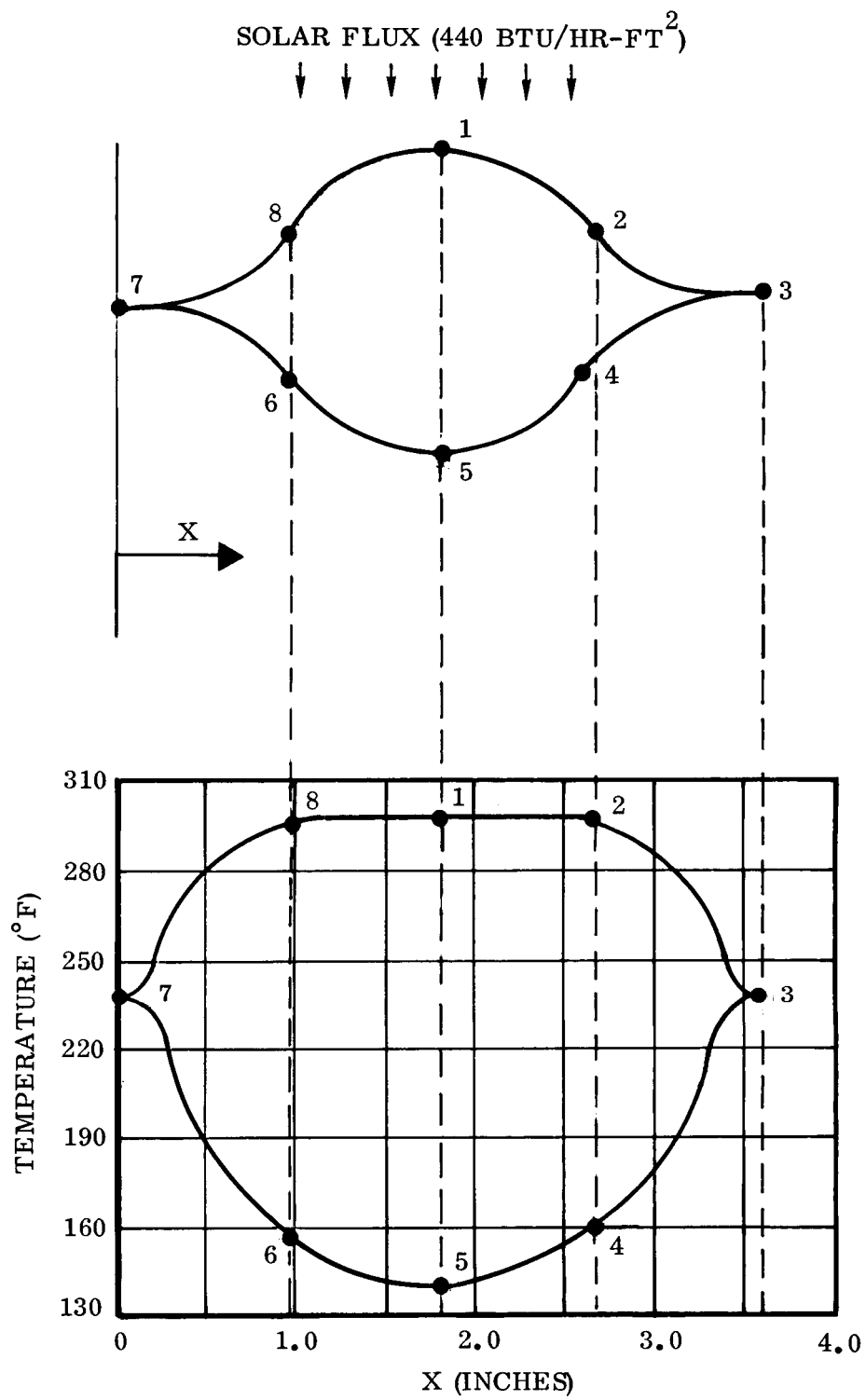


Figure 26 Temperature Distribution

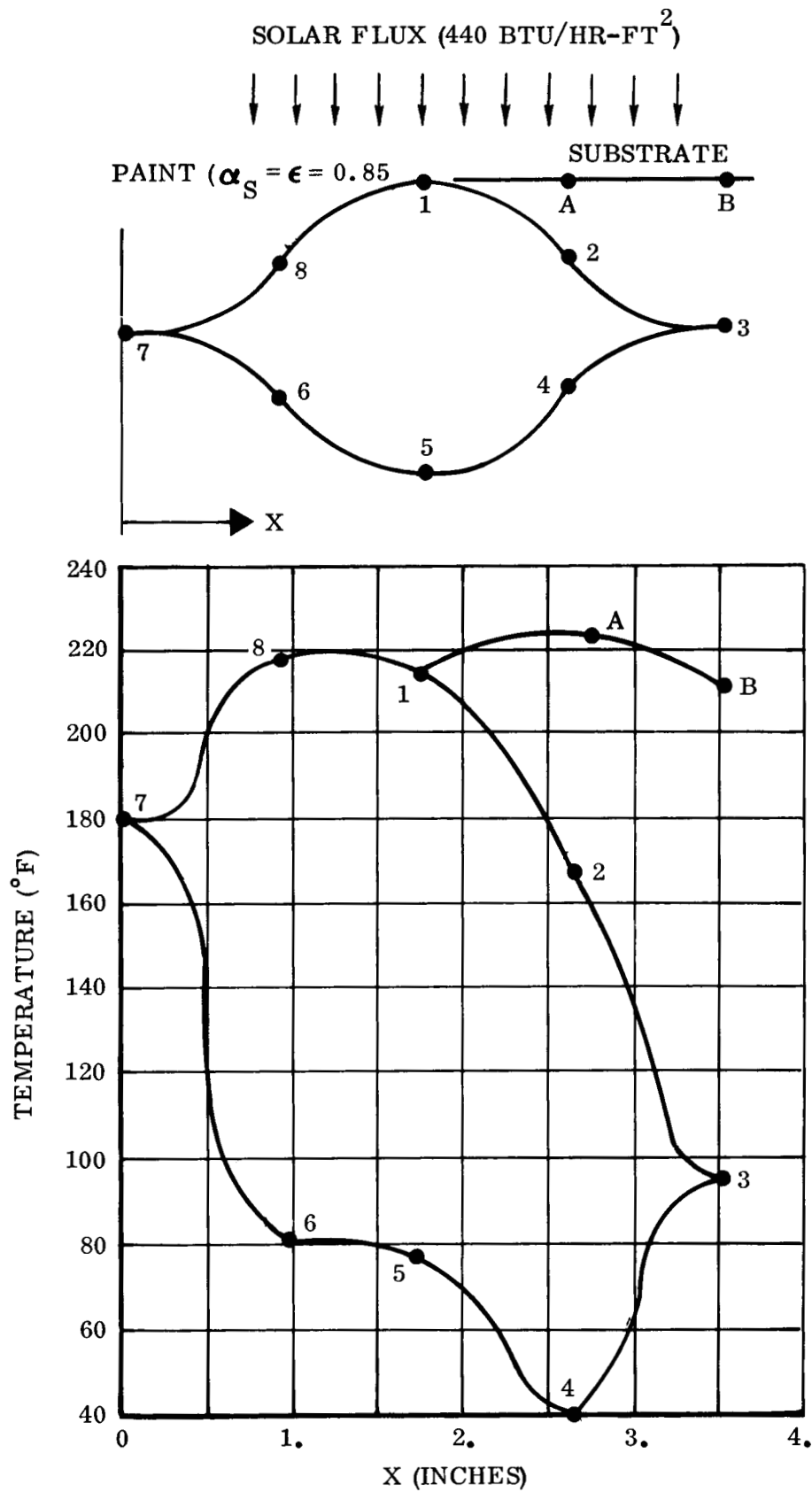


Figure 27 Temperature Distribution - Substrate Attachment

Table 1.
THERMAL PROPERTIES

DESCRIPTION	α_{S1}	ϵ_1	$\epsilon_{1'}$	$\epsilon_{2'}$	ϵ_2	k [BTU/hr-ft-°R]	T_1 [°R]	T_2 [°R]	$T_1 - T_2$ [°R]
Bare, polished, unoxidized titanium surfaces.	0.5	0.18	0.18	0.16	0.16	0	854.	665.	189.
Bare, fully oxidized titanium surfaces (possible range of values)	0.85	0.65	0.65	0.65	0.65	0	695.	561.	134.
(Also applies to glass fiber-epoxy.)	0.85	0.8	0.8	0.8	0.8	0	657.	539.	118.
Bare, partly oxidized titanium surfaces.	0.85	0.49	0.49	0.43	0.43	**0	755.	604.	151.
(With* or without** conduction)	0.85	0.49	0.49	0.43	0.43	*4.5	753.	608.	145.
Surface 1 chemically cleaned or etched to get in "as received" condition, other surfaces partly oxidized.	0.5	0.2	0.49	0.44	0.44	4.7	758.	614.	144.
Surfaces 1' and 2' painted (selected black or white paint), other surfaces partly oxidized titanium.	0.85	0.48	0.85	0.85	0.44	4.7	731.	652.	79.
Surface 2 given low emissivity coat (as with vapor deposited aluminum or adhesive foil), other surfaces partly oxidized titanium.	0.85	0.48	0.48	0.43	0.04	4.7	805.	781.	24.
Surface 2 with low emissivity coat, surfaces 1' and 2' painted, surface 1 partly oxidized titanium.	0.85	0.48	0.85	0.85	0.04	4.7	802.	791.	11.
References for thermal properties: Titanium (6Al-4V): A. Goldsmith, et al, "Thermophysical Properties of Solid Materials", WADC-TR-58-476V2, November 1960, Section V-C-1. Black or White Paint, "Space Materials Handbook", M1-TDR-64-40, January 1965, Pages 155, 605-606. Adhesive Foil;									

6.0 STRUCTURAL DYNAMICS

6.1 INTRODUCTION AND SUMMARY OF ANALYSIS RESULTS

The analysis consists of determining the first three uncoupled bending and torsional natural frequencies of the array in its deployed configuration. The results are as follows:

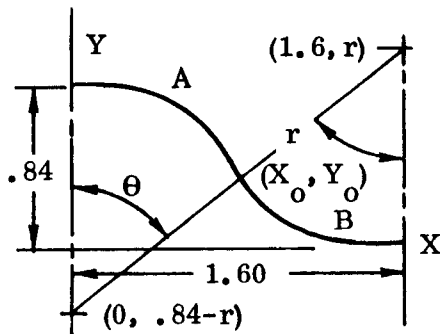
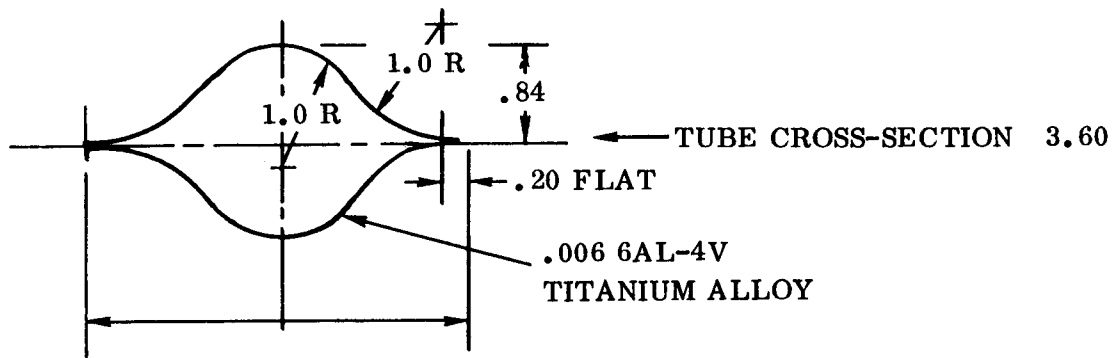
<u>Mode</u>	<u>Frequency (cps)</u>
1st Bending	0.43
2nd Bending	2.71
3rd Bending	7.60
1st Torsion	8.77
2nd Torsion	14.62
3rd Torsion	20.42

It is noted that the fundamental bending frequency of 0.43 cps falls below the specified minimum value of 0.50 cps, a 14% deficiency in frequency. Therefore, in order to bring the frequency up to specification value, it is recommended that one or a combination of the following steps be taken: increase the section moment of inertia of the deployed tubes; reduce the weight per square foot of the substrate and cells; reduce the unsupported length of the array. The changes by each method alone necessary to provide the indicated frequency increase are 35% increase, 35% decrease, and 7% decrease, respectively.

6.2 ANALYSIS

Mass Properties:

We first determine r , the radius necessary to meet the geometrical constraints of .84 inch half height and 1.60 inch half width for the arced portion.



The distance between points 1 and 2 is $2r$. Using $d^2 = \Delta x^2 + \Delta y^2$,

$$4r^2 = (1.6)^2 + [r + (r - .84)]^2$$

Solving for r ,

$$r = 0.9719 \text{ in}$$

The y coordinate of point 1 is $.84 - r = -0.1319$ in

The coordinates of the tangency point are given from symmetry of the arcs,

$$x_o = \frac{1.60}{2}, \quad y_o = \frac{.84}{2} = .42$$

The angle θ is determined from

$$\sin \theta = \frac{x_o}{r} = \frac{0.8}{.9719} = .82313 \quad \cos \theta = .5678 \quad \tan \theta = 1.4496$$

$$\theta = 55^\circ 24.0' = .9669 \text{ rad}$$

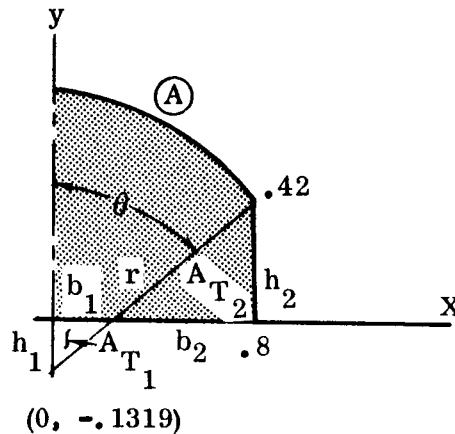
The arc lengths S_A and S_B are

$$S_A = S_B = r \theta = .9719 \cdot .9669 = .9397 \text{ in (1/8 of total section)}$$

The total arc length S of the section is

$$S = 8 S_A = 8 \cdot .9397 = 7.5176 \text{ in (omits flats)}$$

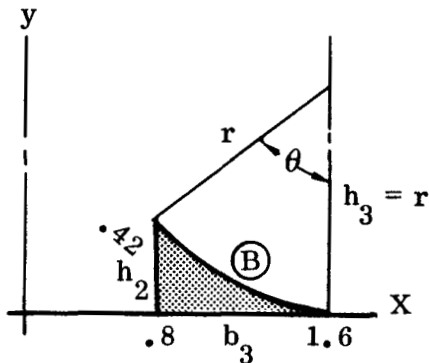
For the area A_A under the arc A ,



$$\begin{aligned} A_A &= A_{\text{Shaded Portion}} \\ &= A_{\text{sector}} - A_{T1} + A_{T2} \\ &= \frac{1}{2} r^2 \theta - \frac{1}{2} h_1 b_1 + \frac{1}{2} h_2 b_2 \\ h_1 &= .1319 \\ b_1 &= h_1 \tan \theta = .1319 \cdot 1.4496 \\ &= .1912 \\ h_2 &= .4200 \\ b_2 &= .8000 - .1912 = .6088 \end{aligned}$$

$$\begin{aligned} A_A &= \frac{1}{2} (.9446 \cdot .9669 - .1319 \cdot .1912 + .6088 \cdot .4200) \\ &= .5719 \text{ in}^2 \end{aligned}$$

For the area A_B under the arc B,



$$A_B = A_{\text{Shaded Portion}}$$

$$= A_{\text{Trapezoid}} - A_{\text{Sector}}$$

$$= \frac{1}{2} (h_2 + h_3) \cdot b_3 - A_{\text{Sector}}$$

$$= \frac{1}{2} (.4200 + .9719) \cdot .8 - .9133$$

$$= .1001 \text{ in}^2$$

$$A_A + A_B = .6720 \text{ in}^2 \text{ (1/4 of}$$

total section)

The total cross sectional area A of the section is

$$A = 4 (A_A + A_B) = 4 \cdot .6720 = 2.6680 \text{ in}^2$$

Mass μ per inch of length of array:

For 6AL4V Ti Alloy, the weight density is $.160 \text{ lb/in}^3$ (Ref. MIL-HDBK-5)

For one tube, the wt/in of span is

$$w_T = t (S + S_{\text{flats}}) \rho = .006 (7.1776 + .8000) \cdot .160$$

$$= .007985 \text{ lb/in}$$

$$w_1 = 2 \cdot .007985 = .0160 \text{ lb/in (both tubes)}$$

For the substrate and cells, the surface weight density is 0.40 lb/ft^2 and the array is 3.00 ft. wide. Thus,

$$w_2 = \frac{.40.3}{12} = 0.1000 \text{ lb/in}$$

For the connecting strips, the surface density is assumed to be 1/4 that of the substrate and cells. The strips are 1.0 inch wide each, (2 inches total width). Thus,

$$w_3 = \frac{1}{4} \cdot \frac{.100}{36} \cdot 2 = .0014 \text{ lb/in}$$

The total weight per inch is

$$\begin{aligned} w_1 &= w_1 + w_2 + w_3 = .0160 + .1000 + .0014 \\ &= .1174 \text{ lb/in (total array)} \end{aligned}$$

Note that most (85%) of the array weight is associated with the substrate and cells.

The mass μ per inch of length is, using $g = 386.04 \text{ in/sec}^2$

$$\mu = \frac{w}{g} = \frac{.1174}{386.04} = .0003041 \text{ lb sec}^2 \text{ in}^2 \text{ (total array)}$$

Mass moment of inertia γ per inch of length:

Tubes:

$$I_1 = 2 w_T d_1^2 + 2 I_O = 2 w_T (d_1^2 + \bar{r}^2)$$

It is assumed that $I_O = w_T \bar{r}^2$, where r is the radius of a circle with the same enclosed area as the actual tube.

$$\pi \bar{r}^2 = A = 2.6680.$$

$$\text{Solving for } \bar{r} \text{ gives } \bar{r} = .9250 \text{ } (\bar{r}^2 = .8556)$$

Also, the tube G_L 's are 41.6 inches apart, making $d_1 = 20.8$ in.

$$I_1 = 2 \cdot .007985 (20.80^2 + .86) = 6.92 \text{ lb in}^2/\text{in}$$

Substrate and Cells:

$$I_2 = \frac{1}{12} w_2 l^2 = \frac{.1000(36)^2}{12} = 10.80 \text{ lb in}^2/\text{in}$$

Connecting Strips:

$$I_3 = 2 \left(\frac{w_3}{2} \right) d_3^2 = 2 \cdot .0007 (18.5)^2 = 0.49 \text{ lb in}^2/\text{in}$$

(The strip Q_L 's are 37 inches apart, making $d_3 = 18.5$ in.)

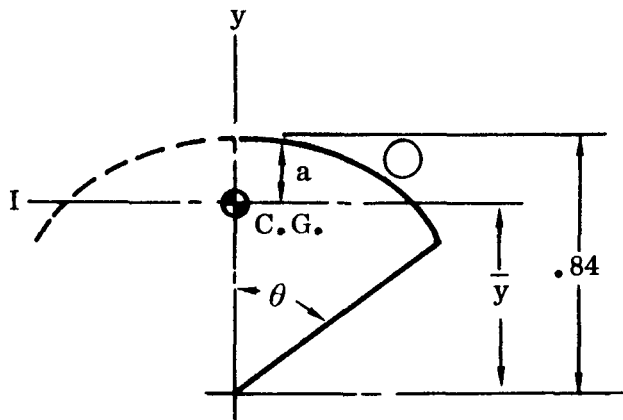
The weight moment of inertia I per inch is

$$\begin{aligned} I &= I_1 + I_2 + I_3 = 6.92 + 10.80 + 0.49 \\ &= 18.21 \text{ lb in}^2/\text{in} \end{aligned}$$

The mass moment of inertia per inch of length is

$$\gamma = \frac{I}{g} = \frac{18.21}{386.04} = .04717 \text{ lb sec}^2 \text{ in}/\text{in}$$

Stiffness Properties



For arc A:

$$I_{1-1} = \frac{1}{2} r^3 t \left(\theta + \sin \theta \cos \theta - \frac{2 \sin^2 \theta}{\theta} \right)$$

$$a = r \left(1 - \frac{\sin \theta}{\theta} \right)$$

(Ref. Roark, 1st Ed. P6. 64, Case 12)

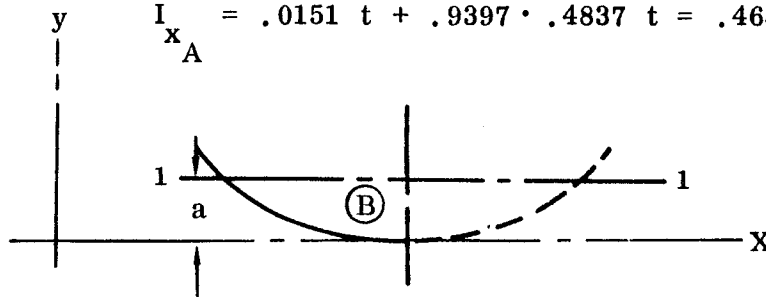
$$I_{x_A} = I_{1-1} + S_A t \bar{y}^2$$

$$I_{1-1} = \frac{1}{2} (.9719)^3 t \left[.9669 + .82313 \cdot .56785 - \frac{2(.82313)^2}{.9669} \right] = .0151 t \text{ in}^4$$

$$a = .9719 \left(1 - \frac{.82313}{.9669} \right) = .1445 \text{ in}$$

$$\bar{y} = .84 - a = .8400 - .1445 = .6955 \text{ in } (\bar{y}^2 = .4837 \text{ in}^2)$$

$$I_{x_A} = .0151 t + .9397 \cdot .4837 t = .4688 t \text{ in}^4$$



For arc B:

$$I_{x_B} = I_{1-1} + S_B t a^2 = .0151 t + .9397 (.1445)^2 t$$

$$= .0347 t \text{ in}^4 \quad (\text{Note } S_B = S_A = .9397 \text{ in})$$

The section moment of inertia I is

$$I = 4 (I_{x_A} + I_{x_B}) = 4 (.4688 t + .0347 t)$$

$$= 2.0140 t \text{ in}^4 = 2.0140 \cdot .006 = .01208 \text{ in}^4/\text{tube}$$

and the bending stiffness EI of the array is, using modulus of elasticity $E = 16.4 \cdot 10^6 \text{ lb/in}^2$ (Ref. MIL-HDBK-5):

$$EI = 16.4 \cdot 10^6 (2 \cdot .01208) = 3.962 \cdot 10^5 \text{ lb in}^2$$

(total array)

For one tube, the torsional moment of inertia J is

$$J = \frac{4A^2}{\int_t ds} = \frac{.006 \cdot 4 (2.688)^2}{7.5176} = .02307 \text{ in}^4 \text{ (per tube)}$$

$$\text{(Note } \int_t ds = \frac{s}{t} \text{ since } t \text{ is constant)}$$

Using modulus of rigidity $G = 6.2 \cdot 10^6 \text{ lb/in}^2$ (Ref. MIL-HDBK-5), the torsional stiffness is

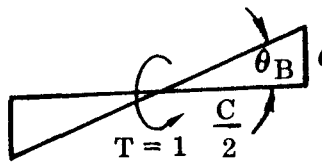
$$GJ = 6.2 \cdot 10^6 \cdot 2 \cdot .02307 = 2.870 \cdot 10^5 \text{ lb in}^2$$

(uncorrected for differential bending stiffness)

With a unit torque applied at the tip, the twist due to the tube system alone is

$$\theta_T = \frac{TL}{GJ} = \frac{1}{GJ} L$$

and due to differential bending alone,



$$\theta_B = \frac{2\delta}{C} \text{ where } \delta = \frac{1}{3} \frac{PL^3}{EI} \text{ and } P = \frac{1}{C}$$

$$\text{so } \theta_B = \frac{2}{C} \cdot \frac{1}{3} \cdot \frac{1}{C} \frac{L^3}{EI} = \frac{2}{3} \frac{L^3}{C^2 EI}$$

The ratio of θ 's is

$$\begin{aligned}\frac{\theta_T}{\theta_B} &= \frac{L}{GJ} \cdot \frac{3C^2EI}{2L^3} = \frac{3}{2} \frac{C^2}{L^2} \frac{EI}{GJ} \\ &= \frac{3}{2} \left(\frac{41.60}{216} \right)^2 \cdot \frac{1.461 \cdot 10^5}{2.870 \cdot 10^5} = .04865\end{aligned}$$

Note that this ratio is constant, since P is applied only at the end closure rib. C is the ϕ separation of the tubes, 41.60 inches, and L is the unsupported length of the array, 216 inches.

Thus, the total torsional stiffness is 1.04865 times the torsional stiffness due to the tubes alone:

$$GJ = 2.870 \cdot 10^5 \cdot 1.04856 = 3.010 \cdot 10^5 \text{ lb.in}^2 \text{ (total array includes differential bending stiffness).}$$

Frequencies

Bending frequencies (cantilever beam):

The bending frequencies are given by:

$$\omega_n = a_n \sqrt{\frac{EI}{\mu L^4}} \text{ (Ref. Dan Hartog, Mechanical Vibration, 3rd Ed., Page 459)}$$

where ω_n = circular natural frequency (rad/sec)

$$\text{in } \eta^{\text{th}} \text{ mode } f_n = \frac{\omega_n}{2\pi}$$

$$a_1 = 3.52, a_2 = 22.04, a_3 = 61.7$$

$$EI = 3.962 \cdot 10^5 \text{ lb in}^2$$

$$\mu = .0003041 \text{ lb sec}^2 \text{ in}^{-2}$$

$$L = 216 \text{ in } (L^4 = 2.177 \cdot 10^9 \text{ in}^4)$$

$$\sqrt{\frac{EI}{\mu L^4}} = \sqrt{\frac{3.962 \cdot 10^5}{3.041 \cdot 10^{-4} \cdot 2.177 \cdot 10^9}} = .7736$$

Mode	a	$\omega = .7736a$ (rad/sec)	$f = \frac{\omega}{2\pi}$ (cps)
1	3.52	2.723	.43
2	22.04	17.05	2.71
3	61.7	47.73	7.60

Torsional frequencies (torsional cantilever):

The torsional frequencies are given by:

$$\omega_n = a_n \sqrt{\frac{GJ}{\gamma L^2}} \quad (\text{Ref. Dan Hartog Pgs. 458 and 459})$$

$$\text{where } a_n = (n + \frac{1}{2} \pi)$$

$$a_1 = \frac{3}{2} \pi = 4.712$$

$$a_2 = \frac{5}{2} \pi = 7.854$$

$$a_3 = \frac{7}{2} \pi = 10.996$$

$$GJ = 3.010 \times 10^5 \text{ lb-in}^2$$

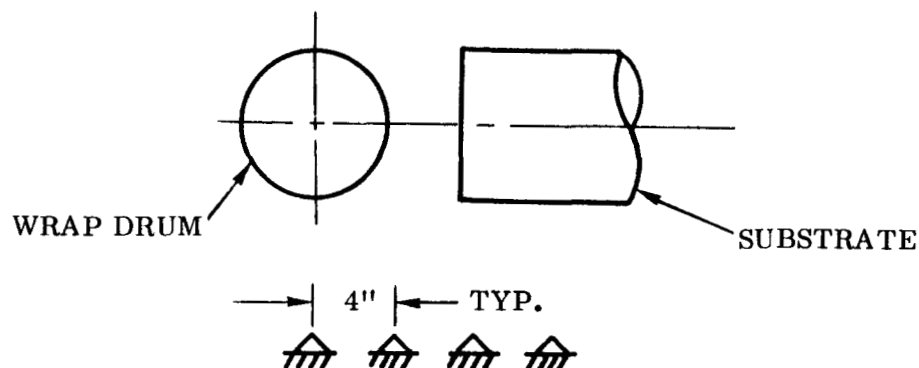
$$\gamma = .04717 \text{ lb sec}^2 \text{ in/in}$$

$$L = 216 \text{ in } (L^2 = 46,656 \text{ in}^2)$$

$$\sqrt{\frac{GJ}{\gamma L^2}} = \sqrt{\frac{3.010 \times 10^5}{.04717 \times 46,656}} = 11.70$$

Mode	a	$\omega = 11.70a$ (rad/sec)	$f = \frac{\omega}{2\pi}$ (cps)
1	4.712	55.13	8.77
2	7.854	91.89	14.62
3	10.996	128.30	20.42

Interference between layers - stowed configuration:



It is assumed that the substrate and cells have zero bending stiffness - the stowed array behaves as a membrane. Also, it is assumed that the membrane is flat, i.e., the cylinder curvature is neglected.

Mass/inch of span (μ)

$$\begin{aligned} \text{Wt. of substrate and cells} &= .40 \text{ lb/ft}^2 \\ &= .00278 \text{ lb/in}^2 \end{aligned}$$

For a 1 in-wide strip, $w = .00278 \text{ lb/in}$

$$\mu = \frac{.00278}{386} = 7.20 \cdot 10^{-6} \text{ lb/sec}^2 \text{ in}^{-2}$$

Extensional stiffness AE (1 in-wide strip)

Material is equivalent .008 fiberglass ($E = 2.0 \cdot 10^6$ in spanwise, y, direction)



$$AE = .008 \cdot 1 \cdot 2.0 \cdot 10^6 = 16,000 \text{ lb}$$

The fundamental frequency of a membrane (string) is $\omega_1 = \frac{\pi}{\ell} \sqrt{\frac{T}{\mu}}$

where T is the initial tension T on the string (Dan Hartog, Pg. 175)

Actually, in the intermediate bays T is, without deformation, zero. It reaches a maximum at full throw. The T in ω , should be replaced by the average value of T, which is $.707 T_{\max} = .707 T$ for a sine mode shape.

$$\text{So } \omega_1 = \frac{\pi}{\ell} \sqrt{\frac{.707T}{\mu}}$$

The change in length of the string from  to 

$$\text{is } \delta = \Delta \ell = S - \ell = \frac{T \ell}{AE}$$

$$S = \int ds = \int_0^{\ell} \sqrt{1 + \left(\frac{dy}{dx}\right)^2} dx = \int_0^{\ell} \sqrt{1 + y_o^2 \sin^2 \frac{1+x}{\ell}} dx = s(y_o)$$

$s(y_o)$ must be evaluated.

Solving $s - \ell = \frac{T \ell}{AE}$ for T

$$T = \frac{AE}{\ell} (s - \ell) = AE \frac{s}{\ell} - 1 = T(y_o)$$

Substitution of $T(y_o)$ in $\omega_1 = \frac{\pi}{\ell} \sqrt{\frac{T}{\mu}}$ gives $\omega_1 = \omega_1(y_o)$.

Substitution of this in the K.E. eq. gives K.E. = $f_1(y_o)$

For elongation, we have P.E. = $\frac{1}{2} K \delta^2$

$$K = \mu \text{ for 1-in deflection or } 1 = \frac{K \ell}{AE} \text{ or } K = \frac{AE}{\ell}$$

$$\text{So P.E.} = \frac{1}{2} \frac{AE}{\ell} (s - \ell)^2 = \frac{1}{2} AE \ell \left(\frac{s}{\ell} - 1 \right)^2$$

Finding the y_o where P.E. = K.E. (intersection of curves) gives the required y_o .

By graphical interpolation, y_o at K.E. = P.E. is 0.090 and ω_1
= 1670 rad/sec (f_1 = 266 cps)

$$y_o = .090 \text{ in}$$

Amplitude (D.A. = 0.180 in at
resonance)

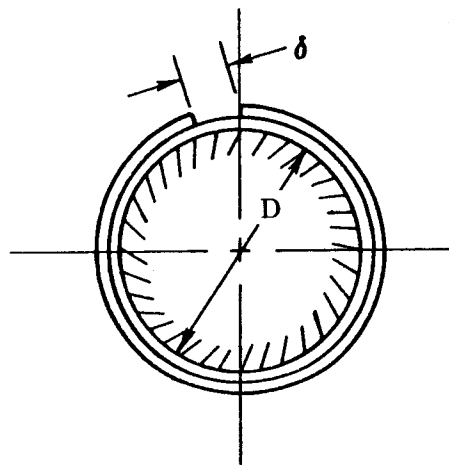
$$f_1 = 266 \text{ cps}$$

7.0 STRUCTURAL ANALYSIS

Conventional methods have been employed in the analysis conducted for the substantiation of design. In some cases, empirical data derived from tests conducted specifically for this task have been employed for analysis of the structure.

7.1 BEAM WRAPPING ON STORAGE DRUM

The mechanics of wrapping the beam on the 12-inch storage drum are such that, geometrically, the outer layer of the beam section must travel a longer distance than the inner layer. Since the two layers of the beam section are continuously attached, the beam layers will complete each revolution around the drum together unless the mode of attachment fails in longitudinal shear. This shear load is computed in the following manner:



Drum diameter = 12 in

Mean circumference of inner sheet

$$C_1 = \pi (D+t)$$

Mean circumference of outer sheet

$$C_2 = \pi (D+3t)$$

$$= C_2 - C_1 = 2 \pi t$$

It is assumed that both layers deform in the wrapping process. The outer layer stretches one half the distance, and the inner layer compresses the same amount. Assuming the modulus of elasticity to be equal in tension and compression.

$$\delta = \frac{PL}{AE}$$

$$\text{or } P = \frac{\delta AE}{L}$$

The longitudinal shear flow $q = \frac{P}{2C}$ (lb/in)

Expanding the equation by substituting the following relationships,

$$\delta = 2 \pi t$$

$$L = 2 \pi R$$

$$A = bt \quad \text{where } b = \text{width}$$

$$c = 2 \pi R$$

$$q = \frac{(2 \pi t) (bt) (E)}{(2 \pi R) (2) (2 \pi R)} = \frac{b E t^2}{4 \pi R^2}$$

The shear flow is calculated based on beam parameters as determined and presented later in this section.

$$b = 4 \text{ in}$$

$$E = 16 \times 10^6 \text{ psi, 6AL-4V titanium annealed}$$

$$t = .0065 \text{ in}$$

$$R = .90 \text{ in}$$

$$q = \frac{(4) (16 \times 10^6) (.0065)^2}{(4) (\pi) (.90)^2} = \frac{.0027 \times 10^6}{10.178} = 260 \text{ lb/in.}$$

For the closed-section type beam, the shear flow is 130 lb/in per seam weld.

$$f_s = \frac{q}{t} = \frac{130}{.0065} = 20,000 \text{ psi}$$

$$F_{su} = 76,000 \text{ psi}$$

$$M.S. = \frac{76}{20} - 1 = \text{HIGH}$$

Minimum Bending Radius Precluding Yield of Material

The mathematical expression for the radius of curvature is introduced by

$$\frac{1}{R} = \frac{M}{EI} \quad (3)$$

The bending stress is given by

$$f_b = \frac{Mc}{I} \quad (4)$$

Letting the bending stress equal the yield stress,

$$F_{ty} = \frac{Mc}{I} \quad (5)$$

or

$$\frac{M}{I} = \frac{R_{ty}}{c} \quad (6)$$

Restating Equation (3)

$$\frac{M}{I} = \frac{E}{R} \quad (7)$$

Equating Equation (7) and (6)

$$\frac{F_{ty}}{c} = \frac{E}{R} \quad (8)$$

or

$$R = \frac{E c}{F_{ty}} \quad (9)$$

In using Equation (9), c is equal to the beam material thickness in the beam wrapping process and it is equal to one-half of the thickness in the beam flattening process.

The minimum radius for which yielding will not occur is given in the following analysis for the beam configuration selected.

$$R = \frac{E c}{F_{ty}}$$

$$E = 16.0 \times 10^6$$

6AL-4V titanium annealed

$$F_{ty} = 120,000 \text{ psi}$$

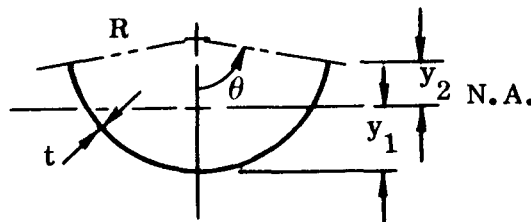
$$c = t/2 = .0065/2 = .00325 \text{ inches}$$

$$R = \frac{16 \times 10^6 \times .00325}{120,000} = 0.433 \text{ inches}$$

7.2 BEAM SECTION PROPERTY STUDIES

The studies which were conducted to determine the best beam section were limited to those sections which could be easily fabricated and would be acceptable to the materials being considered. Two basic sections were considered in the study. These will be referred to as the open and closed sections, respectively. In order to facilitate and expedite the evaluation of the various configurations, simple design graphs were constructed.

Open Section Beam ($0^\circ < \theta < 90^\circ$)



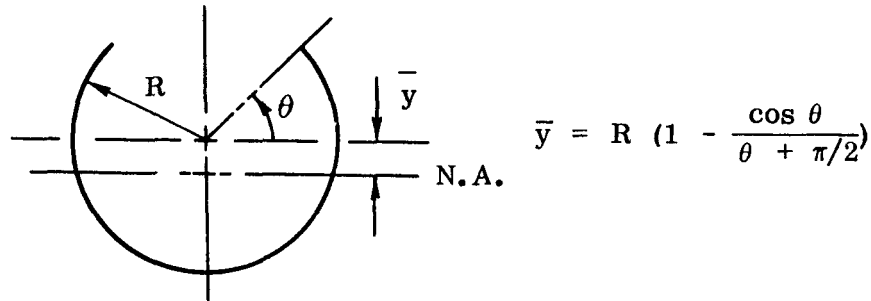
$$I_{na} = R^3 t \theta + \sin \theta \cos \theta - \frac{2 \sin^2 \theta}{\theta}$$

$$y_1 = R \left(1 - \frac{\sin \theta}{\theta} \right)$$

$$y_2 = R \left(\frac{\sin \theta}{\theta} - \cos \theta \right)$$

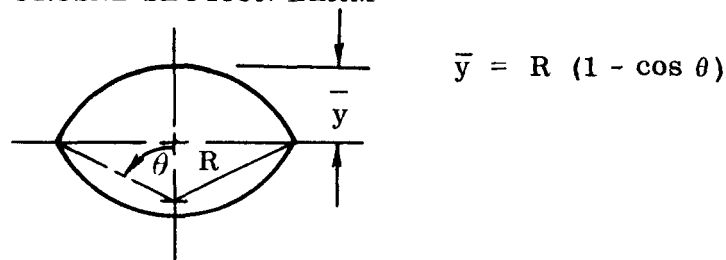
Open Section Beam ($0^\circ < \theta < 90^\circ$)

OPEN SECTION BEAM



$$I_{na} = 2tR^3 \left\{ \left[\frac{\theta}{2} - \frac{1}{4} \sin 2\theta + \frac{\pi}{4} \right] - \cos^2 \theta \right\}$$

CLOSED SECTION BEAM



$$I_{na} = 2R^3 t \left[\theta + \sin \theta \cos \theta - \frac{2 \sin^2 \theta}{\theta} + 2\theta \left(\frac{\sin \theta}{\theta} - \cos \theta \right)^2 \right]$$

Beam Tests (Closed Sections)

Beam tests have been conducted to assist in the development of an empirical method for predicting the buckling allowable for closed section designs. The method of analysis for predicting buckling is based on analysis for and tests which are presented in NACA TN-2875. The method presented in the above reference is modified to the extent that a buckling coefficient which is dependent upon the modulus of elasticity is used. The relationship between the buckling coefficient K and the modulus of elasticity was determined from tests conducted on closed beam segments of various materials. With few exceptions, the theoretically predicted strengths were within 5% of the actual strengths determined by tests.

The referenced report suggests use of the following equation for buckling strength if the R/t ratio is less than 720. In the proposed configurations, the R/t ratios are all very much lower than 720.

$$F_{CR} = \frac{.36 E t}{R}$$

where

R = Radius of circular arc, inches

t = Thickness of material, inches

E = Modulus of elasticity, psi

This equation accurately predicted the test results within 5% of the failure load for steel. However, when titanium and glass fiber beams were tested, unacceptable errors resulted. An attempt was made to develop an empirical equation which would satisfy the buckling prediction for all materials. Examination of the buckling equation indicates that the only term which can be considered a variable is coefficient. The following procedure was employed:

Let M = Bending moment causing beam failure

I = Moment of inertia of test beam

c = Distance to outer fiber from neutral axis

f_b = Bending stress - calculated

$$f_b = \frac{Mc}{I}$$

If the bending stress is equated to the buckling stress,

$$f_b = \frac{K E t}{R}$$

or

$$K = \frac{f_b R}{E t}$$

A plot of the coefficients K required to yield a theoretical buckling stress equal to the calculated bending stress is shown in Figure 28. The buckling coefficient is plotted against the modulus of elasticity.

A summary of the beam tests conducted is presented in Table 2. Also listed are the theoretically predicted values.

Titanium has been selected as the material for the deployable beams. The primary reason for this selection was based on the energy required to flatten a deployed beam for wrapping. For an equivalent beam section, the theoretical force requirements for flattening are a ratio 14:1 in favor of titanium. It is a function of the modulus of elasticity and the cube of the material thickness. For a similar section, glass fiber requires approximately three times the thickness of titanium. It should be noted that there is very little weight advantage in favor of either material. The density ratio for titanium and glass fiber is approximately .163 to .065 or a ratio of 2.5:1.

Therefore, the density factor in favor of glass fiber is offset by the thickness factor in favor of titanium.

7.3 SUBSTRATE STUDIES

The achievement of the lightest possible substrate design is critical, since the beam strength required is directly related to the cantilevered weight. The function of the substrate is to provide a mounting surface for the solar cells. The studies reflect the result of two configurations of substrate design. One design includes the weight of a dielectric material, mesh and adhesives, and the second design does not include these items.

The basic substrate consists of a 0.003-inch sheet of 113 glass cloth using an epon 828-RP7A resin. The substrate is made up of a series of panels which are 38 inches wide and 56 inches long. The analysis of these panels assumes a simple, supported-edge condition along the long dimensions and a free-edge condition along the short dimensions. The method of analysis is taken from Ref. 1, this section, pp. A17.6, Section A17.6.

$$S_{\max} = N_2 \left[E \left(\frac{qa}{t} \right)^2 \right]^{1/3} \quad (\text{membrane stress})$$

$$S_{\max} = \text{maximum stress, psi}$$

$$F_{C_R} = \frac{KE}{R/T}$$

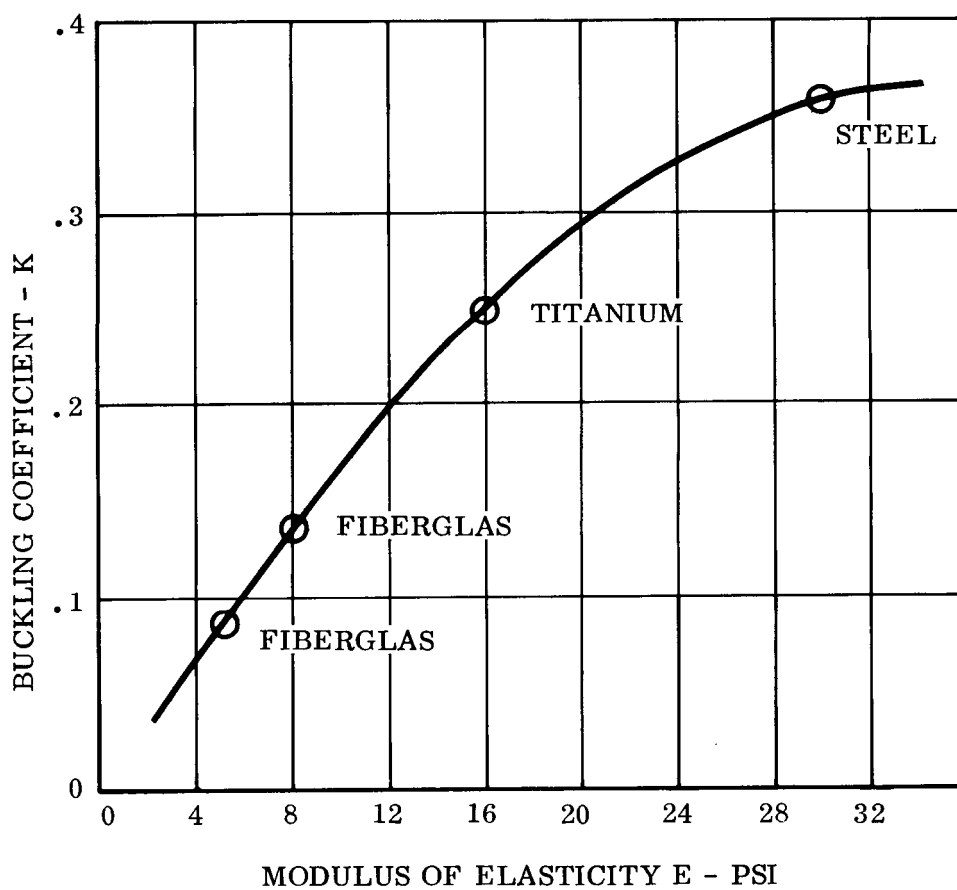


Figure 28 Modulus of Elasticity vs Buckling Coefficient

N_2 = stress coefficient, function of panel aspect ratio a/b

a = length of long side, inches

b = length of short side, inches

E = modules of Elasticity, psi

q = load intensity, psi

t = thickness, inches

$$a/b = \frac{56}{38} = 1.475$$

$$N_2 = 0.37 \text{ Ref. 1, pp. A17.6, Table A17.2}$$

Weight breakdown per complete module (38 x 56)

$$\text{Solar cells: } 0.3 \text{ lb/ft}^2 = .0021 \text{ lb/in}^2$$

$$\text{Weight} = (.0021) (38) (56) = 4.469 \text{ lb}$$

$$\text{Dielectric: } .002 \text{ inches glass fiber 108 cloth, } .065 \text{ lb/in}^3$$

$$\text{Volume} = (.002) (38) (56) = 4.256 \text{ in}^3$$

$$\text{Weight} = 4.256 \times .065 = 0.2766 \text{ lb}$$

$$\text{Adhesive: FM-1044, } .002 \text{ thick, } .010 \text{ lb/ft}^2 @ .002 \text{ in}$$

$$\text{Weight} = (0.010) (38) (56)/144 = 0.1478 \text{ lb}$$

$$\text{Mesh: Exmet Mesh 2 AG 7-2/OE, } .03 \text{ lb/ft}^2$$

$$\text{Substrate: } t = .0030 \text{ glass fiber 113 cloth epon 828-RP7A resin}$$

$$\text{Weight} = (.003) (38) (56) (.065) = 0.4140 \text{ lb}$$

$$\text{Total weight} = 5.7507 \text{ lb}$$

$$\begin{aligned}
 \text{Load density} &= 5.7507/(38)(56) = 0.00270 \text{ lb/in}^2 \text{ (1g)} \\
 &= 0.000540 \text{ lb/in}^2 \text{ (.2g)} \\
 &= 0.000676 \text{ lb/in}^2 \text{ (ULT design)}
 \end{aligned}$$

$$\begin{aligned}
 S_{\max} &= (0.37) \left[5 \times 10^6 \left(\frac{.000675 \times 56}{.003} \right)^2 \right]^{1/3} \\
 &= 342 \text{ psi ultimate}
 \end{aligned}$$

$$W_{\max} = N_1 a \left(\frac{qa}{Et} \right)^{1/3} \quad (\text{membrane deflection})$$

N_1 = deflection coefficient, function of aspect ratio a/b .

$$N_1 = 0.228 \quad \text{Ref. 1, pp A17.6, Table A17.2}$$

$$\begin{aligned}
 W_{\max} &= (0.228)(56) \left(\frac{.000675 \times 56}{5 \times 10^6 \times .0030} \right)^{1/3} \\
 &= 0.1736 \text{ inches}
 \end{aligned}$$

This deflection assumes no lateral deflection of the beams.

7.4 BEAM ANALYSIS

The method of attachment of the substrate to the beams, as illustrated in the following sketch, imposes additional loads which must be sustained by the beams.

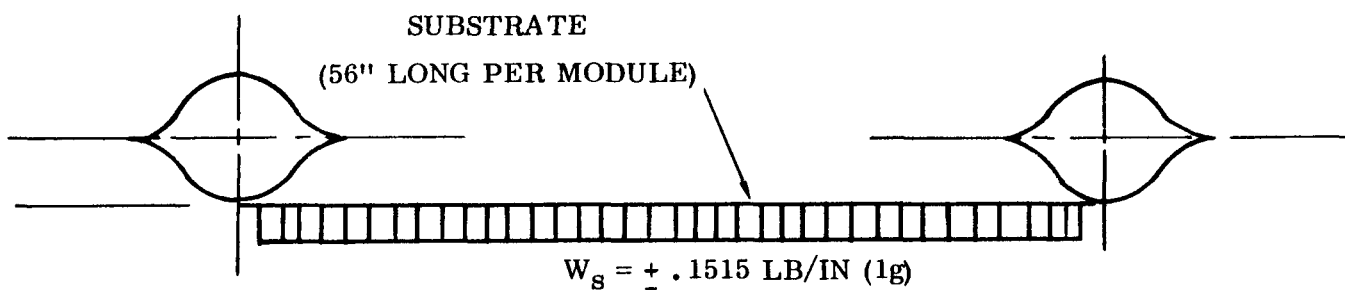
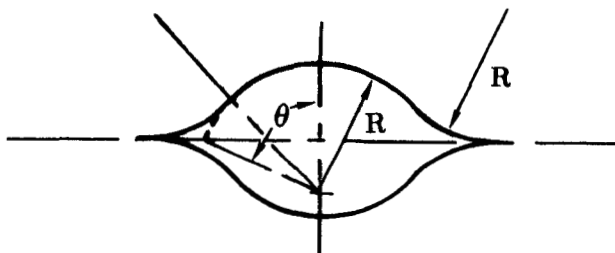


Table 2
SUMMARY - CANTILEVER BEAM TESTS

Test No.	Material	R	t	θ	M _{Test}	M _{Theory}	Remarks
1	Titanium	---	---	---	---	---	Fabricated part was warped, not used.
2	AM355 CRT	1.75	.006	53°	268	359	Error due to excessive flat area in section.
3	AM355 CRT	1.3	.0045	75°	576	546	
4	AM355 CRT	1.06	.0045	73°	420	442.6	
5	Titanium 6AL-4VA	.95	.005	82°	240	240	
6	Titanium 6AL-4VA	.90	.006	93°	288	435.2	Error due to excessive flat plate area in section.
7	Fiberglass 143 Woven	1.15	.018	68°	240	245	Parallel laminated woven
8	XP 251 S	1.60	.018	58.5°	329	352	Non woven cross laminated
9	181 Cloth	1.2	.025	68.5°	459 max. 406 min.	371	Woven parallel laminated
10	Titanium	.9	.006	90°	---	409	Not tested as of writing of this report.

NOTE: Refer to Figure 3 for photograph of test specimens.



The substrate membrane tensile stress induces a distributed load along the beam of

$$W_B = (342) (.003) = 1.026 \text{ lb/in ULT design}$$

This distributed load W_B induces a distributed torque of

$$T_B = (1.026) (.90) = 0.923 \text{ in-lb/in ULT}$$

The torque and distributed load are assumed reacted at each end of the deployable beam.

$$\text{Torque Reaction } R_T = \frac{(.923) (216)}{2} = 99.684 \text{ in-lb ULT}$$

$$\text{Shear Reaction } R_L = \frac{(1.026) (216)}{2} = 110.808 \text{ lb ULT}$$

The total weight of the composite substrate is

$$W_s = \frac{(5.7507) (216)}{56} = 22.2 \text{ lb (1 g)}$$

$$\text{Weight density} = \frac{22.2}{50} = 0.444 \text{ lb/ft}^2 \text{ (substrate only)}$$

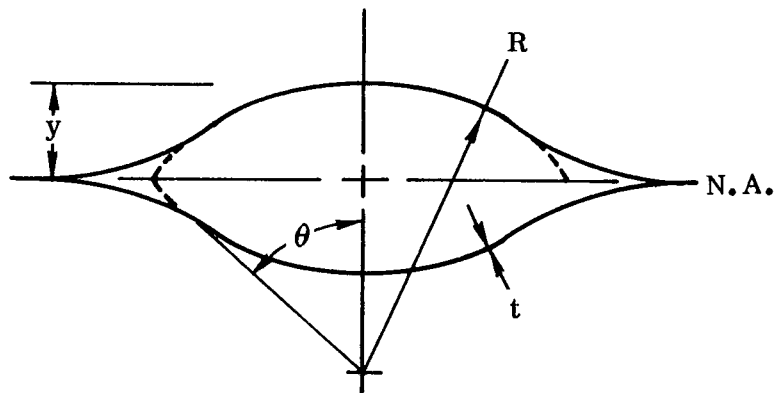
$$\begin{aligned} \text{Beam weight} &= (4) (2) (.006) (216) (.160) \\ \text{(Titanium)} &= 1.659 \text{ lb/beam} \end{aligned}$$

$$\text{Weight density} = \frac{(1.659) (2)}{50} = 0.066 \text{ lb/ft}^2$$

$$\begin{aligned} \text{Total cantilevered density} &= .066 + .444 \\ &= 0.500 \text{ lb/ft}^2 \text{ (1 g)} \end{aligned}$$

$$\begin{aligned} \text{Load per beam} &= \frac{(50) (0.500)}{(2) (216)} = 0.0579 \text{ lb/in (1 g)} \\ &= 0.01158 \text{ lb/in Limit} \\ &= 0.01448 \text{ lb/in ULT} \end{aligned}$$

$$\begin{aligned} \text{Maximum cantilever moment} &= \frac{w l^2}{2} \\ &= \frac{(0.01448) (216)^2}{2} \\ &= 337.79 \text{ in-lb ULT} \end{aligned}$$



$$t = .006 \text{ in}$$

$$R = 0.90 \text{ in}$$

$$\theta = 89^\circ$$

Material:

6AL-4V titanium

$$E = 16 \times 10^6 \text{ psi}$$

$$I = 2R^3 t K_4 \quad (\text{See Figure 29})$$

$$= (2) (.90)^3 (.006) (1.5)$$

$$= .01323 \text{ in}^4$$

$$y = K_5 R \quad (\text{See Figure 29})$$

$$= (0.98) (.90)$$

$$= .882 \text{ in}$$

$$\text{Bending stress} = f_b = \frac{Mc}{I}$$

$$= \frac{(337.79) (.882)}{(0.01323)} = 22450 \text{ psi ULT}$$

$$\text{Buckling allowable} = f_{cr} = KE \frac{t}{R}$$

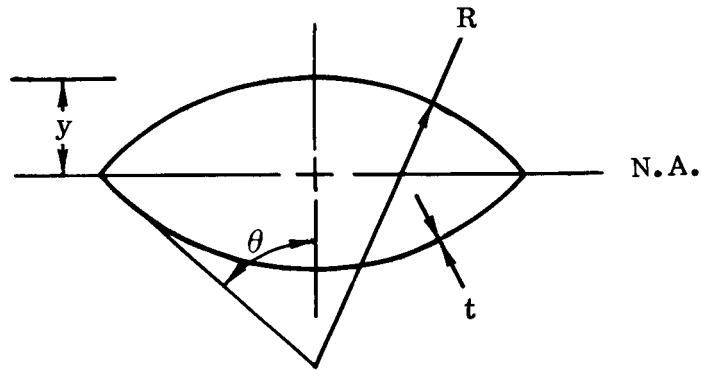
$$K = 0.25$$

$$f_{cr} = \frac{(0.25) (16) (10)^6 (.006)}{.90}$$

$$\text{Torsional stress} = f_{st} = \frac{Tc}{J}$$

$$J = 2I$$

$$= (2) (.01323) = 0.02646 \text{ in}^4$$



$$I_{NA} = IR^3 t \left[\theta + \sin \theta - \cos \theta - \frac{2 \sin^2 \theta}{\theta} + 2 \theta \left(\frac{\sin \theta}{\theta} - \cos \theta \right)^2 \right]$$

$$y = R (1 - \cos \theta)$$

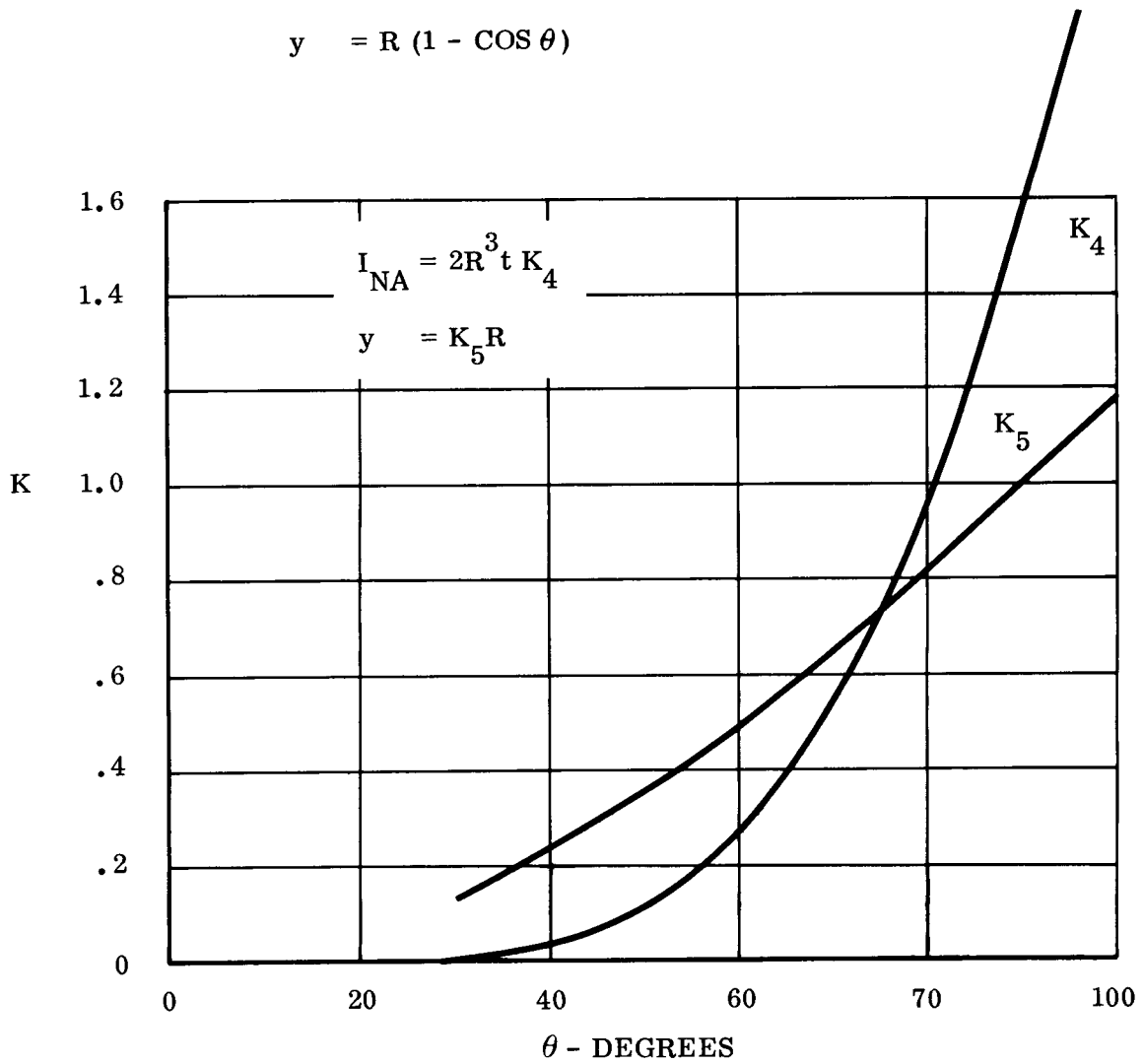
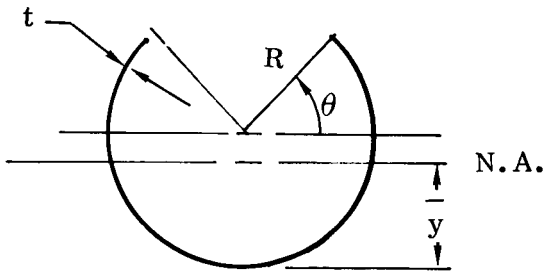


Figure 29 K vs theta - Degrees



$$\begin{aligned} I_{NA} &= 2K_6 R^3 t \\ \bar{y} &= K_7 R \end{aligned}$$

$$I_{NA} = 2tR^3 \left\{ \left[\frac{\theta}{2} - \frac{1}{4} \sin 2\theta + \frac{\pi}{4} \right] - \cos^2 \theta \right\}$$

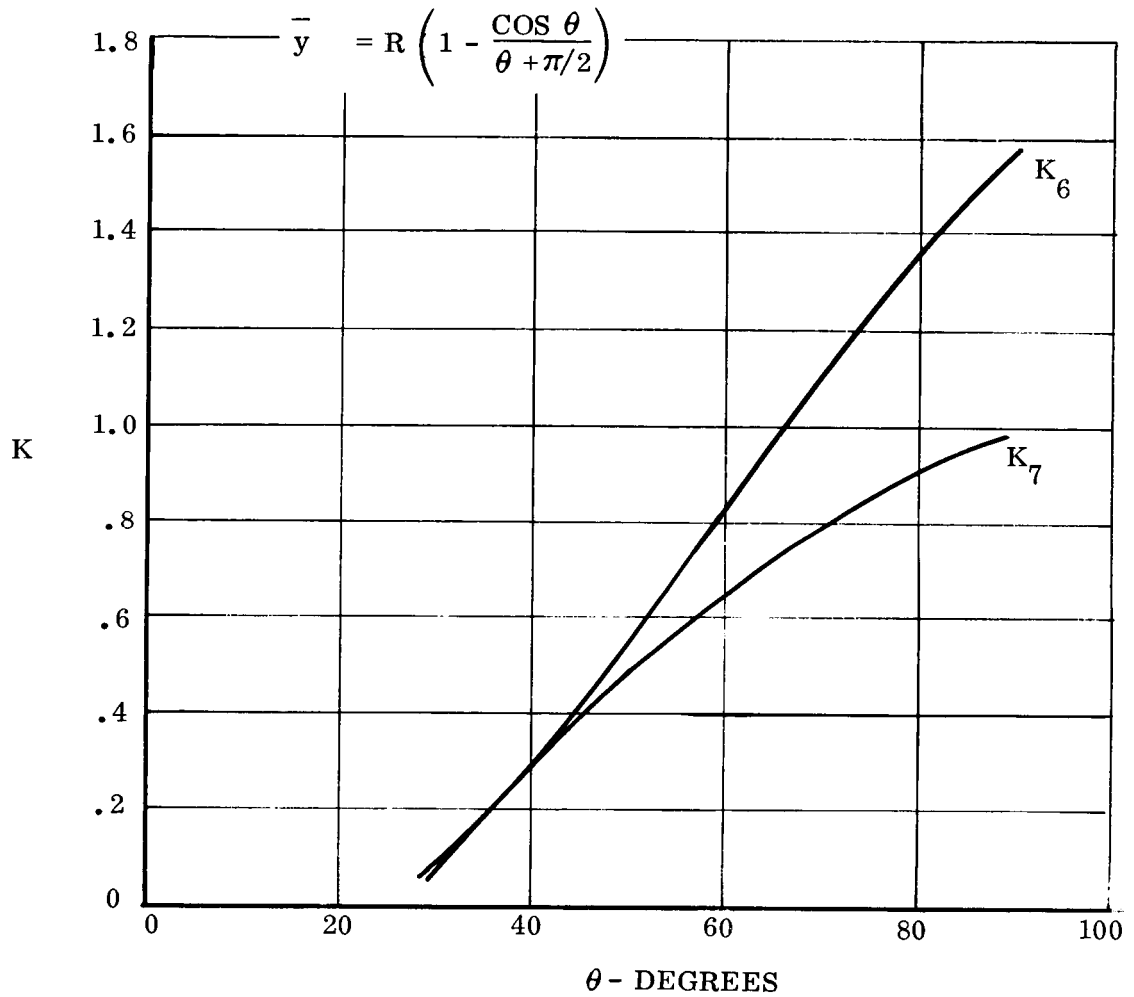


Figure 30 K vs θ - Degrees

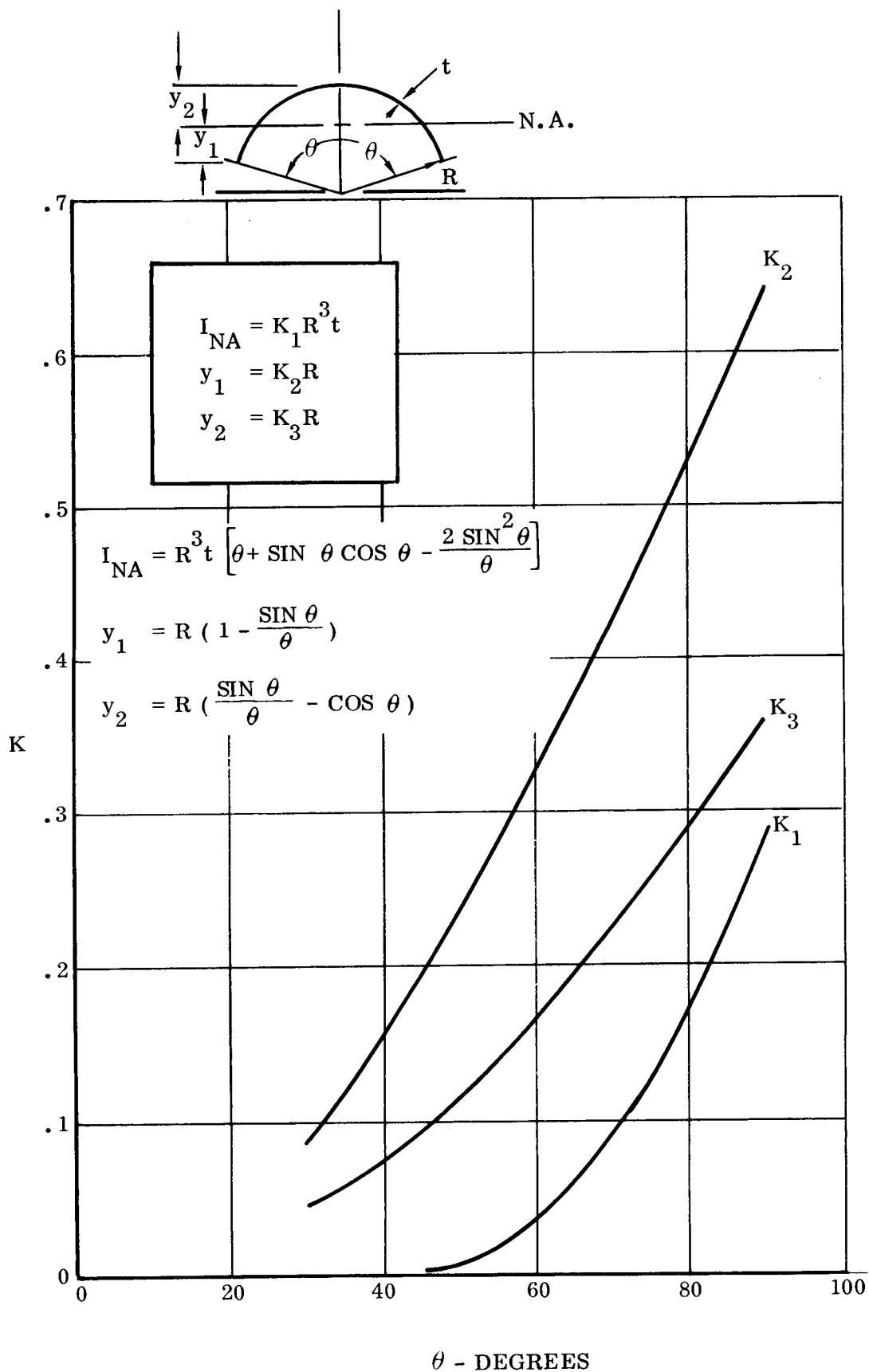


Figure 31 K vs θ - Degrees

$$f_{st} = \frac{(99.684) (.882)}{0.02646} = 3315 \text{ psi ULT}$$

$$\begin{aligned} \text{Lateral shear stress} = f_s &\cong \frac{P_L}{2ht} \cong \frac{P_L}{(2) (D) (t)} \\ &\cong \frac{(\text{No. } 808)}{(2) (1.8) (.006)} \cong 5130 \text{ psi ULT} \end{aligned}$$

$$\text{Shear buckling allowable} = F_{s_{cr}}$$

$$= KE \left(\frac{t}{b} \right)^2 + K_1 E \left(\frac{t}{R} \right) \quad \text{Ref. 2, this section}$$

$$\frac{a}{b} = \frac{216}{2.83} = 76.4$$

$$K = 4.8 \text{ (asymptotic value)}$$

$$K_1 = 0.10$$

$$\begin{aligned} F_{s_{cr}} &= (4.8) (16) (10)^6 \left(\frac{.006}{2.83} \right)^2 + (.10) (16) (10)^6 \left(\frac{.006}{.90} \right) \\ &= 345.17 + 10667 = 11,012 \text{ psi} \end{aligned}$$

Stress ratios:

$$R_s = \frac{8445}{11012} = .766$$

$$R_B = \frac{22450}{26650} = .843$$

This produces a small negative margin. Therefore, the design incorporates a small local doubler at the root of the cantilever beam. The doubler is a titanium sheet 0.50 inch wide and 0.006 inch thick. The length is determined by the following analysis.

$$R_B^2 + R_s^2 = 1$$

$$\begin{aligned}
 R_B &= (1 - R_s^2)^{1/2} \\
 &= (1 - .766^2)^{1/2} \\
 &= 0.642
 \end{aligned}$$

$$\begin{aligned}
 R_B &= \frac{f_b}{F_{cr}} \\
 &= (0.642) (26650) = 17100 \text{ psi}
 \end{aligned}$$

$$\frac{Mc}{I} = 17100$$

$$\frac{I}{c} = \frac{M}{17100} = \frac{337.79}{17100} = 0.01875 \text{ Required at root}$$

The added doubler increases the section modulus by the transfer theorem:

$$I = Ay^2$$

$$A = (0.50) (.006) = .003 \text{ in}^2$$

$$y = (0.90)$$

$$I = .00243 \text{ in}^4$$

$$I_{\text{tot}} = 0.01323 + 2 (.00243) = .01809 \text{ in}^4$$

$$= \frac{I}{c} = \frac{.01809}{.90} = 0.0201 \text{ in}^3$$

$$\text{Root margin of safety} = \frac{.0201}{.01975} - 1 = 0.02$$

To make the doubler effective, a length of 15 inches outboard and 6 inches inboard from the outer face of the outboard beam support is used. To confirm the adequacy of the length of this doubler, the following analysis is made:

$$M = \frac{W l^2}{2} = \frac{(0.01448) (201)^2}{2} = 292.5 \text{ in-lb ULT}$$

$$\begin{aligned}
 T &= T_{\text{root}} - T_B \quad (15) \\
 &= 99.684 - (0.923) \quad (15) \\
 &= 86.529 \text{ in-lb ULT}
 \end{aligned}$$

$$\begin{aligned}
 P_L^1 &= P_L = W_B \quad (15) \\
 &= 110.808 - (1.026) \quad (15) \\
 &= 96.198 \text{ in-lb ULT}
 \end{aligned}$$

$$f_b = \frac{(292.5)(.882)}{(0.01323)} = 19500 \text{ psi ULT}$$

$$R_B = \frac{19500}{26650} = 0.732$$

$$f_{st} = \frac{(86.53)(.882)}{(0.02646)} = 2884 \text{ psi ULT}$$

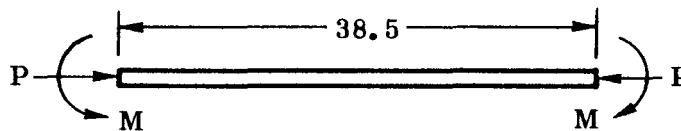
$$f_s = \frac{99.12}{(2)(1.8)(.006)} = 4589 \text{ psi ULT}$$

$$R_s = \frac{7473}{11012} = 0.679$$

$$M.S. = \frac{1}{\left(\frac{.679^2}{.679^2} + \frac{.732^2}{.732^2} \right)^{1/2}} - 1 = .0017$$

7.5 SOLAR ARRAY END BEAM ANALYSIS

The end beam, which ties the ends of the two cantilevered beams together, is loaded as a beam column



$$M = 99.684 \text{ in-lb ULT}$$

$$P = 110.808 \text{ lbs ULT}$$

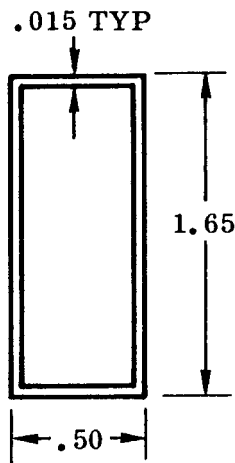
$$M_{\text{Max}} = M \sec \frac{1}{2} U \text{ at mid-length}$$

$$y_{\text{Max}} = \frac{M}{P} \left(\frac{1 - \cos \frac{U}{2}}{\cos \frac{U}{2}} \right) \text{ at mid-length}$$

$$U = \frac{\ell}{j}$$

$$j = \sqrt{\frac{EI}{P}}$$

Section Properties



$$I = \frac{(2) (1.65)^3 (.015)}{(12)} + (0.50)(.015)(.825)^2 (2)$$

$$= 0.01123 + 0.0102$$

$$= 0.02143 \text{ in}^4$$

$$j = \frac{(.02143) (10^7)}{110.808} = 44$$

$$U = \frac{38.5}{44} = 0.875$$

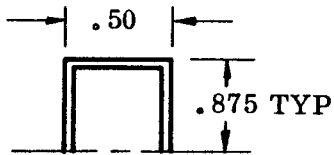
$$M_{\text{Max}} = M \sec \frac{U}{2}$$

$$= (99.684) \sec \frac{0.875}{2}$$

$$= 110 \text{ in-lb}$$

$$f_b = \frac{Mc}{I} = \frac{(110) (.875)}{0.02143} = 4491 \text{ psi ULT}$$

Buckling Allowable



$$t = 0.015 \text{ Al. Alloy 2024-T3}$$

$$\frac{a + b}{2t} = \frac{.875 + .25}{.030} = 37.5$$

Ref.

Needham, R.A.: The Ultimate Strength of Aluminum Alloy Formed Structural Shapes in Compression Journal Aeronautical Sciences, Vol. 21, April 1954

$$\frac{F_{ec}}{\sqrt{F_{cy} E}} = .023$$

$$F_{ec} = .023 (37000 \times 10^7)^{1/2} = 13,984 \text{ psi}$$

$$M.S. = \frac{13984}{4491} - 1 = \underline{\underline{High}}$$

$$y_{max} = \frac{M}{P} \left[\frac{1 - \cos \frac{U}{2}}{\cos \frac{U}{2}} \right]$$

$$= \frac{99.684}{110.808} \left[\frac{1 - \cos \frac{.875}{2}}{\cos \frac{.875}{2}} \right]$$

$$= .093 \text{ inches at mid-span}$$

Weight breakdown per module (substrate only)

$$\text{Cells: } 0.3 \text{ lbs/ft}^2 = .0021 \text{ lb/in}^2 \quad Wt = 4.469 \text{ lb}$$

Substrate: $t = .003$ glass fiber 113 cloth Epon 828-RP7A
 (38 x 56) Weight = $(.003) (38) (56) (.065) = 0.4140$ lb

Beam Wt: Wt = $(4) (2) (.006) (216) (.160)$
 (Titanium) = 1.659 lb/beam

Length = 216 in

$$\begin{aligned}\text{Substrate wt density} &= \frac{4.883}{38 \times 56} = .00229 \text{ lb/in}^2 \\ &= .339 \text{ lb/ft}^2 \quad (1g) \\ &= .000458 \text{ lb/in}^2 \quad (.2g) \\ &= .000606 \text{ lb/in}^2 \text{ ULT}\end{aligned}$$

$$\begin{aligned}s_{\max} &= (0.37) 5 \times 10^6 \left(\frac{.000606 \times 56}{.003} \right)^2 \quad 1/3 \\ &= 318.6 \text{ psi ULT} \quad \begin{array}{l} \text{Substrate Membrane} \\ \text{stress tensile} \end{array}\end{aligned}$$

Distributed lateral load on beams induced by substrate tensile stress is

$$W_B = (318.6) (.003) = 0.956 \text{ lb/in ULT}$$

This distributed load W_B induces a distributed torque of

$$T_B = (0.956) (.90) = 0.86 \text{ in-lb/in ULT}$$

The torque and distributed load are assumed reacted at each end of the deployable beam.

$$\text{Torque reaction } R_T = \frac{(0.86) (216)}{2} = 92.88 \text{ in-lb ULT}$$

$$\text{Shear reaction } R_L = \frac{(0.956) (216)}{2} = 103.248 \text{ lb ULT}$$

The solar array weight density is

$$.339 + \frac{2 \times 1.659}{50} = 0.405 \text{ lb/ft}^2 \text{ (1g)}$$

(Cantilevered weight density)

$$\begin{aligned} \text{Load per beam} &= \frac{(50) (.405)}{(2) (216)} = .0468 \text{ lb/in (1g)} \\ &= .00936 \text{ lb/in limit} \\ &= .0117 \text{ lb/in ULT/beam} \end{aligned}$$

$$\begin{aligned} \text{Maximum cantilever moment} &= \frac{w \ell^2}{2} \\ &= \frac{(.0117) (216)^2}{2} \\ &= 277.44 \text{ in-lb ULT} \end{aligned}$$

$$I = 0.01323 \text{ in}^4$$

$$y = 0.882 \text{ in}$$

$$\begin{aligned} \text{Bending stress} &= f_b = \frac{Mc}{I} \\ &= \frac{277.44 (.882)}{.01323} = 18460 \text{ psi ULT} \end{aligned}$$

$$\begin{aligned} \text{Buckling allowable} &= F_{cr} = KE t/r \\ &= 26650 \text{ psi} \end{aligned}$$

$$\begin{aligned} \text{Torsional stress} &= f_{st} = \frac{Tc}{J} \\ &= \frac{(92.88) (.882)}{(.02646)} = 3092 \text{ psi ULT} \end{aligned}$$

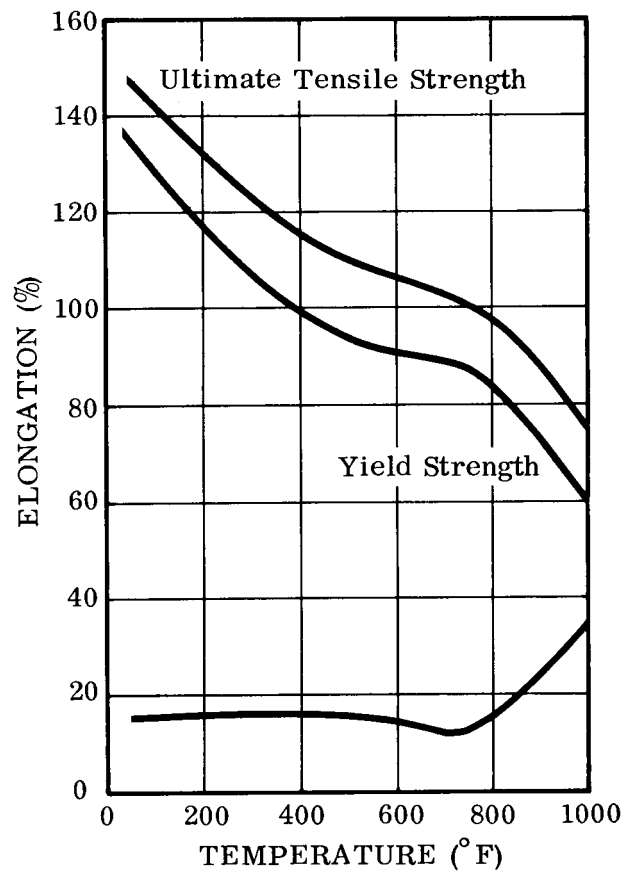
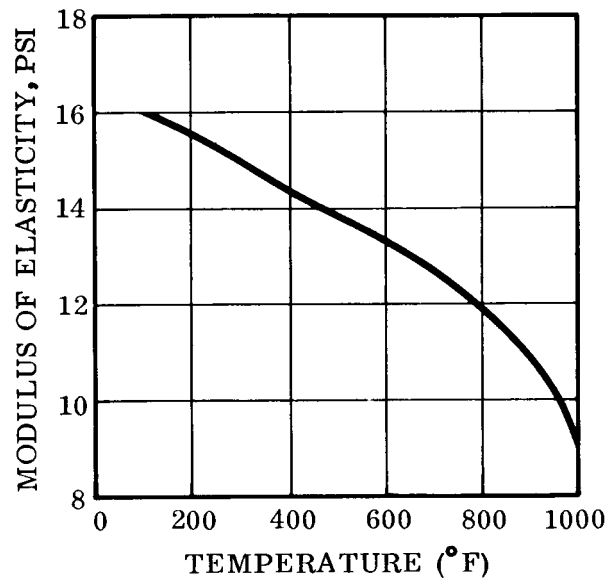


Figure 32 Elevated Temperature Properties

$$\text{Lateral shear stress} = \frac{P}{2ht}$$

$$= \frac{103.248}{(2) (1.8) (.006)} = 4785 \text{ psi ULT}$$

$$\text{Shear buckling allowable} = F_{scr} = KE (t/b)^2 + K E \frac{t}{R} \quad \text{Ref: 2}$$

$$= 11,012 \text{ psi}$$

Stress Ratios:

$$R_B = \frac{18460}{26650} = 0.6925$$

$$R_S = \frac{7877}{11012} = 0.715$$

$$M.S. = \frac{1}{(0.6925)^2 + 0.715^2}^{1/2} - 1 = \underline{\underline{0.005}}$$

7.6 THERMAL STRESS AND DEFORMATIONS

The analysis presented here is a preliminary study to investigate the effects of the temperatures and temperature gradients which have been determined in the heat transfer analysis. Based on the highly polished titanium surface the maximum temperatures to be expected would be approximately 850° R. Realistically, the maximum temperatures which can be expected are on the order of 750° R. This temperature is based on a partially oxidized surface. The effects of temperature on titanium (6AL-4V) are presented in Figure 32. Should these temperatures present a problem, proper surface conditions can reduce the temperature levels to the range of 650 to 700° R.

For the purposes of this analysis, the partially oxidized condition, with its corresponding temperature level of 750° R (290° F), is assumed. The maximum thermal gradient between the upper and lower surfaces of the beam is 151° F. Although a preliminary temperature distribution around the cross section of the beam is presented in Section 5.0, the maximum gradient of 151° F is used in the analysis.

The fictitious bending stress induced by the thermal gradient is given by

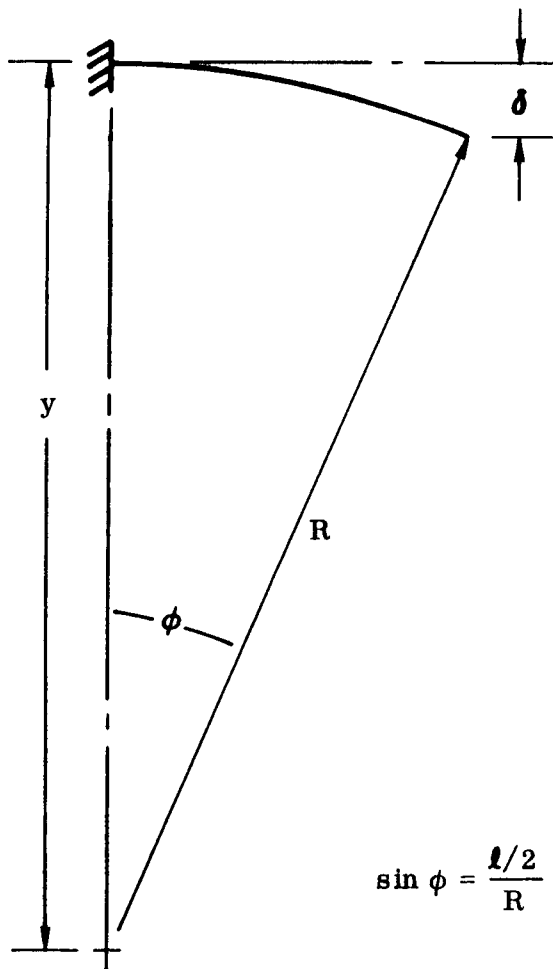
$$f_b = E \alpha \Delta T$$

E = Modulus of elasticity, 15.1×10^6 psi, avg.

α = Coefficient of thermal expansion, 5.2×10^{-6} in/in/° F

$$f_b = 15.1 \times 10^6 \times 5.2 \times 10^{-6} \times \frac{151}{2}$$

$$= 5929 \text{ psi}$$



$$\frac{1}{R} = \frac{M}{EI}$$

$$M = \frac{f_b I}{c}$$

$$\frac{1}{R} = \frac{f_b I}{cEI} = \frac{f_b}{cE}$$

$$R = \frac{cE}{f_b}$$

$$c = .882 \text{ in}$$

$$E = 15.1 \times 10^6 \text{ psi at } 290^\circ \text{ F}$$

$$f_b = 5929 \text{ psi thermal stress (fictitious)}$$

$$R = \frac{(.882)(15.1 \times 10^6)}{5929} = 2240 \text{ in}$$

$$l = 216 \text{ in, beam cantilever length}$$

$$R = 2240 \text{ in}$$

$$\sin \phi = \frac{l/2}{R}$$

$$\sin \phi = \frac{(108)}{(2240)} = .0482$$

$$\phi = 2^\circ 46'$$

$$\delta = R - y$$

$$\cos \phi = \frac{y}{R}$$

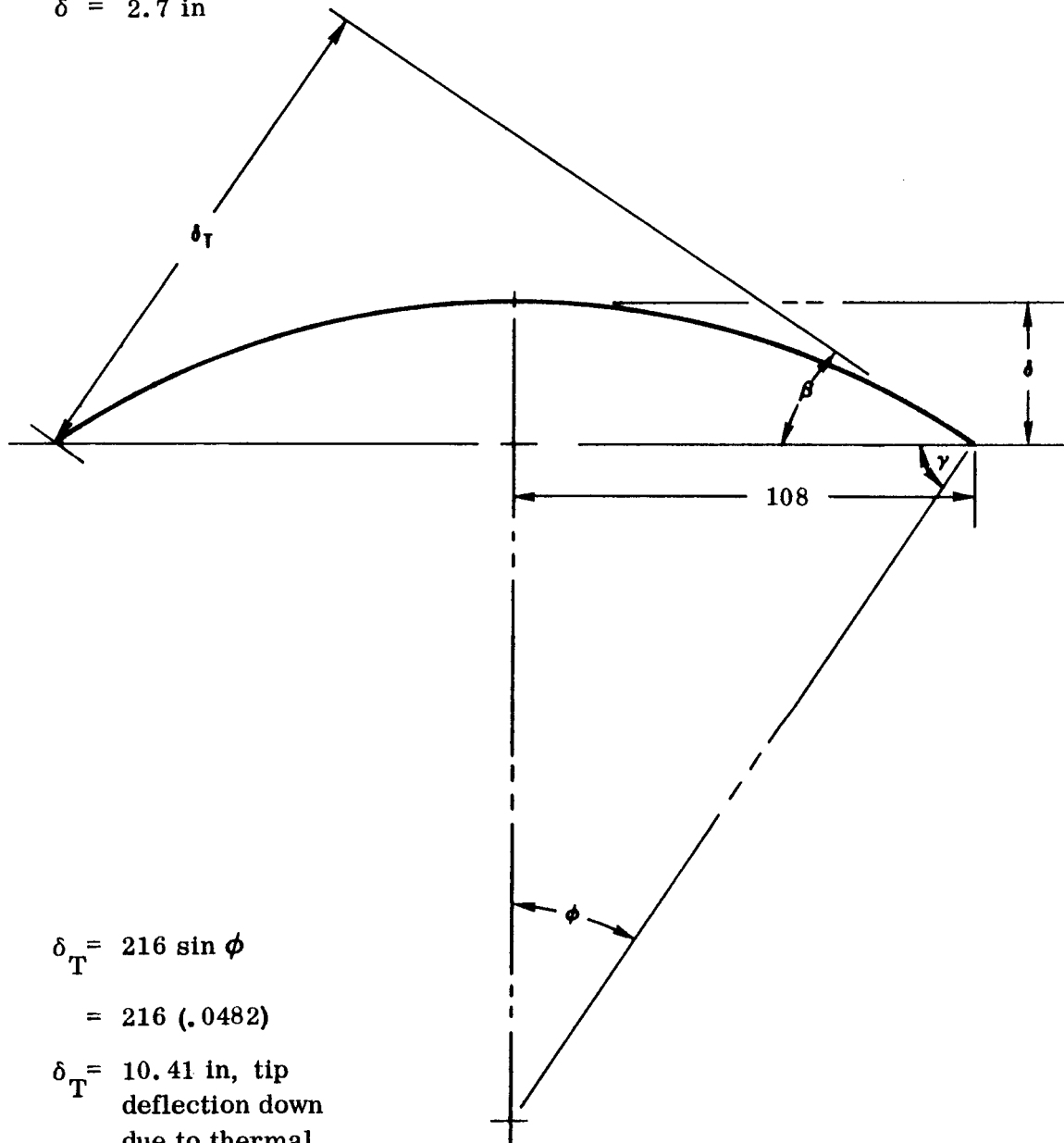
$$y = R \cos \phi$$

$$\delta = R - R \cos \phi$$

$$= R (1 - \cos \phi)$$

$$= 2240 (1 - .9988)$$

$$\delta = 2.7 \text{ in}$$



$$\delta_T = 216 \sin \phi$$

$$= 216 (.0482)$$

$$\delta_T = 10.41 \text{ in, tip deflection down due to thermal deformation}$$

To alleviate the problem presented by the tip deflection, the beam surfaces will be given a surface treatment which yields a gradient of 79° F and a maximum temperature level of 731° R . The surface conditions to attain this level of temperatures are for a black or white painted surface on the inside and a partly oxidized surface on the outside.

$$f_b = E \alpha \Delta T$$

$$E = 15.2 \times 10^6 \text{ psi at } 271^{\circ}\text{ F}$$

$$\alpha = 5.2 \times 10^{-6} \text{ in/in/}^{\circ}\text{ F}$$

$$\Delta T = 79^{\circ}\text{ F}$$

$$\begin{aligned} f_b &= (15.2 \times 10^6) (5.2 \times 10^{-6}) \frac{(79)}{2} \\ &= 3115 \text{ psi (thermal stress), fictitious stress} \end{aligned}$$

$$R = \frac{cE}{f_b}$$

$$= \frac{(.882) (15.2 \times 10^6)}{3115} = 4300$$

$$\sin \phi = \frac{108}{4300} = .025$$

$$\phi = 1^{\circ} 26'$$

$$\delta_T = 216 \sin \phi$$

$$\beta = \phi$$

$$\delta_T = (216) \sin 1^{\circ} 26'$$

$$= 5.4 \text{ in}$$

$$M.S. = \frac{1}{(R_B^2 + R_S^2)} - 1 = 0$$

$$R_B^2 + R_S^2 = 1$$

$$R_B = (1 - R_S^2)^{1/2}$$

$$= (1 - .715^2)^{1/2}$$

$$= (1 - .511)^{1/2}$$

$$= .699$$

$$R_B = \frac{f_b}{F_{CR}} = \frac{M/Z}{KE t/R} = \frac{M R K_5 R}{KE t 2R^3 t K_4}$$

where

$$I = 2R^3 t K_4$$

$$y = K_5 R$$

$$t^2 = \frac{M K_5}{2KER K_4 R_B} = \frac{(277.44) (.98)}{(2) (.23) (15.2 \times 10^6) (.90) (1.5) (.699)}$$

$$= \frac{271.89}{6.598 \times 10^6} = 41.208 \times 10^{-6}$$

$$t = .00642 \text{ in required}$$

This thickness requirement is for the lightweight version of the substrate design.

The substrate design, which includes the dielectric, adhesives, and mesh, has a root bending moment of 337.79 in-lb ULT. The following analysis calculates the thickness requirements for this case:

$$t^2 = \frac{M K_5}{2 K E R K_4 R_B}$$

$$= \frac{337.79}{6.598 \times 10^6} = 51.20 \times 10^{-6}$$

$$t_{\text{req'd}} = 0.00723 \text{ in}$$

This greater thickness requirement would increase the solar array weight density from 0.500 lb/ft² to 0.512 lb/ft². It would also increase the cantilever moment from 337.8 in-lb ULT to 345.9 in-lb ULT.

On the basis of the preceding analysis, it is recommended that a 0.0065-in sheet of titanium be employed for the beam and an internal or external resistance-welded doubler be used at the beam root to increase the beam strength to that required to sustain the added stresses caused by the thermal gradient. Other acceptable means would be to chem-mill a greater thickness of material, tapering the thickness requirements as needed.

7.7 DEPLOYMENT CONSIDERATIONS FOR RETROFIRE

The selected beam configuration is analyzed to determine the acceptable cantilever length which will sustain retrofire loads. The retrofire load factors are as follows:

$$n_v = 6g \quad \text{vertical down}$$

$$n_L = 1g \quad \text{lateral}$$

Running load per beam = .0579 lb/in vertical (1g)

$$\text{Max. vert. moment per beam} = \frac{(.0579) (6) (1.25) (1^2)}{2}$$

$$= 0.217 \frac{2}{1} \text{ lb/in ULT}$$

$$\ell_1 = \frac{M_v}{.217}^{1/2} \quad \text{for vertical moment}$$

$$\text{Lateral running load per beam} = \frac{1.659}{216} = .00767 \text{ lb/in (1g)}$$

(own weight)

$$\text{Substrate Weight} = 22.2 \text{ lbs (1g)}$$

Assuming that all of the substrate inertial force in the lateral direction is resisted by one beam, the running load is

$$\text{Lateral running load} = \frac{22.2}{216} = .1027 \text{ lb/in (1g)}$$

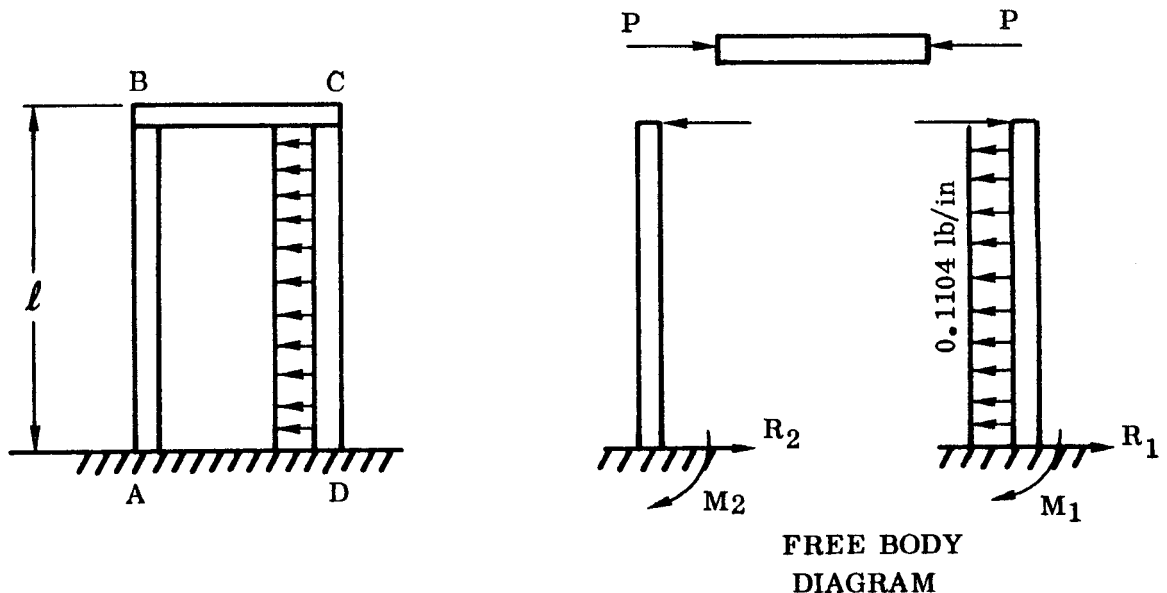
(substrate weight)

This lateral running load induced into the beam by the substrate weight causes a running torsion load of

$$T^1 = .1027 \text{ lb/in} (.90) = .09243 \text{ in-lb/in (1g)}$$

$$\text{Torque arm} = 0.90 \text{ in}$$

Lateral Loads Analysis



In order to determine the internal load distribution of the distributed load on member CD, the analysis assumes that the tip deflection of beam AB must equal the tip deflection of beam CD. The joints at B and C are assumed pinned.

$$\delta_B = \delta_C$$

$$\delta_B = \frac{P\ell^3}{3EI}$$

$$\delta_C = \frac{W\ell^4}{8EI} - \frac{P\ell^3}{3EI}$$

$$\frac{2P\ell^3}{3EI} = \frac{W\ell^4}{8EI}$$

$$P = \frac{3W\ell}{16}$$

$$\ell_{\text{Allow}} = \frac{16P}{3W}$$

$$M_2 = P$$

$$P = M_{2/\ell}$$

$$\ell_{\text{Allow}}^2 = \frac{16 M_2}{3 W} \quad \text{based on } M_2$$

$$M_1 = \frac{w\ell^2}{2} - P\ell$$

$$P = \frac{M_1 - \frac{w\ell^2}{2}}{\ell}$$

$$\ell_{\text{Allow}} = \frac{16}{3W} \left(\frac{M_1 - \frac{w\ell^2}{2}}{\ell} \right)$$

$$\ell_{\text{Allow}}^2 = \frac{16 M_1}{3W} - \frac{8}{3} \ell^2$$

$$\ell_{\text{Allow}}^2 + \frac{8}{3} \ell^2 = \frac{16 M_1}{3W}$$

$$\ell^2 \left(1 + \frac{8}{3}\right) = \frac{16 M_1}{3W}$$

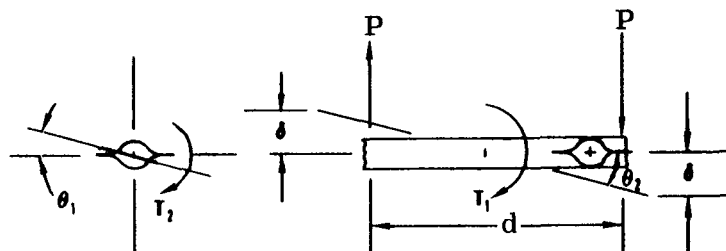
$$\ell_{\text{Allow}}^2 = \frac{16 M_1}{3W \left(1 + \frac{8}{3}\right)} = \frac{(16) M_1 (3)}{3W (3 + 8)}$$

$$\ell_{\text{Allow}}^2 = \frac{16 M_1}{11W} \quad \text{based on } M_1$$

Since the allowable load in either beam is equal, the maximum beam length allowable is given by

$$\ell_{\text{Allow}} = \sqrt{\frac{16 M_{\text{Allow}}}{11W}} \quad \text{for lateral moment}$$

Torsional Load Analysis



VIEW LOOKING INBOARD

Torsional load is assumed distributed in a 3:1 ratio.

T = Total torque, in-lb

$$T_2 = 0.75 T$$

$$T_1 = 0.25 T$$

$$T = W(.9) \ell$$

$$\therefore T_2 = .75 W (.9) \ell$$

$$= (.75) (.1104) (.9) \ell$$

$$= .0745 \ell$$

$$f_{s_t} = \frac{T_c}{J}$$

$$= \frac{(.0745 \ell) (.882)}{.02646} = 2.483 \ell$$

Let

$$f_{s_t} = F_{s_{cr}}$$

$$\ell_{\text{Allow}} = \frac{F_{s_{cr}}}{2.483}$$

Allowable Deployed Spans

The allowable deployed spans calculated are based on individual loading conditions only. A combined loading analysis has not been attempted at this stage of the program. This analysis has been made to obtain an indication of the allowable span which could be deployed without jeopardizing its structural integrity during the retrofire sequence.

Maximum vertical bending moment:

$$\ell_{\text{Allow}} = \left(\frac{M_v}{.217} \right)^{1/2}$$

$$M_v = 337.5 \text{ in-lb ULT allowable}$$

$$= \left(\frac{337.5}{.217} \right)^{1/2} = 39.4 \text{ in}$$

Maximum torsional moment:

$$\ell_{\text{Allow}} = \frac{F_{s_{\text{cr}}}}{2.483} = \frac{11012}{2.483} \text{ not critical}$$

Maximum lateral bending moment:

$$\ell_{\text{Allow}} = \left(\frac{16M_L}{11W} \right)^{1/2}$$

Since test data are lacking on the moment capability of the beam to resist lateral loads, the moment M_L is given the value of M_V . This is a conservative assumption.

$$\ell_{\text{Allow}} = \left(\frac{16 \times 337.5}{11 \times .1104} \right)^{1/2} = 66.6 \text{ in}$$

The maximum allowable length for the retrofire condition would be something less than 39.4 inches. There does not appear to be any advantage in providing for a partially extended solar array during the retrofire mode.

7.8 TORQUE DRUM

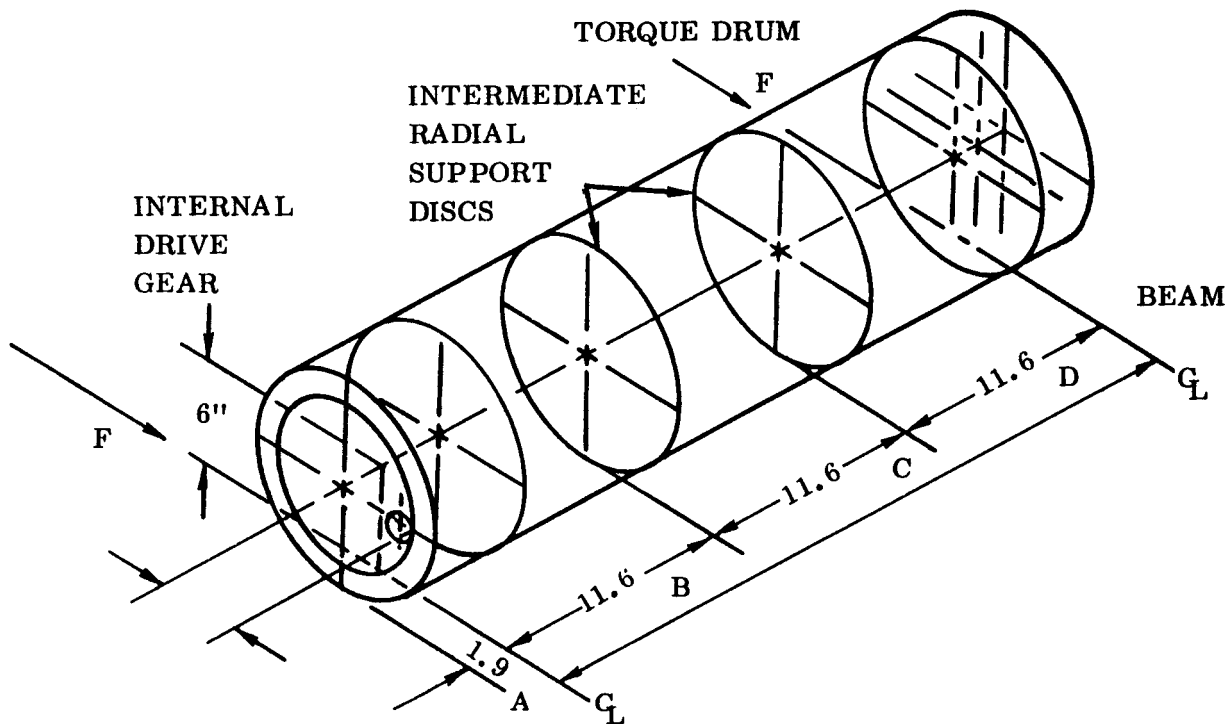
The torque drum is designed to transmit the drive torque to the two deployable beams. A drive torque based on a 20-lb axial beam force is considered for analysis. Temperatures are considered, conservatively, not below 75° F.

Tangential shear load on gear teeth

$$= 2(F) \left(\frac{6}{5} \right)$$

$$= 2 (20 \times 1.25) \left(\frac{6}{5} \right) = 60 \text{ lb ULT}$$

$$\cong \frac{60}{2} = \underline{\underline{30}} \text{ lb ULT/tooth}$$

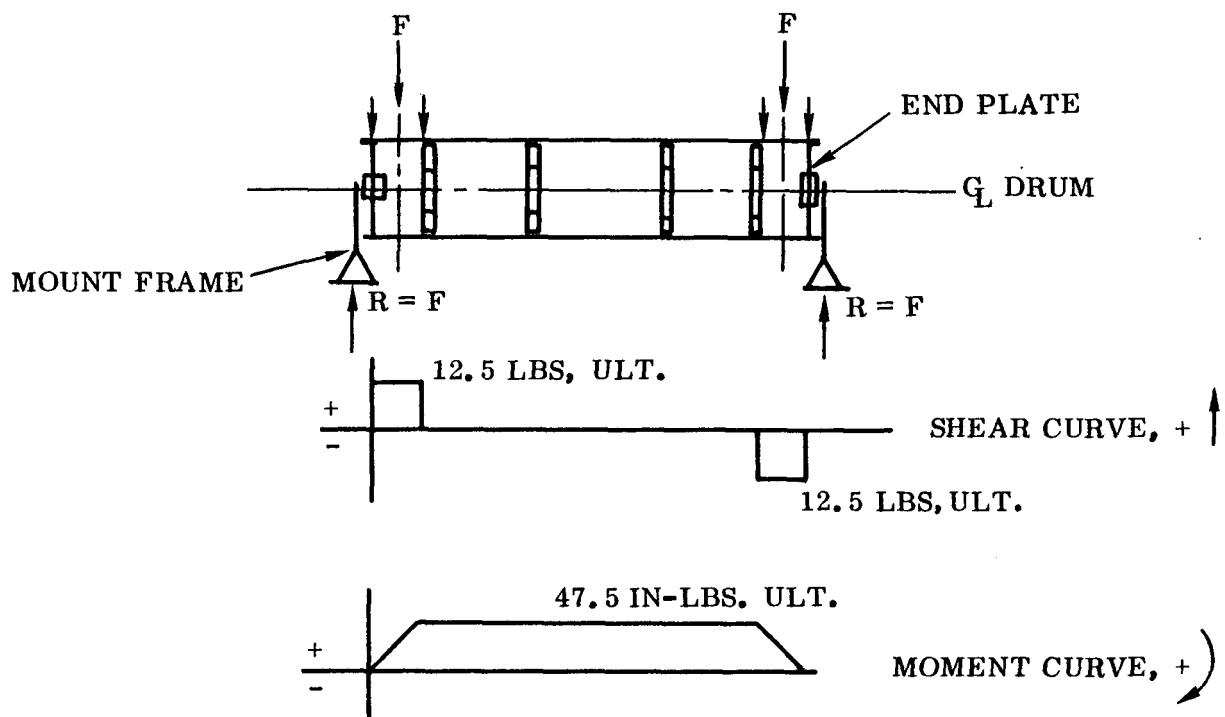


$$\text{Torque in motor shaft} = 60 \times .375'' = \underline{22.5} \text{ in-lb ULT}$$

$$\begin{aligned} \sum \text{Torque in torque drum} &= (F \times \frac{1}{2} F) \times 6 \\ &= (20 \times 1.25 + \frac{1}{2} \times 20 \times 1.25) \times 6 \\ &= \underline{225} \text{ in-lb ULT} \\ &= \text{Max. torque in Section A} \end{aligned}$$

$$\begin{aligned} \text{Torque in Sections B, C and D} &= (F) \times 6 \\ &= (1.25 \times 20) \times 6 \\ &= \underline{150} \text{ in-lb ULT} \end{aligned}$$

Only one-half the shear due to forces, F , is carried as a beam in the torque drum. The other half is transmitted directly into the mount frame through the end plate.



The above curves are slightly conservative because radial support provided by the rollers, which transmit radial load through springs to the roller housing, is neglected.

If we consider the torque drum as a continuous drum between beam centerlines without intermediate support discs,

$$F_{S_{CR}} = KE \left(\frac{t_{\text{Effective}}}{r} \right)^{1.35} \quad \text{Ref. Roark, Pg. 317 for clamped ends}$$

$$K \cong .60 \text{ (by extrapolation)}$$

$$\text{For } \frac{l}{r} = \frac{38.5}{6} = 6.4$$

$$t_{\text{Effective}} = .70 \times t = .70 \times .020 = .014$$

$$F_{S_{CR}} = .60 \times 10^7 \left(\frac{.014}{6} \right)^{1.35} = 1680 \text{ psi}$$

$$f_s = \frac{\tau}{2A} = \frac{\tau}{2\pi r^2 t} = \frac{150}{2\pi \times 6^2 \times .014} = 47 \text{ psi ULT}$$

M.S. \rightarrow HIGH

Torsion analysis of the torque drum indicates that the prime concern is radial load-carrying ability and not torsion.

If we assume the drum is infinitely long when under a uniform radial pressure, such as would occur with the substrate in the stowed position, the elastic stability allowable is

$$P_{CR} = \frac{3 EI}{r^3} \quad \text{Ref. Roark, Pg. 318}$$

$$I_{\text{Effective}} = \frac{t^3}{12} \times .70 = \frac{.020^3}{12} \times .70$$

$$= .47 \times 10^{-6} \text{ in}^4/\text{in}$$

$$P_{CR} = \frac{3 \times 10^7 \times .47 \times 10^{-6}}{6^3} = .065 \text{ psi} = \underline{9.4} \text{ lb/ft}^2$$

If we consider effects of intermediate radial support discs,

$$P = KE \left(\frac{t}{2r} \right)^3$$

where $K = 120$

Ref. NACA TN

For

$$\frac{l}{r} = \frac{11.6}{6} = 1.9$$

$$\frac{2r}{t_{\text{Eff.}}} = \frac{2 \times 6}{.014} = 857$$

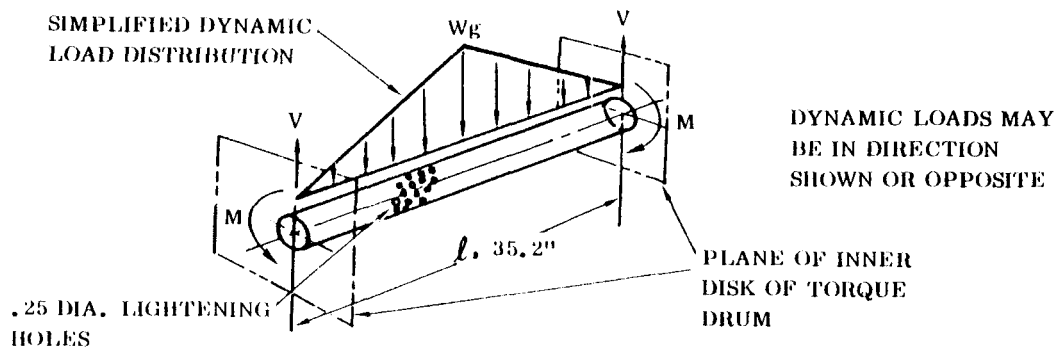
$$P = 120 \times 10^7 \left(\frac{.014}{2 \times 6} \right)^3 = \underline{1.9} \text{ psi}$$

7.9 DRIVE AND SUPPORT MECHANISM

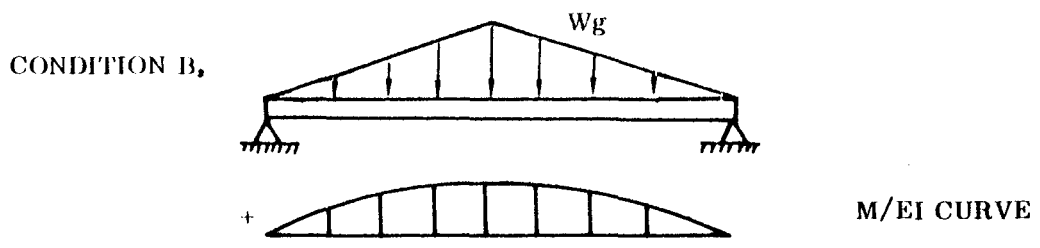
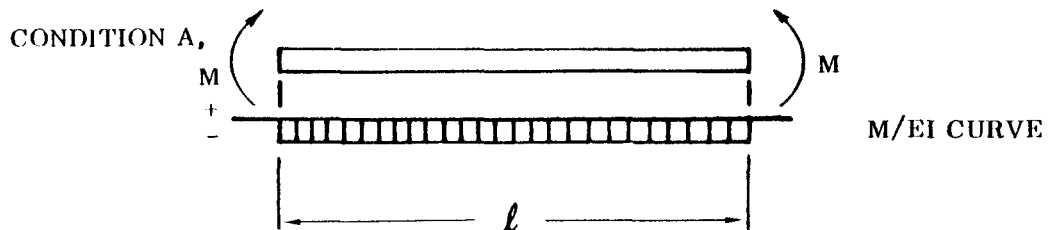
This analysis is based on nominal sheet thicknesses.

Wire Conduit

The wire conduit is analyzed for dynamic vibration which occurs during launch if the tube is excited at its fundamental frequency. Dynamic loads are treated as static loads. A dynamic amplification factor of 16.7:1 is based on a structural damping ratio of .03. Analysis is based on no intermediate support rings. It is considered that dynamic wire loads are not coupled with dynamic tube loads and are therefore not superimposed.



M is maximum at the ends and is determined by letting the sum of the areas under the M/EI curves for the following conditions be equal to the change in slope between the beam ends.



$$\sum \frac{M}{EI} \Big|_0^{\ell} = \text{Slope} = 0$$

EI is cancelled for a uniform beam:

$$\text{Slope} = 0 = \left(\frac{Wg \ell^2}{12} \right) \left(\frac{2}{3} \right) - M$$

$$\begin{aligned} M_{(\text{Max})} &= \frac{(W)(g) \ell^2}{18} \\ &= \frac{(.0021)(1.6 \times 1.4.4 \times 16.7 \times 1.25) \times 35.2^2}{18} \\ &= 6.8 \text{ in-lb ULT} \end{aligned}$$

$$\begin{aligned} V &= \frac{(W)(g)}{2} = \frac{(.0021)(1.6 \times 1.414 \times 16.7 \times 1.25) \times 35.2}{2} \\ &= \underline{1.7} \text{ lb ULT} \end{aligned}$$

$$f_{s(\text{Avg.})} = \frac{V}{Dt_{(\text{Eff.})}} = \frac{1.7}{2 \times (.010 \times .5)} = \underline{54} \text{ psi avg.}$$

$$f_b = \frac{Mr}{I}$$

$$I_{(\text{Effective})} = .50 (r^3 t) = .50 (1^3 \times .010) = .016 \text{ in}^4$$

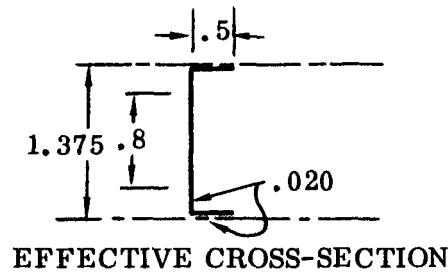
$$f_b = \frac{6.8 \times 1}{.016} = 425 \text{ psi}$$

$$F_{CR} = \frac{.225 E_c}{r/t} = \frac{.225 \times 3 \times 10^6}{1/.010} = 6750 \text{ psi}$$

M.S. → HIGH

The conduit should be considered designed from a handling standpoint rather than for an environmental loading condition.

Elastic Stability of Intermediate Rings under a Uniform External Radial Pressure



$$I = 2(A)d^2 + \Sigma \frac{t(2d)^3}{12} = 2(.5 \times .040) (.70)^2$$

$$+ \frac{.020}{12} \left[(1.375)^3 - (.8)^3 \right]$$

$$I = .0196 + .0035 = .0231 \text{ in}^4$$

$$P = \frac{3EI}{R^3} = \frac{3 \times 10^7 \times .0227}{(5.3)^3} = 4570 \text{ lb/in}$$

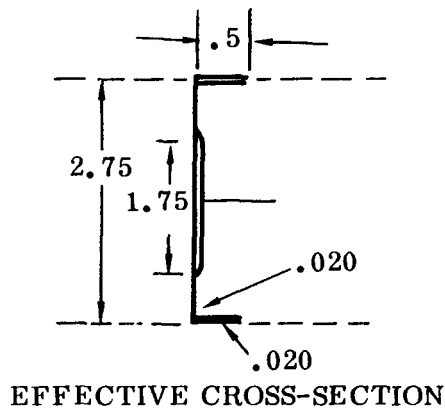
$$\text{Compression Stress} = \frac{PR}{A} = F_{cy}$$

$$P = \frac{F_{cy} \cdot A}{R} = \frac{35000 \times .0515}{5.3} = 340 \text{ lb/in yield}$$

Required capability based on elastic buckling of torque drum cylinder

$$= 1.9 \times 12 = 23 \text{ lb/in}$$

Elastic Stability of End Rings under a Uniform External Radial Pressure



$$I = 2(A)d^2 + \Sigma \frac{t(2d)^3}{12} = 2(.5 \times .040) (1.375)^2$$

$$+ \frac{.020}{12} [(2.75)^3 - (1.75)^3]$$

$$I = .0756 + .0257 = .1013 \text{ in}^4$$

$$P = \frac{3EI}{R^3} = \frac{3 \times 10^7 \times .1013}{(4.6)^3} = 31220 \text{ lb/in, neglecting conservative effects of cylinder.}$$

$$\text{Compression stress} = \frac{PR}{A} = F_{cy}$$

$$P = \frac{F_{cy} \cdot A}{R} = \frac{35000 \times .060}{4.6} = 457 \text{ lb/in yield}$$

Required capability based on elastic buckling of torque drum cylinder

$$= 1.9 \times 7.6 = \underline{14} \text{ lb/in}$$

M.S. → HIGH

7.10 SOLAR ARRAY GROWTH POTENTIAL

Growth potential of the size of the total solar array system beyond the 200 square feet reflected in the design presented in this report is illustrated in Figure 33. Such growth is obtained by an increase in cantilever length, since the width restriction and the four-blade concept must be maintained. The analysis made in the development of results shown in Figure 33 makes use of the same general beam parameters as those given previously in this report.

A further study has been made with respect to the addition of the variable parameter of aspect ratio. The results of this study are presented in Figure 34.

7.11 REFERENCES

E. F. Bruhn, "Analysis and Design of Flight Vehicle Structures," Tri-State Offset Company, 1965.

D. J. Perry, "Aircraft Structures," McGraw-Hill Company, New York, N.Y.

- NOTES:
1. STUDY BASED ON 38.5 INCH WIDTH
 2. WEIGHT DOES NOT INCLUDE DRIVE MECHANISM OR SUPPORT STRUCTURE
 3. BASED ON ONE BLADE OF A FOUR BLADE SYSTEM
 4. INCLUDES 0.3 LB/FT^2 FOR SOLAR CELLS AND PROVISIONS

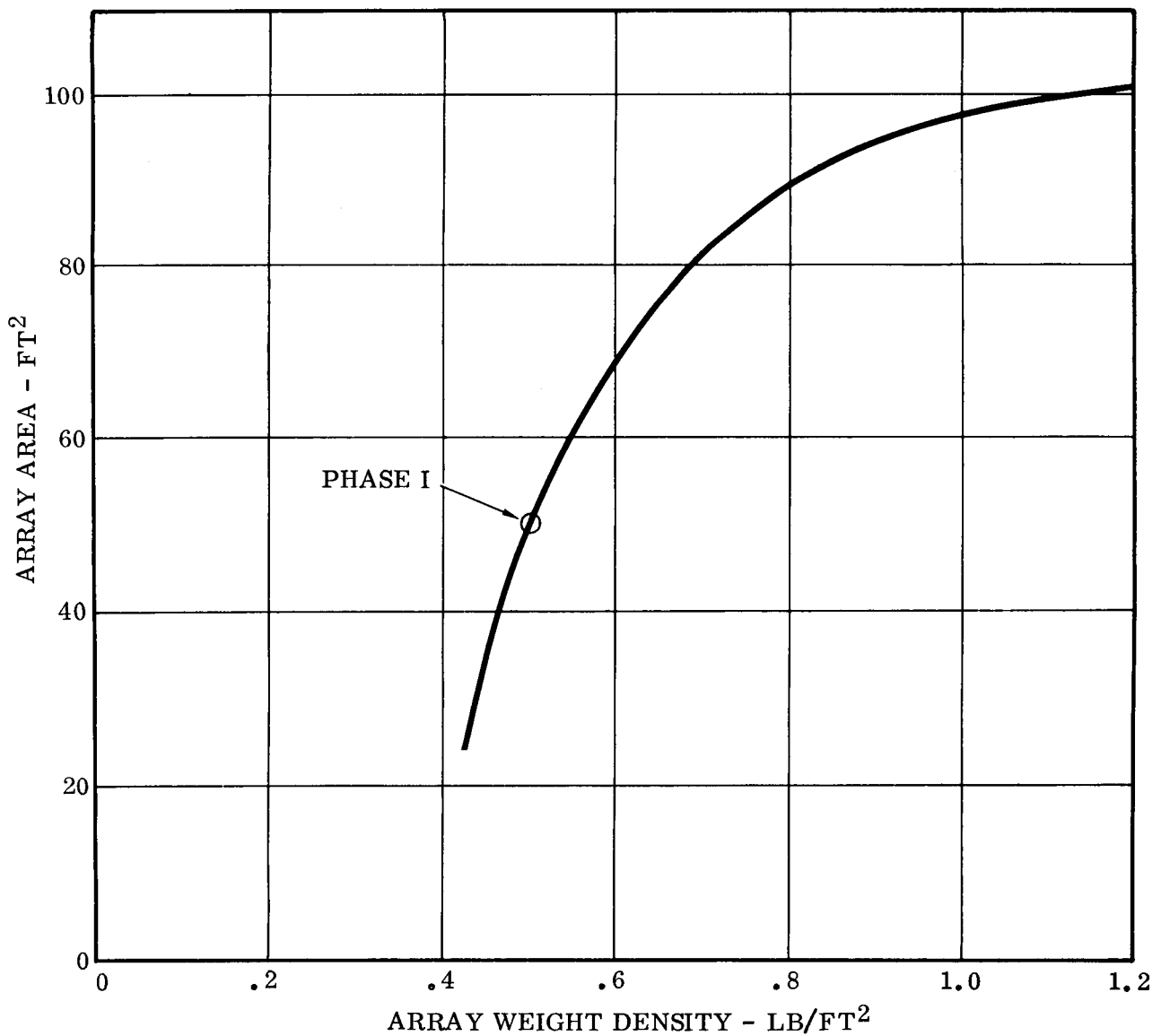


Figure 33 Solar Array Growth Potential

- NOTES: 1. WEIGHT DOES NOT INCLUDE DRIVE MECHANISM OR SUPPORT STRUCTURE
2. BASED ON ONE BLADE OF A FOUR BLADE SYSTEM
3. INCLUDES 0.3 LB/FT² FOR SOLAR CELLS AND PROVISIONS
4. THIS FIGURE SHOULD BE USED FOR COMPARISON STUDIES ONLY

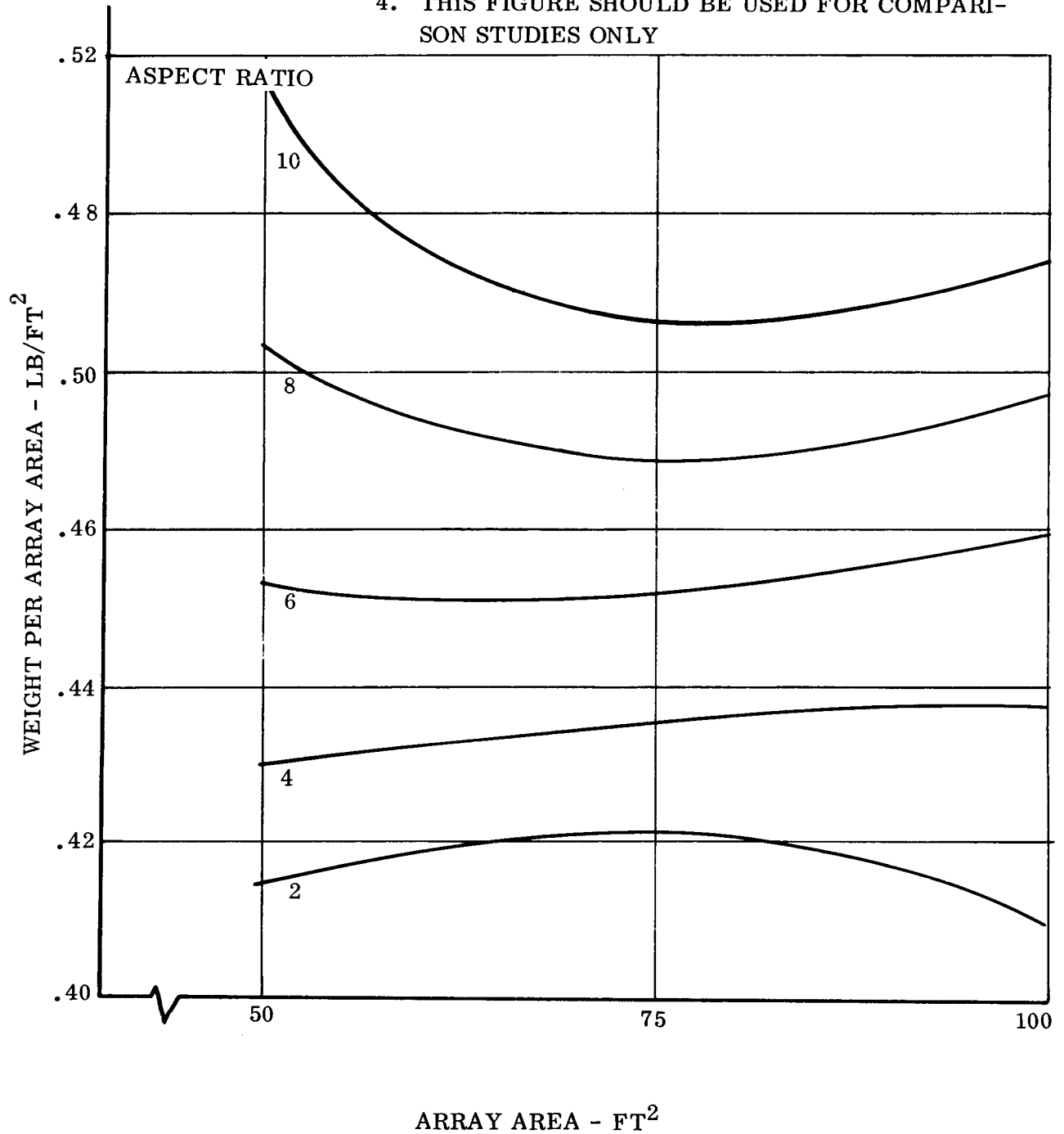


Figure 34 Parametric Studies

8.0 WEIGHT ANALYSIS

The weight analysis given below was calculated for both minimum and maximum values of commercial sheet tolerances. Under normal fabrication procedures, it is impractical to control overall weight deviation from nominal design values through selection of material. However, Ryan experience with solar panel fabrication indicates that an overall deviation not exceeding 4% can be expected based on nonselective use of material. The weights listed are for one-quarter of the total array. (See Figure 35.)

Item	Mill Weight, Lb	
	Minimum	Maximum

Drive and Support Housing (excludes substrate)

Ref. Figure 5

Wire conduit (2'-dia x .010' wall glass fiber tube with 50% area lightening holes)	0.086	0.105
Torque drum (.020' wall aluminum with 30% area lightening holes)	2.038	2.620
Gear motor and drive	1.0	
Pinion gear (nylon)	0.007	
Internal gear (nylon)	0.362	0.400
44 Rollers (.3" dia. x .020' wall drawn aluminum tubing)	0.354	0.434
4 radial support discs (.02"-thick aluminum sheet with 30% area lightening holes)	0.894	1.038
End plates (magnesium machining to .040')	0.548	0.606
Retaining nuts (magnesium machining)	0.019	0.021
Ball bearings	0.26	
End channels (magnesium machining to .040')	0.371	0.410

Item	Mill Weights, Lb	
	Minimum	Maximum
End covers (.020' aluminum sheet)	0.597	0.729
Roller casings (.020' aluminum sheet)	0.819	1.001
Beam guides (machined magnesium)	0.464	0.512
44 roller springs (.032" fiberglass sheet)	1.050	1.167
Inboard shear plates (.020" aluminum sheet)	0.162	0.198
8 tie angles (.020' aluminum)	0.070	0.086
Tie tee (.040' aluminum extrusion)	0.301	0.326
1/2 of mount frame (.020' aluminum)	0.728	0.854
Total (Drive & Support Housing)	10.130	11.774

Weight deviation = $\pm 7.5\%$ from nominal

$$\text{Unit weight} = \frac{\text{weight}}{\text{substrate area}} = \frac{\text{weight}}{50 \text{ ft}^2}$$

$$\text{Unit weight} = \underline{0.203} \text{ lb/ft}^2 \text{ min.}$$

$$\underline{0.235} \text{ lb/ft}^2 \text{ max.}$$

Substrate, Including Solar Cell Installation -- Ref. Figure 4

Installed solar cell modules (includes wire mesh at .03 lb/ft ²)	15.0	
2 deployable beams (.006 6AL-4V titanium)	3.025	3.575
Substrate (.003" RP7A-828 resin-impregnated glass cloth)	1.261	1.541

Substrate stiffeners and hinges (glass fiber tube)	0.241	0.295
Dielectric (.002"-thick 108 glass cloth)	0.842	1.030
Tip intercostal (.015" aluminum)	0.230	0.280
Protection strips (.125" thick x 2" wide x 10 lb/ft ³ silicone sponge)	1.751	2.140
Total (Substrate including Solar Cell Installation)	22.350	23.861

Unit weight = 0.447 lb/ft² min.

0.477 lb/ft² max.

Weight deviation = $\pm 3.2\%$ from
nominal

If we eliminate the wire mesh and dielectric,

Unit weight = 0.400 lb/ft² min.

0.426 lb/ft² max.

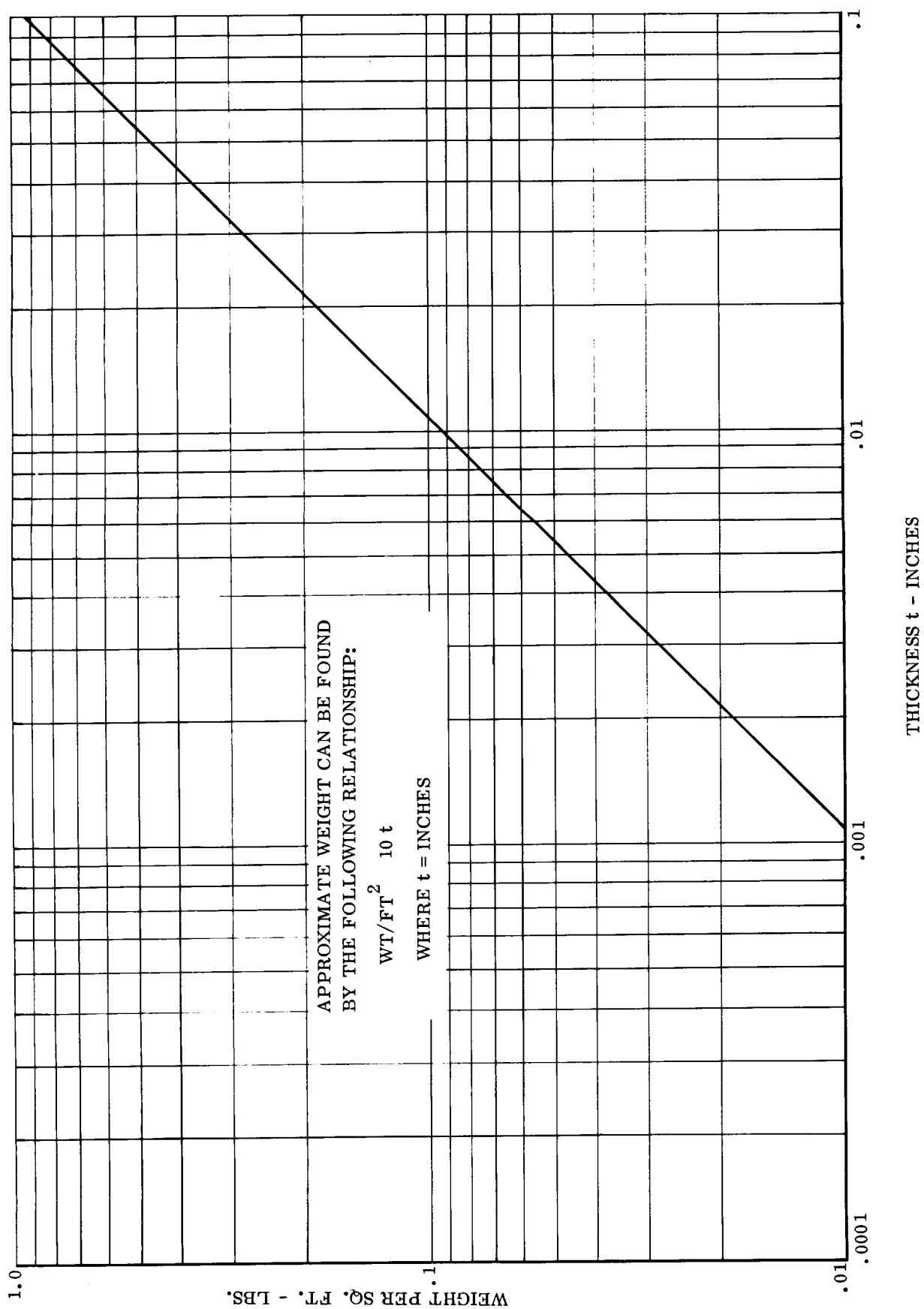


Figure 35 Weight of Glass Fiber Substrate

9.0 MATERIAL AND PROCESS DEVELOPMENT

The Phase I material and process development effort includes the following studies:

1. Basic properties of beam materials.
2. Process methods necessary to meet design objectives.
3. Suitability of materials to withstand environmental conditions.
4. Substrate material and method of attachment to beam.
5. Bending and wrapping tests on several beam configurations.
6. Cushioning materials to protect solar cells in stowed position.

9.1 BEAM MATERIALS

Both metallic and non-metallic beam materials were considered. Titanium was selected as the preferred beam material, because of stability in the thermal environment and superior wrapping properties. Several glass fiber-reinforced plastic systems have also been found satisfactory, and can be used as alternates if necessary.

The following materials were evaluated:

<u>Code</u>	<u>Material</u>	<u>Reinforcement</u>	<u>Resin Type</u>
A	Stratoglas 300 T	Non-woven S glass	Epoxy
B	Ryan MPD 139	1667 E glass	Epon 828-Dion RP-7A
C	3M Scotch Ply XP-251S	Non-woven S glass	Epoxy
D	3M Scotch Ply 1009 S	Non-woven S glass	Epoxy
E	Ryan MPD 139	143 E glass cloth	Epon 828-Dion RP-7A
F	Ryan MPD 139	1557 E glass cloth	Epon 828-Dion RP-7A
G	Narmco 534	181 E glass cloth	Phenyl-silane
H	Std. Insulation 58-68R	143 E glass cloth	Epon 1031 - NMA
I	3M Scotch Ply 1007	Non-woven E glass	Epoxy-Anhydride
S	AM 355 - CRT Steel	--	--
T	6AL-4VA Titanium	--	--

Materials G, H, I and T will satisfy the design and environmental requirements. The other plastic materials creep at the 295° F sterilization temperature when in the stowed position. However, they can be used if sterilization is by means of ethylene oxide only. Material S was useful in developing the beam shape, but does not meet the non-magnetic material requirement.

Four principle evaluation tests were conducted to measure properties needed for beam design. These tests were:

Flexural strength and modulus (Paragraph 9. 2. 1)

Beam sector wrapping (Paragraph 9. 2. 2)

Beam section bending moment (Paragraph 9. 2. 3)

Creep at 295° F (Paragraph 9. 2. 4)

9. 2 DESCRIPTION OF EVALUATION TESTS

9. 2. 1 Flexural Strength and Modulus Test

The purpose of these tests was to determine the effect of glass fiber orientation on the strength and modulus of elasticity of the reinforced plastic beam materials. Flat panels 12" x 12" x .030" were constructed with the fiber warp direction as shown in Figures 36 and Table 3.

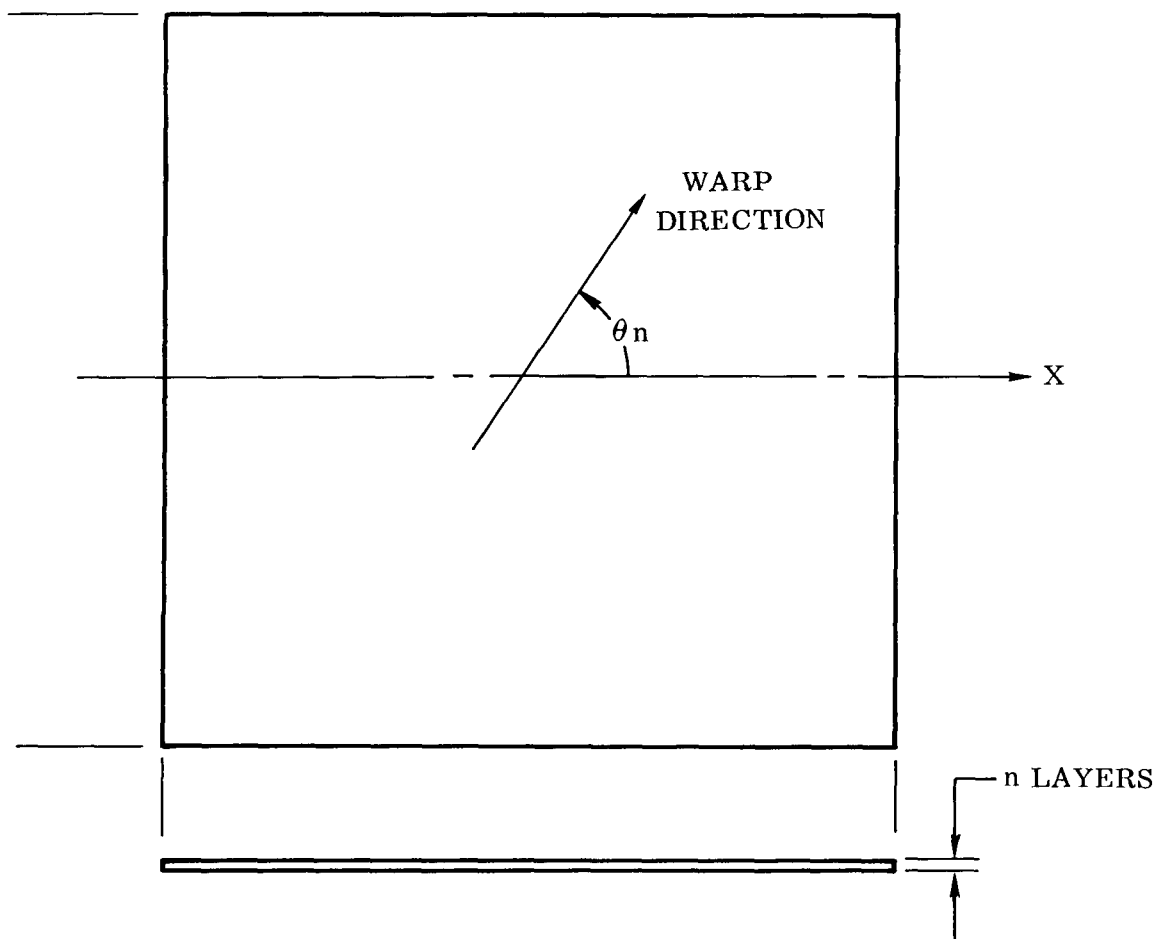
These test panels demonstrated the wide variation in properties available. The fiber orientation in the cross-laminated panels was chosen to simulate the original design concept. The outer fibers at θ_n equals 90° would be circumferential on the beam and the inner fibers at θ_n equals 0° longitudinal on the beam.

Materials A and B (see Paragraph 9. 1) were not tested because of processing difficulties. Test laminates made from material A delaminated before specimens could be prepared. The style 1667 glass cloth used in Material B is too easily distorted during lamination for satisfactory control of fiber orientation in the laminate. Flexural tests on Materials S and T were not conducted, since properties are readily available in the literature.

The test results are summarized in Table 4. Manufacturer's data is shown for comparison where available.

The specimens were tested by method 1031 of Federal Specification L-P-406. Specimen width was 0.50 inch. Span length was 1.7 inches. The flexural strength and modulus values of some materials were unexpectedly high. This was caused in part by a bias in the test method toward thin specimens.

The effect of fiber orientations on material properties was shown in these tests. Strength and modulus properties can be varied over a broad range to suit the design requirements.



θ_n = ANGLE BETWEEN X AXIS AND WARP DIRECTION
OF nTH LAYER

n = NUMBER OF LAYERS

SEE TABLE 3 FOR CONSTRUCTION OF EACH LAMINATE

Figure 36 Test Panel for Flexural Strength and Modulus

Table 3.

PANEL REQUIREMENTS

Qty.	Identification	Material	Process	Construction	
				Nth Layer	θ_n
(1)	I-A-1	Stratoglas 300T	Vacuum Bag Cure 1 hr 325° F	1, 6 2-5	90° 0°
(1)	I-A-2	Stratoglas 300T	Same	1-6	0°
(1)	I-C-1	Scotchply XP-251S	Per 3 M Instruction Sheet	1, 4 2, 3	90° 0°
(1)	I-C-2	Scotchply XP-251S	Same	1-4	0°
(1)	I-D-1	Scotchply 1009-26S	Same	1, 4 2, 3	90° 0°
(1)	I-D-2	Scotchply 1009-26S	Same	1-4	0°
(1)	I-E-1	143 Volana 828 RP-7A	Vacuum Bag Per MPD 139	1-3	0°
(1)	I-F-1	1557 Volana Epon 828 RP-7A	Same	1-5	0°
(1)	I-G-1	Narmco 534 181 Cloth	Per Narmco Process	1-3	0°
(1)	I-H-1	Std. Insul. 58-68R 143 Cloth	Per Std. Insul. Process	1-3	0°
(1)	I-I-1	Scotchply 1007	Per 3M Instruction Sheet	1, 2 3	0° 90°
(1)	I-I-2	Scotchply 1007	Same	1-3	0°

Table 4.

MECHANICAL PROPERTIES OF BEAM MATERIALS

Material Identification	Angle Loading (Degree)	Flexural Strength psi x 10 ⁻⁶		Flexural Modulus of Elasticity psi 10 x ⁻⁶	
		.03 Thick Specimen	Manufacturer's Data (t = .12)	.03 Thick Specimen	Manufacturer's Data (t = .12)
I-C-1	0	(1)	---	2.5	---
I-C-1	90	236	170	8.2	5.0
I-C-2	0	275	200	11.0	8.0
I-C-2	90	8	---	2.4	---
I-D-1	0	(1)	---	3.0	---
I-D-1	90	217	---	9.5	---
I-D-2	0	246	210	11.0	7.9
I-D-2	90	12	---	1.9	---
I-E-1	0	153	---	8.3	---
I-E-1	90	31	---	.9	---
I-F-1	0	140	---	7.7	---
I-F-1	90	39	---	2.9	---
I-G-1	0	94	74	6.4	3.7
I-G-1	90	67	---	4.3	---
I-H-1	0	(1)	---	10.1	---
I-H-1	90	(1)	---	1.7	---

(1) Specimen deflected to 105° Angle without breaking.

9.2.2 Beam Sector Wrapping Tests

The purpose of these tests was to study the wrapping characteristics of the beam materials. The specimen configuration shown in Figure 37 is a half-cylinder similar to the beam shape originally proposed. Materials and construction method are given in Table 5. The test consisted of flattening the convex side of the section against a 12-inch-diameter drum, then wrapping the flattened sheet around the circumference of the drum. The capability of the material to be wrapped without failure was visually determined.

It should be noted that the orientation of surface fibers is extremely important in the non-woven fiber reinforced plastics. The surface fibers must be parallel to bending stresses in order to work most effectively. When tension loads are normal to fiber direction, crazing and resin cracks occur at very low stress levels. Such crazing has only a small effect on parallel loaded properties. In the sections tested, fibers on the concave surface are oriented circumferentially to support the tension stress imposed by flattening. The convex surface fibers were, in some cases, oriented parallel to the concave fibers, but this construction required flattening forces exceeding practical limits. The most effective construction locates the convex surface fibers circumferentially. In a two-layer laminate of this construction, the radius of the molded part is substantially longer than the radius of the cylindrical mold surface. This effect can be attributed to the unbalanced orientation of reinforcing fibers, resulting in dissimilar contraction rates on each surface during the resin cure cycle.

The results of wrapping tests are summarized in Table 6. Wrapping difficulties first occur with the inability of the section to conform smoothly to the drum surface. When forced to conform, failure occurs either by delamination at sites of local buckling, or by tearing at the edge of the open sector. Approximate practical limits on thickness/radius relationships were established by these tests.

Following the wrapping evaluation, the open beam sectors were loaded as cantilever beams to measure their ultimate bending moment capability. The test arrangement is shown in Figure 38. Some difficulty was experienced in obtaining a uniform bearing at the fixed support, so that some of the beam sectors failed by tearing or splitting at the support instead of buckling, as expected. When buckling failures occurred, local delamination was observed at the failure site. Table 7 summarizes the test results. Figure 39 shows the group of beam specimens tested. Figure 40 shows typical failure modes experienced.

Table 5.

TEST SECTOR REQUIREMENTS

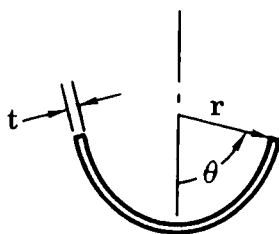
Qty.	Identification	Material	Construction		Size	
			Layer	Fiber Angle θ_n	Radius in.	Length in.
(1)	H-1.0A - 2	Stratoglas 300T	1 2	90° 0°	1.0	12.0
(1)	H-1.0A - 3	Stratoglas 300T	1,3 2	90° 0°	1.0	12.0
(1)	H-1.0A - 4	Stratoglas 300T	1,4 2,3	90° 0°	1.0	12.0
(1)	H-1.0A - 5	Stratoglas 300T	1,5 2,3,4	90° 0°	1.0	12.0
(1)	H-1.0A - 6	Stratoglas 300T	1,6 2,3,4,5	90° 0°	1.0	12.0
(1)	H-1.0C - 30	Scotchply XP 251-S	1 2,3	90° 0°	1.5	12.0 Cure 1 hr at 300° F plus 2 hr at 350° F
(1)	H-1.5C - 30	Scotchply XP 251-S	1 2,3	90° 0°	1.5	12.0 Cure 1 hr at 300° F plus 2 hr at 350° F
(1)	H-1.0E - 1	E43 Cloth 828 - RP 7A	1	0°	1.0	12.0 Cure Per MPD 139
(1)	H-1.0E - 2	E43 Cloth 828 - RP 7A	1,2	0°	1.0	12.0 Cure Per MPD 139
(1)	H-1.0C - 20	XP 251-S	1 2	90° 0°	1.0	12.0 1 hr at 300° F 2-4 hrs at 350
(1)	H-1.0D - 30	Scotchply 1009-26 S	1 2,3	90° 0°	1.0	12.0 Cure 1 hr at 300° F plus 2 hr at 350° F
(1)	H-1.5D - 30	Scotchply 1009-26 S	1 2,3	90° 0°	1.5	12.0
(1)	H-1.5C - 20	XP 251-S	1 2	90° 0°	1.5	12.0 1 hr at 300° F 2-4 hr at 350
(1)	H-1.0D - 20	Scotchply 1009-26 S	1 2	90° 0°	1.0	12.0 1 hr at 300° F 2-4 hrs at 350
(1)	H-1.5D - 20	Scotchply 1009-26 S	1 2	90° 0°	1.5	12.0 1 hr at 300° F 2-4 hrs at 350

Table 6.
WRAPPING TESTS ON BEAM SECTORS
(11.9 in. Diam. Drum)

Identity	Radius (r)	Thickness (t)	Length (L)	Center Half-Angle θ	Remarks	Wrapping Results
H-1.0A - 2	1.03	.014	12.0	88	Laminate has some voids	Wraps easily - Interlaminar shear failure when buckled
H-1.0A - 3	1.00	.021	11.9	90	Outer surface wavy	Difficult to wrap - Tears on edge
H-1.0A - 4	1.00	.026	12.1	90		Not practical to wrap
H-1.0A - 5	1.00	.025	11.9	90		Too stiff to wrap
H-1.0A - 6	1.00	.037	12.0	90		Cannot wrap
H-1.0C - 20	1.23	.015	11.7	68	Unbalanced construc- tion causes radius increase	Wraps very well
H-1.0C - 30	1.33	.024	11.7	67		Wraps OK - Problems if stiffer
H-1.0D - 20	1.02	.015	11.6	83		Wraps very well
H-1.0D - 30	1.35	.021	11.7	67		Wraps OK - Problems if stiffer
H-1.0E - 1	1.06	.0092	12.4	85	Unbalanced construc- tion causes radius increase	Wraps easily
H-1.0E - 2	1.07	.017	12.5	85		Wraps very well
H-1.5C - 20	1.93	.0155	11.7	70		Wraps very well
H-1.5C - 30	2.18	.024	11.6	63		Wraps well - would be improved if stiffer
H-1.5D - 20	1.68	.015	11.7	80	Unbalanced construc- tion causes radius increase	Wraps very well
H-1.5D - 30	2.08	.021	11.7	67		Wraps well - would be improved if stiffer

Table 7.

BENDING MOMENT TESTS - OPEN BEAM SECTOR



Specimen Identity	Radius (r) in	Thickness (t) in	Center Half-Angle (θ)°	Bending Moment in/lb.	Failure Mode
H-1.0A - 2	1.03	.014	88	44	Interlaminar shear
H-1.0A - 3	1.00	.021	90	187.5	Root long. shear
H-1.0C - 2U	1.23	.015	68	122	Root long. shear
H-1.0C - 3U	1.33	.024	67	270	Root long. shear
H-1.5C - 2U	1.93	.0155	70	181.5	Compression buckling
H-1.5C - 3U	2.18	.024	63	345	Long. shear
H-1.0D - 2U	1.02	.015	83	80	Root long. shear/interlaminar shear
H-1.0D - 3U	1.35	.021	67	287	Root long. shear/interlaminar shear
H-1.5D - 2U	1.68	.015	80	111	Compression buckling
H-1.5D - 3U	2.08	.021	67	304	Long. shear
H-1.0E - 1	1.06	.0092	85	27.9	Compression buckling
H-1.0E - 2	1.07	.017	85	100	Long. shear - root

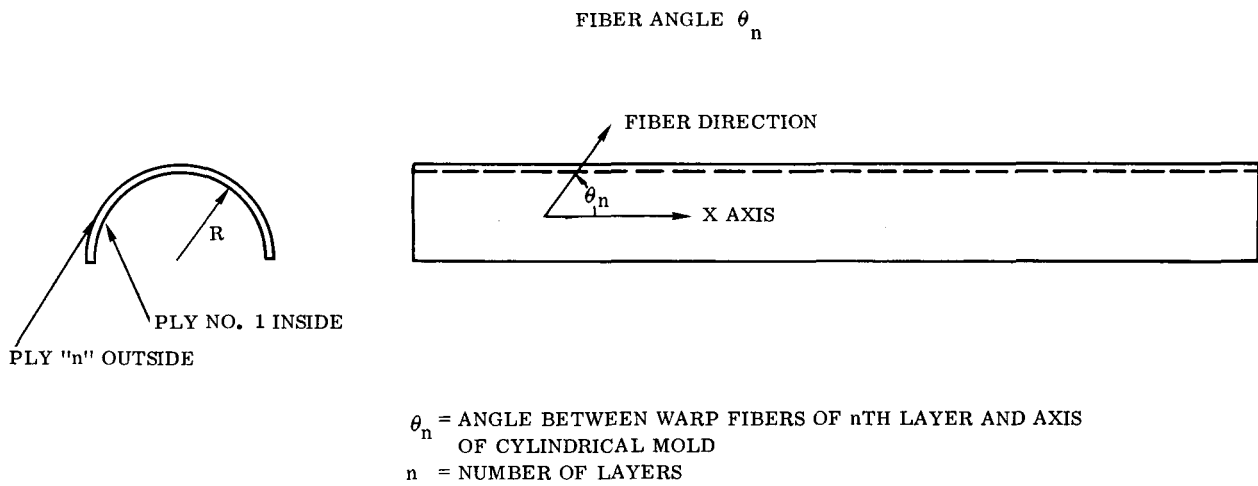


Figure 37 Test Section

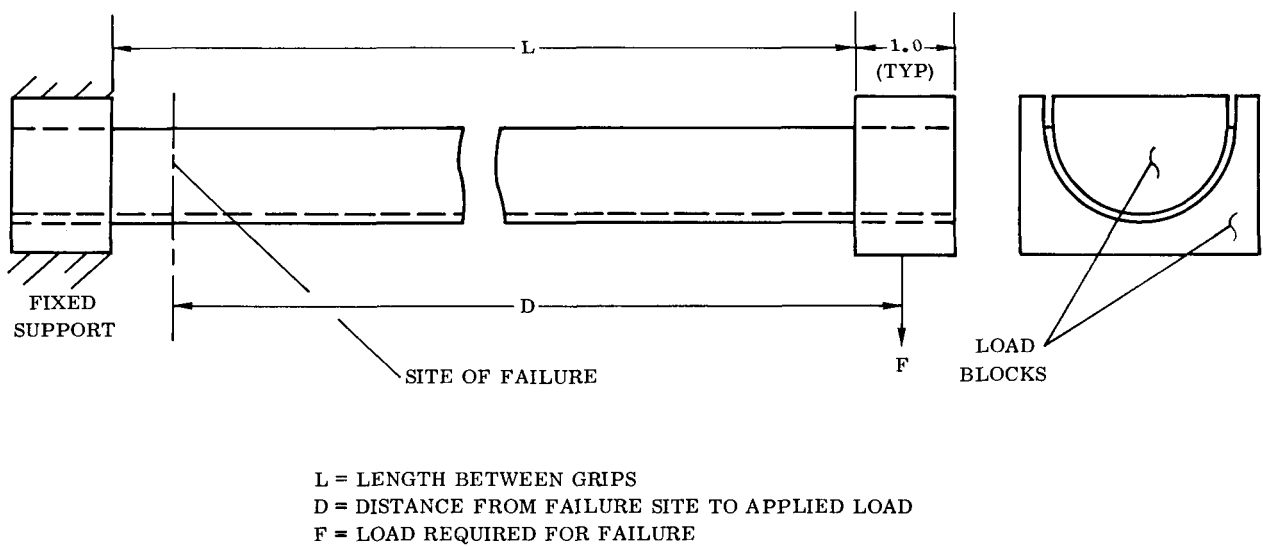


Figure 38 Test Method - Beam Buckling

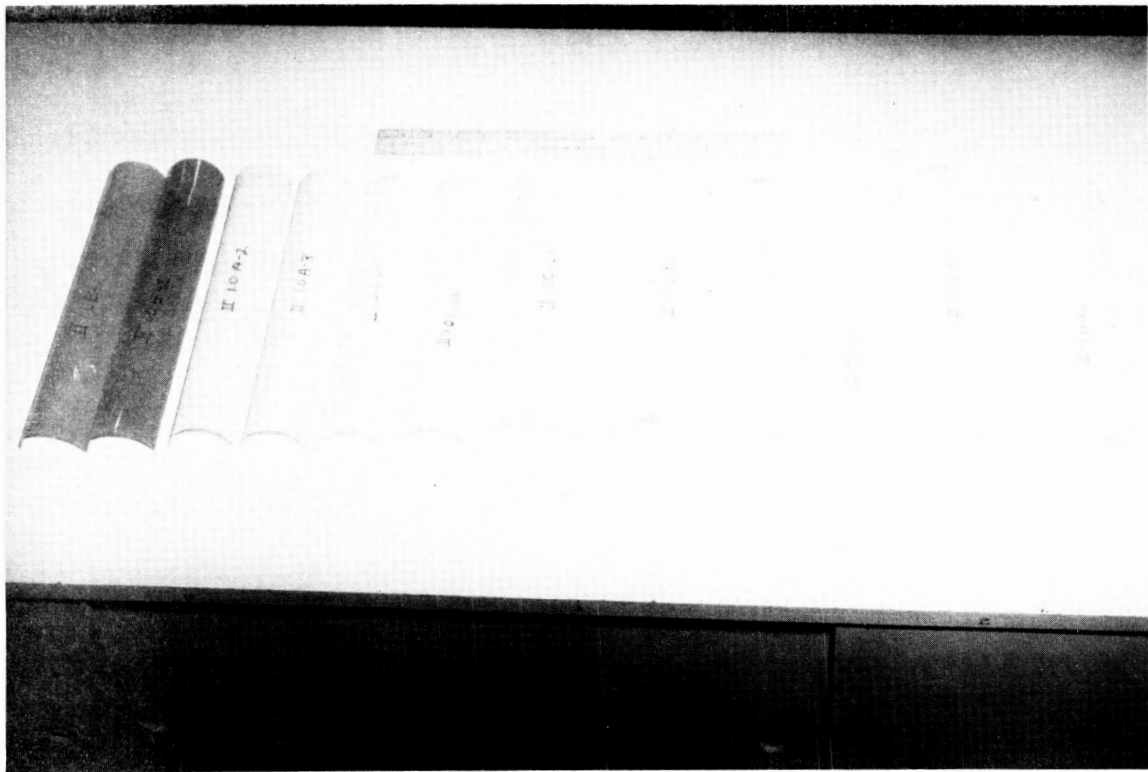


Figure 39 Beam Specimens

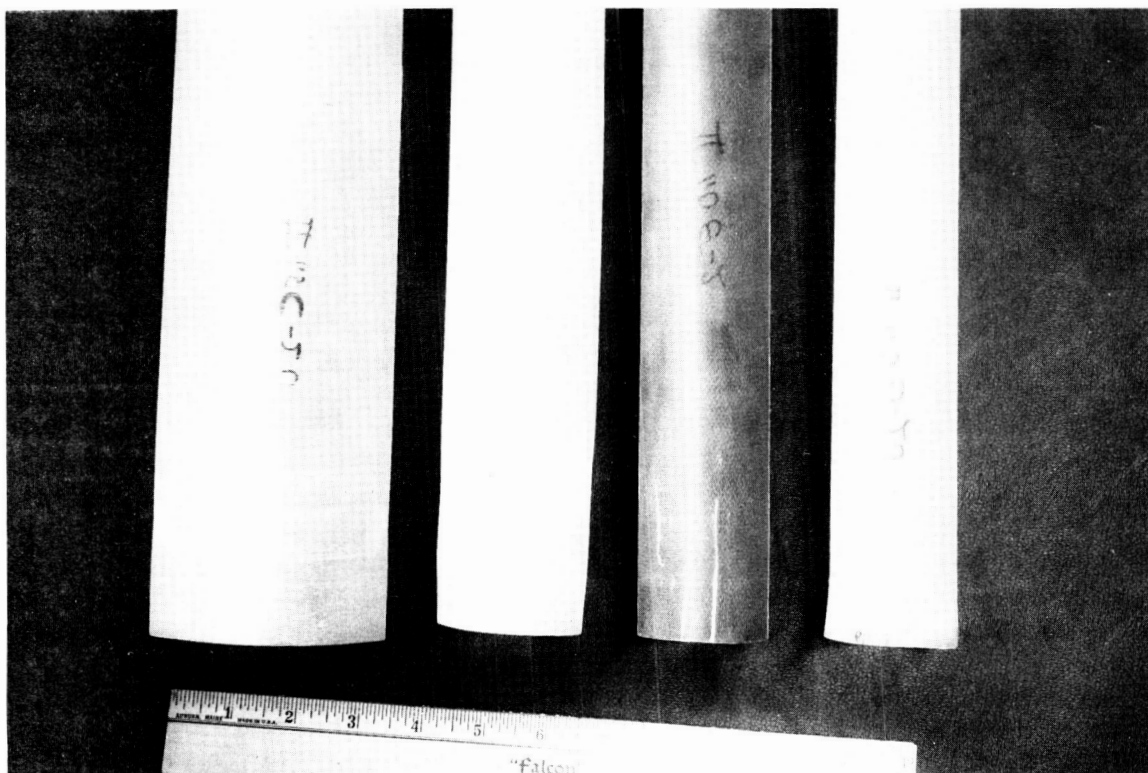


Figure 40 Typical Failure Modes

9.2.3 Beam Section Bending Moment Tests

After selection of the closed beam configuration as the preferred cross-section, several test beam sections were prepared to determine actual bending strength. The metal beam sections were joined by seam welding the edges. Glass fiber beam sections were joined using FM-1000 Nylon-epoxy adhesive. Figure 3 shows the group of beams tested.

The beam sections were cantilevered beams as shown in Figure 41. Test results are summarized in Table 8. Before testing, every beam was wrapped around a 12-inch diameter drum to demonstrate wrapping capability, and to impose preliminary loads expected prior to deployment. Glass fiber materials exhibit higher modulus of elasticity values on initial loading than on subsequent load cycles. This is attributed to crazing of the resin-glass interface when first bonded. The test method measured the secondary modulus properties of the beams representative of the actual application.

Failure mode in the metal beams tested was always compression buckling. The failure mode of the parallel laminated 143 cloth beam was longitudinal shear of the transverse fibers. The other glass fiber beams failed in compression buckling.

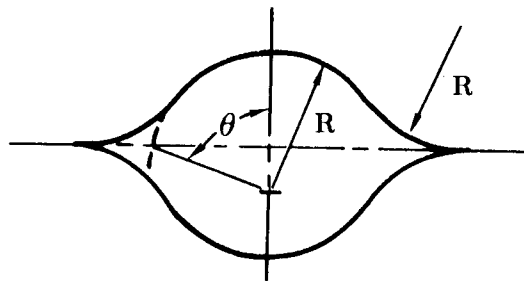
Beam strength was varied by changing material properties and thickness, keeping the basic section shape constant. In some cases, the metal beam did not form to the radius intended. Variations due to shape factors were encountered. The shape variation was a flat region on the side of the beam which permitted the beam to buckle at less than theoretical loads.

One expected advantage of glass fiber construction was its ability to obtain a higher modulus longitudinally than circumferentially, by suitably orienting the glass fibers in the laminate. However, it was found that the chosen beam shape required almost equal stiffness in both directions for optimum strength. The glass fiber beam, using style 143 unidirectional glass cloth (parallel laminated), failed at a lower load than the cross laminated beams. due to insufficient circumferential support of the beam shape.

Table 8.

CANTILEVER BEAM TEST RESULTS

Test No.	Material	R-in	T-in	θ°	M-in lb	Failure Mode
1	AM 355 CRT	1.75	.006	53	268	Compression buckling
2	AM 355 CRT	1.3	.0045	75	576	Compression buckling
3	AM 355 CRT	1.06	.0045	73	420	Compression buckling
4	Titanium 6AL-4VA	.95	.005	82	240	Compression buckling
5	Titanium 6AL-4VA	.90	.006	93	288	Compression buckling
6	143 Glass fiber Parallel Laminated	1.15	.018	68	240	Longitudinal shear
7	Scotchply XP-251S Cross Laminated	1.60	.018	58.5	329	Compression buckling
8	181 Glass fiber Parallel Laminated	1.2	.025	68.5	459	Compression buckling



9.2.4 Creep at 295° F

Preliminary selection of materials was based on ability to withstand, and to function in the imposed environments. The most severe environment experienced by the beam material will be during sterilization at 295° F while wrapped on the drum. Plastic materials tend to creep at elevated temperatures under sustained loads, even at temperatures above the heat distortion temperature.

In order to evaluate specific materials under consideration, a creep test was conducted. A 1 inch x 10 inch x .030 inch sample of each material was wrapped on a 2 inch radius drum and soaked 24 hours at 295° F. The stress imposed in this loading arrangement was approximately equivalent to the stress level required to flatten the chosen beam section. Following testing, the samples were removed and the change in radius of curvature measured. Figures 42, 43 and 44 show the test arrangement before and after test. Table 9 shows the radius of curvature measured.

The least creep occurred in the titanium sample. The samples of materials G(Narmco 534), H(Std. Insulation 58-68) and I (Scotchply 1007) with a radius greater than 20 inches, are considered satisfactory. The other materials could not be expected to maintain beam shape after sterilization at 295° F.

The amount of creep was also influenced by the orientation of glass fiber reinforcement. These tests show the necessity for circumferential fiber orientation on the concave surface.

Table 9.

CREEP AT 295° F

Identification	Angle of Loading	Radius After 24 Hrs @ 295° F
I-C-1	90	2.1
I-C-2	0	2.7
I-D-1	90	2.1
I-D-2	0	3.1
I-E-1	0	4.8
I-E-2	90	2.5
I-F-1	0	4.7
I-F-1	90	2.5
I-G-1	0	21.0
I-G-1	90	21.8
I-H-L	0	29.4
I-H-1	90	4.3
I-I-1	0	10.5
I-I-2	0	22.8
6-4 Ti	-	84

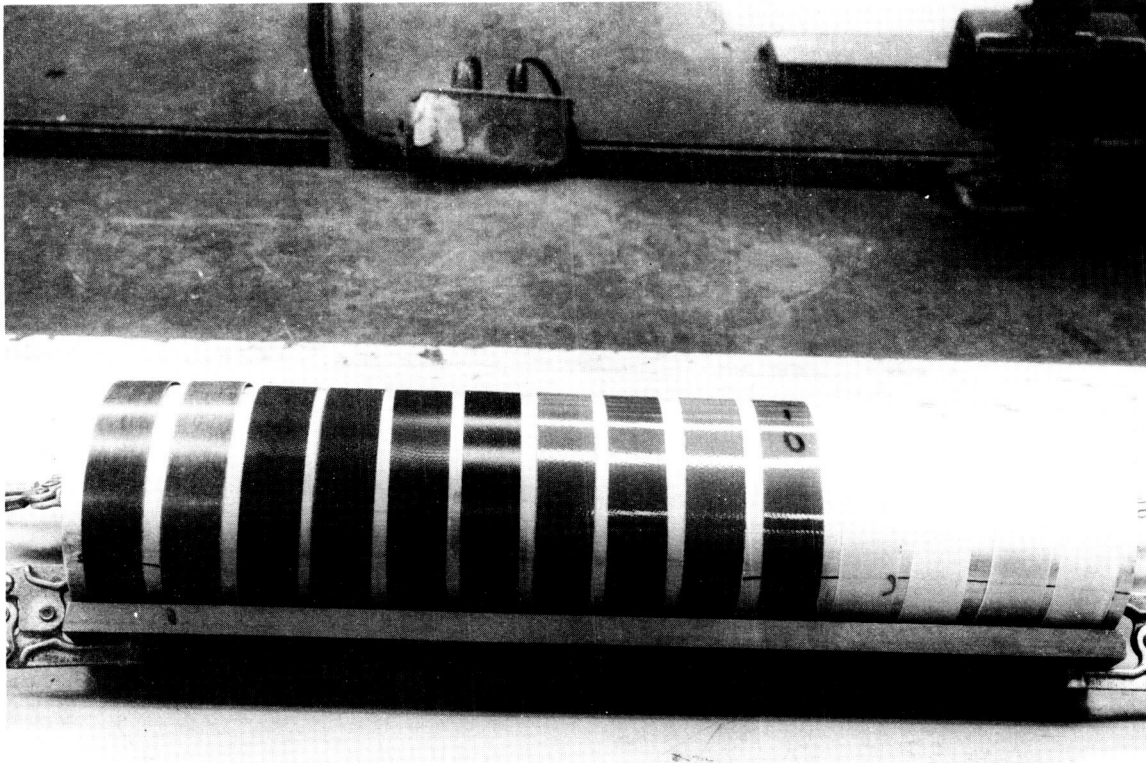


Figure 43 Creep Specimen During Test

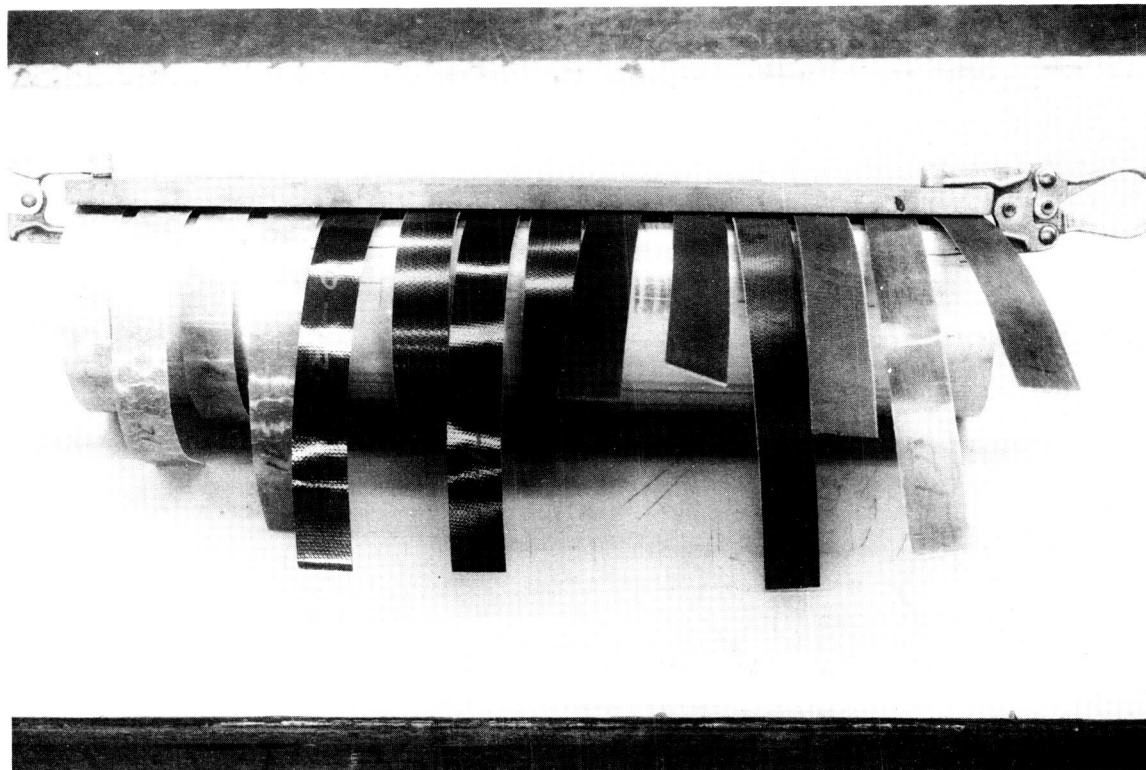


Figure 44 Creep Specimen After Test

9.3 BEAM PROCESS DEVELOPMENT

Selection of glass fiber reinforced plastic as the beam material in the design proposal was largely influenced by two factors. These were their ability to be formed straight and accurately to relatively unlimited lengths, and their flexibility with respect to orientation of mechanical properties. It was expected that difficulties in maintaining straightness would prevent use of metal.

During the Phase I development, it became apparent that the closed beam shape was much less subject to warping or twisting than the open beam shape originally proposed. Process methods for forming titanium were developed which are less elaborate than those required for the reinforced plastic beam.

The glass fiber-plastic materials require cure on a mold at 350° F. Post-cures at 500° F are required to obtain high temperature properties.

The beam halves were adhesive bonded at 350° F. It is essential for proper wrapping that both halves of the beam be flattened when they are assembled. A special tool was made to hold the molded glass fiber beam-halves flat while the adhesive was applied, which would also restore them to their molded shape while maintaining pressure on the bond line during cure. These methods produced acceptable glass fiber beams, but were not in any way superior to the metal forming process.

The grade of titanium selected (Ti-6AL-4V) was based on the following properties:

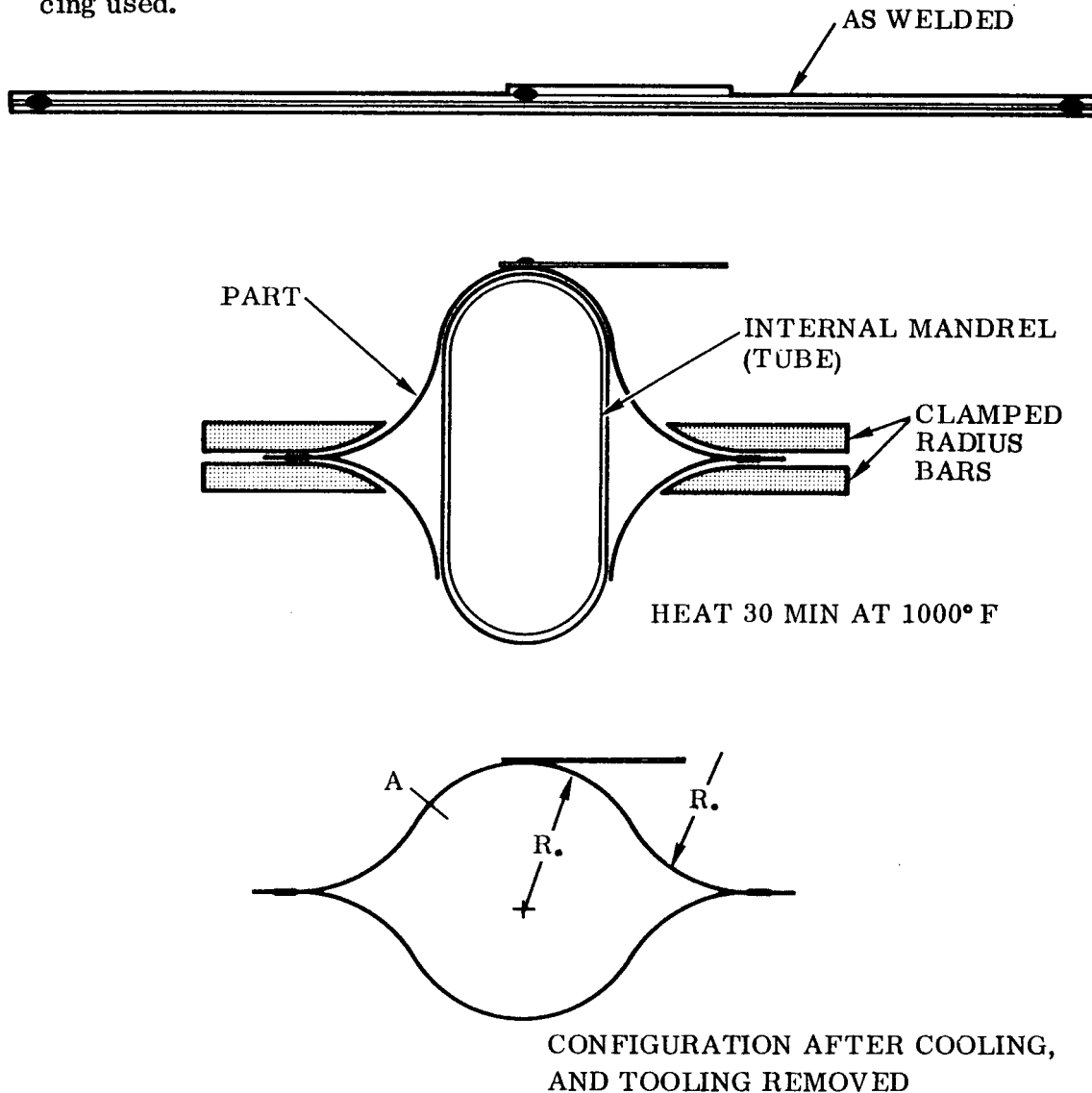
- a) Availability
- b) Acceptability
- c) Stability through temperature range (-423° to +1000° F)
- d) High mechanical properties in annealed state
- e) Weldability
- f) Fatigue property
- g) Creep property

During the development forming program, it was established that seam welding the two sheets comprising the beam before forming was a definite advantage over pre-forming the details, and then seam welding the two halves. The latter method always produced a twisted beam of

varying degrees. Ti-6Al-4V exhibited the property of proportional increase in bend ability relative to elongation at elevated temperatures. This enabled forming many shapes at elevated temperatures which normally cannot be cold formed. An additional advantage of creep forming at elevated temperatures was reduction in springback. This characteristic eliminated the need for a hot-sizing operation.

Forming annealed titanium at elevated temperatures can be accomplished up to 1350° F without affecting mechanical properties. However, forming above 1100° F usually requires descaling and conditioning operations because of the significant oxidation which occurs.

The final process was a 1000° F temperature exposure for 1/2-hour in a forming tool. The following diagram illustrates the tooling and sequencing used.



The tool employed resulted in a structurally desirable beam section and produced a point of inflection at point A. Any length of beam perimeter flat or near flat at point A was undesirable, as it decreased the overall strength of the beam. This was evident by the nature of the buckling strength elements, as opposed to curved elements.

9.4 SUBSTRATE MATERIALS

The preferred material for dielectric and mechanical characteristics of the flexible substrate was glass fiber-reinforced epoxy laminate. Other plastics, such as silicone rubber or Teflon, have greater flexibility but are inferior mechanically.

The resin system selected for the substrate was an aromatic amine epoxy system which has good stability in vacuum over a temperature range from -400 to +350°F. The resin is Epon 828 cured with Dion RP-7A hardener. Substrate thickness is the factor controlling wrapping capability. The stiffness of the glass fiber epoxy laminate will increase only about 25 percent over a 250°F temperature drop.

Substrate thickness in the range of .004 to .010 inch, with intermittent transverse stiffeners, presented no unusual process problems. The principal development consideration was the incorporation of a silver mesh conductor bonded into the substrate laminate. The mesh selected was an expanded metal foil .002 inch thick. The mesh could be laminated as an internal layer when the glass fiber cloth was impregnated and cured. However, problems of resin contamination of solder terminals limited this method.

Several substrate laminates were prepared using Bloomingdale FM 1044R Nylon-epoxy bonding film to laminate the silver mesh to previously cured glass fiber-epoxy sheets. Adhesive film thickness of .002 inch was used on each side of the mesh to provide sufficient adhesive to fill the spaces in the mesh. The mesh was bonded between the basic substrate sheet of 1557 glass fiber-epoxy, and a dielectric sheet of 108 glass fiber-epoxy in an autoclave at 350°F and 80 PSI. Total laminate thickness was .012 inch.

Manual bending tests indicated that the additional reinforcement and thickness due to the silver mesh made the laminate stiffer than needed. Style 113 glass cloth (.003 in. thick) was selected to replace the 1557 glass cloth.

The bonding film thickness was reduced to .001 inch. Two laminates using these components were autoclave-bonded with satisfactory results. Total laminate thickness is .0075 inch outside the mesh and .009 inch in the mesh area. The bond is uniform and continuous in the internal spaces of the mesh.

There was no difficulty in controlling adhesive boundaries near the electrical terminal bars. Cutouts made in the adhesive film before assembly were maintained during cure with negligible adhesive flow.

Figures 45 and 46 show the appearance of the substrate after lamination. The size of the specimen shown is 7.5 x 18.0 inches.

9.5 CUSHIONING MATERIAL

In order to protect the solar cells in the stowed position during launch, a cushion or pad arrangement must be provided on the reverse surface of the substrate. Because the cushion surface will be in direct contact with the solar cell cover glasses, an inert surface material must be chosen. Two material types were considered for this application. These were TFE Teflon and silicone rubber foam. For the bearing surface, Teflon is preferred because of its low coefficient of friction and chemical inertness. The silicone rubber foam will maintain resiliency over a broad temperature range and is most suitable as a cushion. Other foams such as polyurethane become rigid at low temperature. Teflon foam was considered, but was not acceptable as a cushion, because it is not resilient.

Two configurations were determined as suitable. One is a composite of silicone rubber foam faced with a Teflon film surface. The second is a silicone rubber sheet, molded to provide a glossy skin as a bearing surface against the solar cells.

Three silicone rubber foams have been evaluated. These were:

1. General Electric RTV-7
2. Dow Corning Silastic RTV S-5370
3. Hadbar Silicone Sponge - Hadbar 404

Samples of RTV-7 and S-5370 were prepared in sheet form by casting the foam against a primed Teflon film, .002 inch thick. The glossy silicone foam sheets were prepared by casting the foam against unprimed aluminum sheets. Physical properties of the foam materials are summarized in Table 10.

Although the Teflon surface is superior, the higher weights involved suggest additional consideration of the glossy silicone rubber sheet. One requirement is thermal vacuum cleaning of all silicone rubber sheets to remove outgassing products, prior to exposure to the space environment. The use of a Teflon barrier improves reliability relative to cell contamination. However, it will be necessary to demonstrate by environmental tests that the thermal vacuum cleaned silicone sponge is acceptable, before eliminating the use of the Teflon bearing film.

Table 10

PROPERTIES OF SILICONE RUBBER FOAMS

Material	Description	Density lb/ft ³	Compression Deflection 25% psi	Compression Deflection 50% psi
RTV-7	1/8" molded with .002 in. Teflon surface	15.6	.7	2.5
S-5370	1/8" molded with .002 in. Teflon surface	20.1	1	3
S-5370	1/8" molded with glossy surface	18.5	1	3
Hadbar 404	1/2" extruded strip	12-16	.7	2.5
RTV-7	1/8" molded with glossy surface	13.2	.7	2.5

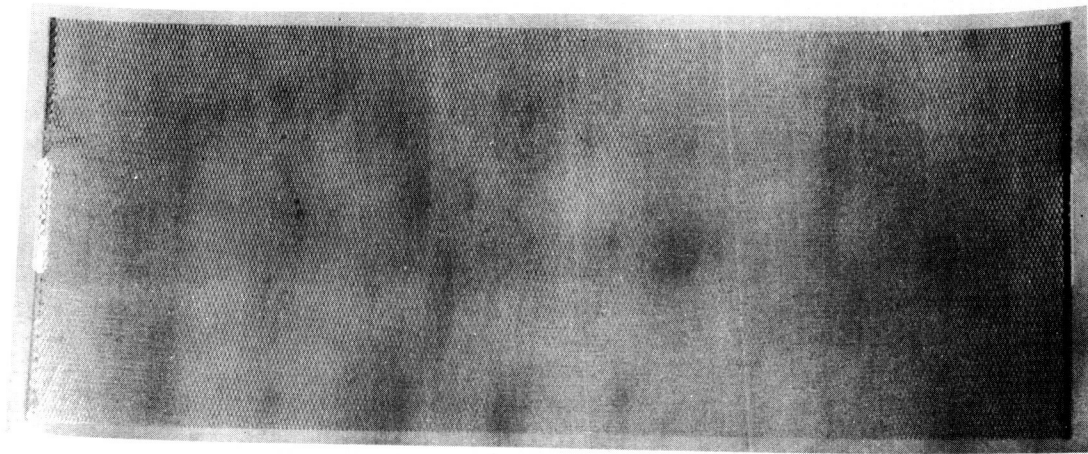


Figure 45 Substrate After Lamination

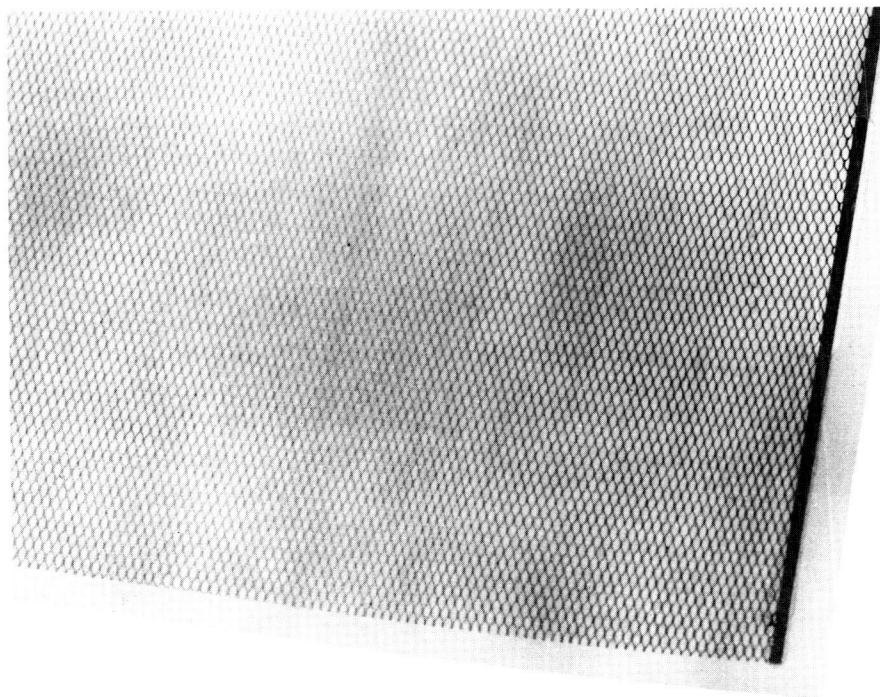


Figure 46 Substrate After Lamination

10.0 RELIABILITY

10.1 PROJECT RELIABILITY AND VALUE ENGINEERING

Project Reliability and Value Engineering is a program of continuous review and assistance to project technical activities. Its purpose is to assist in implementing the achievement of optimum system effectiveness at low cost in Ryan products.

In implementing such a program, Project Reliability and Value Engineering will perform the following tasks:

- (a) Coordinate design assurance activities to assure that all requirements are met.
- (b) Continuously be aware of the latest project technical activities, project technical data drawings and changes, engineering task assignments, equipment specifications and test plans, and similar project documentation.
- (c) Ensure the adherence to sound engineering practices and established engineering policies and procedures.
- (d) Prepare reports of periodic engineering project reliability meetings.
- (e) Coordinate and implement design reviews.
- (f) Review test plans and prototype test data.

10.2 DESIGN REVIEWS

Design reviews are scheduled in order to provide a means for evaluation of design and to point out design deficiencies.

The following specific design reviews are planned:

- (a) Preliminary Review. This is to be conducted at the end of the Development Design phase (Phase I). The purpose will be to review the preliminary design drawings, specifications, and design concepts of the preliminary design phase.

- (b) Detail Design Review. This is to be conducted at the end of the Detail Design Phase (Phase II). The purpose will be to review the final design concepts, choice of components, materials, reliability of vendors, and performance of experimental equipment.
- (c) Layout Review. This is to be conducted prior to preparation of detail manufacturing drawings. The purpose will be to review layout drawings and sketches, consider environmental requirements such as thermal stress, vibration, and also inherent parameters such as weight, finish, producibility, maintainability and value analysis.
- (d) Prototype Performance Review. This is to be conducted to evaluate prototype subsystems and system performance with regard to specification requirements.

Attendees at design reviews will comprise senior technical personnel who are qualified in the areas to be discussed, cognizant production and quality personnel, and design assurance representatives. Customer representatives will also be invited to participate in design reviews.

Prior to each design review, the project engineer will be responsible for dissemination of all pertinent technical information to the prospective attendees.

After each design review, Design Assurance will assemble the following information in a formal report of the design review.

- (a) Type of design review
- (b) List of attendees
- (c) Summary of accomplishments
- (d) List of unsolved problems revealed at the review
- (e) Requests for appropriate action

10.3 RELIABILITY ANALYSIS AND PREDICTION

The following steps constitute the analysis and prediction aspects of the reliability program:

- (a) Preliminary Reliability Prediction. The preliminary reliability prediction will be based on preliminary design phase concepts. These include preliminary materials and parts lists and preliminary stress factors which reflect the most complete information available in this phase.
- (b) Detailed Reliability Predictions. This will be based on final detailed design phase concepts. This prediction will be based on an analysis of parts usage, calculated stresses, predicted environmental parameters, and mechanical and electrical stress measurements performed on Phase II subsystem tests.
- (c) Final Reliability Analysis. This will be based on contractor and customer system and subsystem testing. Here actual failures will be analyzed and compared with predicted data in order to demonstrate the system reliability.

It is the responsibility of the Design Assurance group to provide feedback of theoretical reliability data and failure data to project engineering, design, quality control, and production, as appropriate for study, and to recommend corrective action during all phases of the program.

All engineering and design information will be made available to the reliability assurance organization in order to implement reliability analyses and prediction.

10.4 FAILURE REPORTING AND ANALYSIS

A closed-loop system of failure reporting, analysis and corrective action will be implemented throughout all phases of subsystem and system testing.

The failure reporting and analysis function will be carried out as follows:

- (a) Failure Reporting. All failures will be reported throughout all phases of subsystem and system testing by contractor and customer.
- (b) Tabulation and Reduction. All failure data will be tabulated in order to detect problem areas, failure trends, and possible weaknesses in design.

- (c) Dissemination of Failure Data. All failure data will be disseminated through summary reports and special critical problem reports. Where necessary, specific problem action requests will be initiated.
- (d) Corrective Action. Corrective action will be taken where failure data indicates a need for such action. This will be directed to the applicable project, design, production, or quality engineering group responsible.

The Reliability Assurance organization will have access to all engineering and test data pertinent to an accurate failure reporting system.

10.5 DESIGN STANDARDIZATION

A major effect on reliability, maintainability, and cost is produced by the degree to which design practices and processing procedures are controlled and based on proven approaches. As a part of the Design Assurance responsibility, practices and procedures will be reviewed to determine whether they can be improved by design standardization.

Specific technical areas to be reviewed are:

- (a) Design specifications
- (b) Test procedures
- (c) Inspection procedures
- (d) Process specifications
- (e) Workmanship standards
- (f) Procedures for selection of qualified vendors
- (g) Specification control drawings

Requests for corrective action will be initiated by Design Assurance when deficiencies are found.

10.6 RELIABILITY DOCUMENTATION

The Reliability organization shall be responsible for the following documentation:

- (a) Reliability program plan
- (b) Design review reports
- (c) Reliability prediction and analysis reports
- (d) Failure report summaries and critical problem reports
- (e) Corrective action requests

11.0 CONCLUSIONS

The results of the combined layout, analytical, materials, and test sample investigations have justified confidence in the proposed design as contained in this report. No major problem areas have developed. The results of the studies indicate that the basic roller concept is feasible and that the final design configuration will meet program objectives.

Minor problems may still exist in the area of beam stability at the point of transition from flat to full section. A test model is presently being fabricated to investigate these areas more thoroughly and provide modifications as required.

The roll beam developed here particularly for this solar panel concept is not limited to this application. Many uses in the area of extendable booms, both for space and earth applications are evident. Exploration of these possibilities would be a logical outgrowth of this program.

12.0 RECOMMENDATIONS

It is the recommendation of the Contractor that the detail design activity proceed in accordance with the current program schedule.